Master's thesis

NTNU
Norwegian University of Science and Technology
Faculty of Natural Sciences
Department of Materials Science and Engineering

Jonas Foshaug

Interaction between pre-reduced ilmenite and high titania slag melts

Master's thesis in Materials Science and Engineering
Supervisor: Gabriella Tranell
Co-supervisor: Stephen Lobo
June 2023

NTNU
Norwegian University of
Science and Technology

Jonas Foshaug

Interaction between pre-reduced ilmenite and high titania slag melts

Master's thesis in Materials Science and Engineering
Supervisor: Gabriella Tranell
Co-supervisor: Stephen Lobo
June 2023

Norwegian University of Science and Technology
Faculty of Natural Sciences
Department of Materials Science and Engineering

NTNU
Norwegian University of
Science and Technology

Preface

This master's thesis was done for the course TMT4905 in the master's program for materials science and engineering (MTMT) at the Norwegian University of Science and Technology (NTNU). This work has been carried out at the Department of Materials Science and Engineering at the Norwegian University of Science and Technology, Trondheim, Norway.

I would like to acknowledge my supervisor Prof. Gabriella Tranell and my co-supervisor Ph.D. Stephen Lobo for all the help on the project. I would like to thank all the engineers in IMA and Sintef for the help and guidance in the labs, and I would like to thank Morten Peder Raanes for the EPMA analysis.

Abstract

In the titanium industry, ilmenite is one of the most important raw materials. It is processed using reduction methods involving coke/coal. There is a desired change away from this reduction method in the industry due to the CO_2 emission that this method entails. The use of other reducing gases such as H_2 or a mixture of H_2 and CO is being looked at and is showing promising results. This master thesis aims to examine the interface between different pre-reduced ilmenite pellets and high titania slag. These different pre-reduced ilmenite pellets include H_2 reduced, CO reduced, and a mixture of the two gases.

There has been developed a successful method of dropping ilmenite pellets into melted high titania slag. This method was developed for the Tube Furnace 2 (TF2). TF2 is a furnace at NTNU Trondheim that has a controllable atmosphere, graphite heating elements, and a "quenching" possibility. The experimental work carried out in this master thesis used two different crucible types/systems, Mo and BN-coated SiC, and five ilmenite pellet types with different reduction agents. Three of the pellet types come from earlier and related work, the G-pellets. And two were created specifically for this experimental method, the A-pellets.

- G1 reduced with 100% CO for 2 hours having a conversion degree of 65%
- G3 reduced with a mixture of 60% CO and 40% H_2 for 2 hours having a conversion degree of 83%
- G6 reduced with a 100% H_2 for 2 hours having a conversion degree of 113%
- A1 reduced with 100% CO for 3 hours having a conversion degree of 76%
- A2 reduced with a 100% H_2 for 20 minutes having a conversion degree of 61%

The composition of the slag used is 85%TiO2+10%FeO+5%CaO in wt% and is the same for all experiments run. This slag was created using pure oxides in the laboratory. The G-pellets were used in combination with the BN-coated SiC crucible. The A-pellets were used in combination with the molybdenum crucible.

The BN-coated SiC crucible ended up having major reactions with the slag system. The Fe ended up reducing to a metallic phase, and Si-oxide phases were created. Both these phases were created due to the SiC crucible. An interface between the pellet and the slag could be seen in the experiments with a temperature of 1600°C and 0 min drop time, a visible pellet was found. For the Mo crucible experiments, the crucible had a lesser degree of reaction with the slag system. The Fe was not reduced and was in a Fe-oxide phase, the Mo had small metallic phases scattered around in the slag and were present in an oxide phase. The pellet/slag interface was not found in the Mo crucible experiments since the pellet was completely melted. The melting time for the pellets was found to be very quick, meaning difficulties finding the interface.

Sammendrag

I titanium industrien er ilmenitt ett av de viktigste råmaterialene. Ilmenitt behandles ved bruk av reduksjonsmetoder som involverer kull/koks. Det er et ønske om å bevege seg bort fra kull/koks (CO) reduseringsmetoden som er i bruk i industrien, dette er på grunn av CO2-utslippene som medfører denne metoden. Bruken av andre reduksjonsgasser som H_2 eller en blanding av H_2 og CO blir undersøkt og viser lovende resultater. Denne masteroppgaven har som mål å undersøke grensesnittet mellom ulike pre-reduserte ilmenittpellets og høytitania-slagg. Disse ulike pre-reduserte ilmenittpelletsene inkluderer H_2-reduserte, CO-reduserte og en blanding av de to gassene.

I denne masteroppgaven har det blitt utviklet en vellykket metode for å slippe ilmenittpellets ned i smeltet høytitania-slagg. Denne metoden ble utviklet for Tube Furnace 2 (TF2). TF2 er en ovn ved NTNU Trondheim som har en kontrollerbar atmosfære, grafitt varmings elementer og mulighet for "bråkjøling". Det eksperimentelle arbeidet som ble utført i denne masteroppgaven brukte to forskjellige digel systemer, Mo og BN-belagt SiC. Det var også fem typer ilmenittpellets med ulike reduksjonsmidler. Tre av pellettypene kommer fra relatert arbeid, G-pelletsene, og to ble laget spesielt for denne eksperimentelle metoden, A-pelletsene.

- G1 ble redusert med 100% CO i 2 timer og hadde en reduksjonsgrad på 65%.
- G3 ble redusert med en blanding av 60% CO og 40% H_2 i 2 timer og hadde en reduksjonsgrad på 83%.
- G6 ble redusert med 100% H_2 i 2 timer og hadde en reduksjonsgrad på 113%.
- A1 ble redusert med 100% CO i 3 timer og hadde en reduksjonsgrad på 76%.
- A2 ble redusert med 100% H2 i 20 minutter og hadde en reduksjonsgrad på 61%.

Sammensetningen av slagget som ble brukt, er 85% TiO2 + 10% FeO + 5% CaO i vektprosent, og sammensetningen er den samme for alle eksperimentene som ble utført. Dette slagget er laget ved å bruke rene oksider på laboratoriet. G-pelletsene ble brukt i kombinasjon med BN-belagt SiC-digler. A-pelletsene ble brukt i kombinasjon med molibden digler.

BN-belagt SiC-digelen viste seg å ha store reaksjoner med slagg systemet. Hvor jernet ble redusert til en metallisk fase, Si-oksid faser ble dannet. Begge disse fasene ble dannet på grunn av SiC-digelen. Et grensesnitt mellom pelletene og slagget kunne sees i eksperimentene med en temperatur på 1600°C og 0 minutter drop tid, hvor det var mulig se en ikke smeltet del av pelletene. For eksperimentene med Mo-digelen hadde digelen en mindre grad av reaksjon med slagg systemet. Jernet ble ikke redusert og var fortsatt i en Fe-oksid fase. Mo hadde små metalliske faser spredt rundt i slagget. Det var også Mo til stede i en oksidfase i slagget. Pellet/slagg-grensesnittet ble ikke funnet i eksperimentene med Mo-digel, siden pelleten var fullstendig smeltet i alle forsøkene. Smeltehastigheten for pelletsene var funnet til å være veldig rask, som medførte en vansklighet med å finne grensesnittet.

Contents

Figure list

List of Tables

1 Introduction

1.1 Background and motivation

TiZir Titanium and Iron AS is in the process of developing a more environmentally friendly way of processing ilmenite. This development is looking at replacing the pre-reducing agent from the standard CO made from coke/coal with hydrogen. By replacing the CO the yearly emission of carbon dioxide will be cut significantly. The process emits around 247 861 tons of CO_2-equivalent yearly, this number is from 2022.[1] Most of the CO_2-equivalent emission comes from this pre-reducing step.

In the development of pre-reducing ilmenite using hydrogen, there is a lacking of studies on how the pellets reduced by hydrogen affect the melting process later. That is a topic being looked more closely on in this master thesis. One of the reasons why there is lacking studies is because of the corrosive nature of the high titania slag melt. Once the slag reaches high temperatures it reacts with just about any crucible materials.

1.1.1 Industrial process/Tyssedal process

To more completely understand the work of this master thesis a little background on today's process of TiO_2 is needed. There are many different methods available for the production of TiO_2. A few of these methods are the Becher process in Australia [2], carbothermic smelting of hard rock ilmenite in Quebec [3], and the Tyssedal process in Norway [4]. All these processes start with the raw material ilmenite. The chemical composition of ilmenite is $FeTiO_3$ and is often classified into two categories, which are beach sand ilmenite and rock ilmenite. Beach sand ilmenite is usually found near the sea in sand dunes or in river deltas. The beach sand ilmenite contains a higher amount of TiO_2 than the rock ilmenite. 50-65 wt% in beach sand compared to 35-45% in rock ilmenite. A reason for this is there is usually a higher amount of iron in the rock ilmenite, where a hematite (Fe_2O_3) phase is very common in the rock ilmenite. [4] Norway is a leading producer of ilmenite in the world with the production of about 8% of the world's ilmenite. The ilmenite deposit in Tellenes mined by Titania AS is considered a world-class deposit. [5] The ilmenite used in the tyssedal process is taken from a beach sand deposit located in Senegal.[6] The operation in Senegal goes under the name of The Grande Côte mineral sands Operation, GCO for short. GCO is the largest dredge mineral sand operation in the world. The sand deposit has less impurities due to the weathering effect, the impurities are leached out and the resulting minerals are comparable to rock ilmenite.[7, 8]

The Tyssedal process is the process most interesting and relevant for this master's thesis. The process is divided into two main stages, the first stage is a pre-reducing stage and the second stage is a melting stage. These stages can be seen illustrated very simply in figure 1.1. From start to finish in the Tyssedal process the content of TiO_2 approximately goes from 54% in the first stage to about 87% in the final stage. [8]. The Tyssedal process will be described in greater detail below to give a better context for this master thesis, where the reactions taking place will be explored.

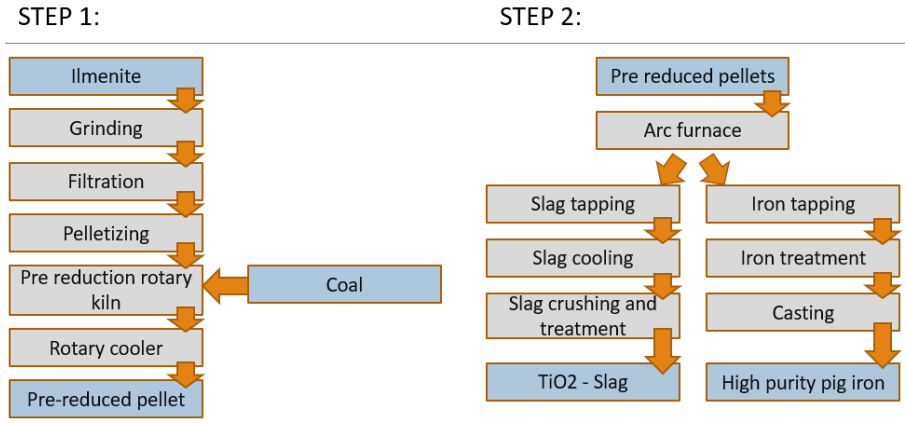

Figure 1.1: A simplified model of the two-step process recreated from metal production in Norway[4].

The process starts out in the pre-reducing stage. Here it starts by feeding ilmenite into a wet ball mill, this mill grinds up the ilmenite into a suitable size. Once the ilmenite has been ground to a desired size it is pelletized. To pelletize the ground-up ilmenite, the ilmenite slurry from the wet ball mill is filtered and mixed with a binder. This product of mixed ilmenite slurry and binder is pelletized into desired shapes and fired to ensure the pellets are strong enough for the next steps. These fired pellets are then ready for the pre-reduction step, where they are inserted into a rotary kiln together with coal/coke. In this rotary kiln, the iron in the pellets will reduce into metallic iron. The main reduction reactions can be seen below in the equations 1.1,1.2, and 1.3. After the pellets have been reduced they are cooled down in a reducing atmosphere in a rotary cooler to ensure a minimal re-oxidation of iron. A temperature of about 1100 °C is the target inside the rotary kiln. This high temperature ensures the reaction 1.2 will be almost completely shifted to the right. Meaning a surplus of CO gas is produced and reduces the $FeTiO_3$. When explaining the metallization degree of ilmenite, we look at the amount of iron oxide reduced. For the Tyssedal process, a high metallization degree is desired. To achieve a high degree of metallization the CO_2/CO needs to be low.

The reactions taking place inside the rotary kiln are:

$$FeTiO_3 + CO\,(g) \rightleftharpoons Fe + TiO_2 + CO_2(g) \tag{1.1}$$

$$CO_2(g) + C \rightleftharpoons 2\,CO\,(g) \tag{1.2}$$

These reactions give us the total reaction:

$$FeTiO_3 + C \rightleftharpoons Fe + TiO_2 + CO\,(g) \tag{1.3}$$

The pellets are then ready for the second stage. In this stage, the pellets are continuously fed into an electric arc furnace where they undergo the last reduction reactions, here they are turned into high titania slag with a temperature exceeding 1500 °C. In this stage, a balance of reduction degree is needed. If the pellets are reduced too much the fluidity will not be adequate for the tapping of the slag. A certain amount of FeO is needed in the high titania slag to accomplish this. The way this balance is achieved is by controlling the amount of reducing agent, aka controlling the carbon balance in the furnace. There are two products being tapped from the furnace. High-purity pig iron and TiO_2 slag. The slag tapped has 87 wt% TiO_2. [8]. A more detailed explanation of the tyssedal process can be found in the book Metal Production in Norway. [4]

The main reactions taking place in the arc furnace are:

$$\mathrm{FeO\,(l) + C \rightleftharpoons Fe\,(l) + CO\,(g)} \tag{1.4}$$

$$\mathrm{2\,TiO_2(l) + C \rightleftharpoons Ti_2O_3(l) + CO\,(g)} \tag{1.5}$$

Table 1.1: An estimate of the ilmenite concentrate and the resulting slag from the 80s [9]

	wt% TiO_2	wt% FeO	wt% Fe_2O_3	wt% SiO_2	wt% MgO	wt% Al_2O_3	wt% Cr_2O_3
Imenite concentrate	44.6	34.8	11.9	2.8	4.7	0.7	0.07
Tyssedal slag	75	7.6	-	5.3	7.9	1.2	0.009

Table 1.1 indicates how the ilmenite transforms during the Tyssedal process. The process has gotten better over the years, from producing slag with 75 wt% to 87 wt% TiO_2. [8, 9]

1.2 Aim and scope of the work

The aim of the master thesis is to better have a look at the interface between ilmenite pellets and high titania slag, more specifically the difference between the CO- and H_2- reduced pellets. This is done by a newly developed setup on the Tube Furnace 2 that allows for the dropping of pellets into liquid slag with the function to 'quench'. The pellets used are from two sources, an earlier work of S. Lobo and newly made pellets from ilmenite powder. Once these experiments are run they will be macro- and microscopically investigated. These investigations include the use of different functions on the EPMA. To make sure the experimental data is usable, the materials chosen are comparative to what is present in the industry, just a little bit simplified. One of the main results will be an EPMA mapping of the interface between pellet and slag.

2 Theory and literature survey

2.1 Literature survey

2.1.1 Ilmenite smelting

Ilmenite smelting is a process to upgrade mineral ilmenite ($FeTiO_3$) to TiO_2 rich slag often used as pigment. A problem in ilmenite smelting is the foaming that sometimes occurs during the process. This foaming can become uncontrollable. It is believed that the foaming happens due to a lack of fluidity in the slag, as well as a gas evolution of CO/CO_2 gas that functions as gas bubbles in the slag. [10, 11]

In the process of high titania slag the liquidus line of the phase system is an important aspect. Numerous studies have been done on the liquidus line in a $FeTiO_3 - Ti_2O_3 - TiO_2$ system. [12, 13, 14] The studies used synthetically made slags with different amounts of FeO in the system, then measuring the liquidus temperature of the composition. Here some relevant measurements are the ones with a wt% of FeO around 10-15%. The liquidus temperature seems to be ranging around a value of 1650-1700 °C. The findings of the experimental investigations are that the liquidus temperature varies quite a lot with the FeO amount. Meaning a slag containing around 31 wt% FeO has a liquidus point at around 1500°C whilst lower amounts of FeO, around 6-8 wt%, shows a liquidus temperature above 1700°C. [12] This research also showed a disconnection in the results Factsage shows, however, these experimental data from Factsage are old ($\tilde{2}010$), and are likely updated. It gives an idea of the uncertainty present in the high titania slag research conducted so far. This research seems to be more accurate than most, the reason for this is the experimental setup used is extremely similar to what is used in the industry. This experiment was done using a water-cooled copper crucible, this means the crucible gets a freeze lining during the experiment. The slag will have minimal reaction from outside sources since it does not directly touch any outside sources(crucibles etc.). [12]

2.1.2 Lining and crucible materials with high titania slag

Freeze lining is one of the most common methods used in ilmenite smelting. This method is common because of the corrosive nature of TiO_2 slag. TiO_2 slag reacts with all refractory materials when melted. The freeze lining method used is a way of cooling the slag down at the crucible surface using a material with a high enough heat conductivity. cooling it down leads to the slag solidifying and becoming the crucible "wall". This is a great method for big production using furnaces with big volumes, but not a great method in a lab environment where the samples are usually quite small. [4] It has been done in a lab environment, and much of the equilibrium data gathered stem from a freeze-lining system. [12] The freeze-lining system is quite sensitive. Meaning it is essential to maintain the freeze lining but at the same time not drop below the liquidus temperature. If the temperature drops below liquidus there will be partial solidification and an increased viscosity as a result. The partial solidification is also believed to be responsible for incidents such as uncontrolled foaming in the furnace.[15] Careful monitoring of the furnace is needed for it to run smoothly, especially when a composition change in the furnace is desired.

A study on different crucible types/coatings used for induction smelting of high titanium alloys was done by S. Fashu et al.[16] The study looked at crucibles such as SiC, Al_2O_3, Mo, BN, and graphite, just to mention a few. The most promising crucibles/coating combination was concluded to be cheap

crucibles such as graphite and Al_2O_3 coated by an inert refractory material such as Y_2O_3. The negative sides were the difficulties of application and the stability of the coating. The Mo crucible coated with this inert refractory material was also a contender. when looking at the BN crucible, it was found to cause aggressive melt contamination.

P. Shen et al. studied the wettability for molten SiO_2–MnO–TiO_2–FeO_x slag with refractory materials.[17] They tested the different materials with the help of the sessile drop method. Meaning measuring the contact angle between a drop of liquid on a refractory metal. The different materials tested were Mo, W, Pt, polycrystalline Al_2O_3, and graphite. The temperature ranged from 1473-1673 K. There was good adhesion between the slag and all these materials. The metal materials had an adhesion in the order of Pt W Mo, and with increasing temperature the wettability gets considerably increased for Mo and W. It was found that the wettability for the graphite crucible was very temperature dependant. The adhesion was originally very low between graphite and slag, but at a certain point, a temperature dependant reaction leads to a considerable decrease in contact angle. There are also signs of foaming behavior in the graphite/slag reaction. [17]

2.1.3 Slag viscosity

The viscosity of slag is usually very temperature dependant, meaning a gradual increase of the viscosity during a decrease in temperature below the liquidus line. However, for high titania slag the rise in viscosity is very sudden and extreme below a certain temperature. Illustrated simply in figure 2.1. In the industry a low viscosity is desired to be able to tap the slag, this means a higher temperature might be necessary.[4] Another factor affecting the viscosity is the FeO content in the system. It was found that the critical temperature for TiO_2 slag seen in figure 2.1 is very dependent on FeO and other oxides such as Ti_2O_3. [18, 19] It has been found that once completely melted the high titania slag has a very low viscosity and is insensitive to temperature and slag composition.

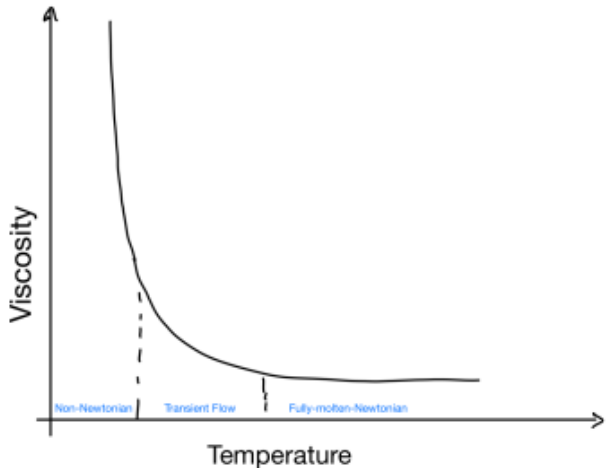

Figure 2.1: An illustration of the viscosity of high titania slag vs temperature.[20]

A viscosity study was done using an experimental setup with molybdenum crucibles and a rotating cylinder viscometer. In the study, it was found that a small inclusion of CaO, SiO_2, and MgO into the TiO_2-FeO system had minimal effect on the viscosity compared to the effect of the TiO_2-FeO ratio.[19, 18] This is one argument why CaO can be included for the slag samples in this master thesis, it is needed to lower the melting temperature of the slag while it does not affect the viscosity a great deal. From the study done by K. Hu et al. [18], there was made viscosity-temperature curve from the viscosity data used in the work. This shows the limiting effect of the small inclusions compared to the TiO_2-FeO ratio, seen in figure 2.2 below.

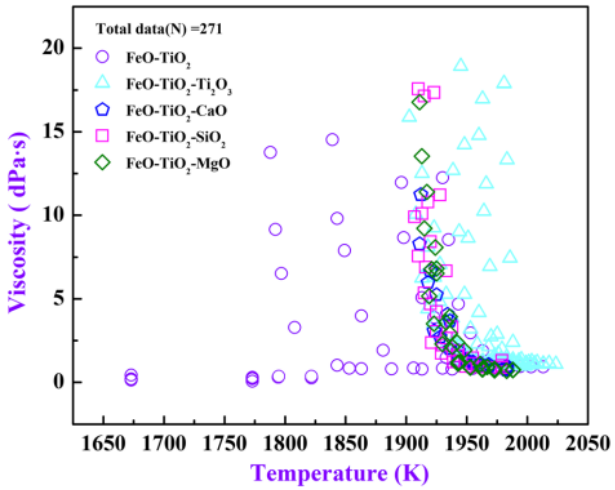

Figure 2.2: Viscosity vs temperature curve taken from K. Hu et al.[18]

2.1.4 Effect of carbon in the high titania slag system

By introducing carbon into a high titania slag system there will be a reducing effect on the oxides present. The most dominant oxides are TiO_2 and FeO. In a study of iron recovery of high titania slag in ESCM (electro-slag crucible melting) the effect of carbon in the system was explored. [21] The experiments run in the ESCM furnace were using a graphite crucible and a graphite electrode. The experiments were run at around 1650 °C to ensure melting. It was found that the TiO_2 started to reduce to Ti_3O_5 and Ti_2O_3, and as a consequence the viscosity of the slag increased. This increase is because of the higher melting temperature of the new phases created by the reduction. The iron in the slag will then be trapped because of the higher viscosity and the iron recovery is greatly reduced.[21]

2.1.5 Direct reduction

Reducing iron without melting is called DRI (direct reduced iron), i.e. Removing oxygen from iron ore or iron-bearing materials. This process is used in the iron production industry, whereas a few different reducing agents are viable. The most common are CO gas, coal or natural gas. [22, 23] Using these reducing agents the byproduct will be either CO_2 or H_2O. This can be seen in the following reactions below. The reason this is interesting in this master thesis is because ilmenite contains about 20 mol% iron so it is safe to assume iron plays a role in the solid state reduction process of the ilmenite. Comparing the reduction of iron pellets using different reduction agents to the reduction of ilmenite pellets is interesting, and can lead to a better understanding of the mechanisms.

The reduction mechanisms using CO can be described as the following:

$$3\,Fe_2O_3 + CO \rightleftharpoons 2\,Fe_3O_4 + CO_2 \tag{2.1}$$

$$2\,Fe_3O_4 + CO \rightleftharpoons 3\,FeO + CO_2 \tag{2.2}$$

$$FeO + CO \rightleftharpoons Fe + CO_2 \tag{2.3}$$

The reduction mechanism using hydrogen can be described as the following:

$$3\,FeTiO_3 + H_2 \rightleftharpoons 2\,Fe_3O_4 + H_2O \tag{2.4}$$

$$2\,Fe_3O_4 + H_2 \rightleftharpoons 3\,FeO + H_2O \tag{2.5}$$

$$FeO + H_2 \rightleftharpoons Fe + H_2O \tag{2.6}$$

It was concluded that hydrogen was a more efficient reducing agent than CO due to a better kinetic behavior.[24] The hydrogen also showed a better diffusion behavior. The explanation being smaller molecule sizes and lower viscosity for hydrogen. [24] Modelling of iron oxide reduction is difficult due to the many parameters influencing reduction rates. This has the following effect when making mathematical models, where the models have to make a lot of assumptions with the parameters. Many studies have been done on iron pellets using reducing gases like CO, H_2, and CH_4. [25, 26] The topics of these studies were the basis of several subsequent studies to develop a model to simulate the reduction zone in the shaft furnace. [27, 28, 29] These models did not consider CO-H_2-CH_4 reducing gas, or transition and cooling sections. It was therefore further developed. [30] This model indicates how iron reduces in different reduction gasses, and how a CH4 reduction gas would work on iron pellets. If used correctly these models can predict certain experimental results quite well, but an overall model is not very accurate yet. [24]

In the paper that concluded that hydrogen was a more efficient reducing agent than CO. A summarized table of rate-determining steps for different temperatures and experimental methods was made. [24] A recreated table can be seen below in 2.1.

Table 2.1: Rate limiting step of iron oxide reduction reported in the literature. This table is recreated from the literature survey [24].

Reference	Reduction step	Temperature range [°C]	Reduction-controlled mechanism	Experimental method
[31]	$Fe_2O_3 \longrightarrow Fe$	460–500	Phase-boundary	Isothermal (H_2)
	$Fe_2O_3 \longrightarrow FeO$	700–910	Phase-boundary	Isothermal (H_2)
[32]	$Fe_2O_3 \longrightarrow Fe$	300–900	First-order and nucleation	Non-Isothermal (H_2)
[33]	$Fe_3O_4 \longrightarrow Fe$	220–430	Phase-boundary and nucleation	Isothermal (H_2)
[34]	$Fe_2O_3 \longrightarrow Fe_3O_4$	25–650	Phase-boundary	Constant rate thermal analysis (H_2)
[35]	$Fe_2O_3 \longrightarrow Fe_3O$	400–500	Phase-boundary and product layer diffusion	Isothermal (H_2)
[36]	$Fe_2O_3 \longrightarrow Fe_3O_4$	250–800	Random nucleation	Non-Isothermal (H_2)
[37]	$Fe_2O_3 \longrightarrow Fe_3O_4$	800–900	Phase-boundary	Isothermal (CO)
	$Fe_3O_4 \longrightarrow FeO$	800–900	Phase-boundary	Isothermal (CO)
	$FeO \longrightarrow Fe$	800–900	Nucleation and growth	Isothermal (CO)
	$Fe_2O_3 \longrightarrow Fe$	700–900	Phase-boundary and diffusion	Isothermal (CO)
[38]	$Fe_2O_3 \longrightarrow FeO$	800–950	Phase-boundary and diffusion	Isothermal (H_2,CO)

2.1.6 Melting of iron pellets

In a study done on the interaction behavior between direct reduced iron and different melts[39] it was found that carbon either in the melt or in the DRI pellet had an effect by increasing the melting rate of the pellet, this was due to an effect on the liquidus temperature. The DRI used were high, low, and carbon-free, which was immersed into different melts and slags. It was also concluded that particle density is a crucial parameter in the melting behavior and that the melting times were significantly longer if the pellets were in contact with the slag on the melt.[39] These longer melting times were in qualitative agreement with the modeling done by Gonazalez.[40] The setup of the experiments in this study is similar to this master thesis, using a high-temperature tube furnace, the difference being they mounted a pellet on a molybdenum wire to be able to lower the pellet into the melt for the dipping process. [39]

In the melting of steel scrap in a molten iron-carbon melt, similar to the investigation explained above, it was found that the main factors controlling the melting and dissolution process were heat

and mass transfer. [41] The melting steps can be described as follows. In the start, there is an initial formation of a solid hot metal layer, this layer gets liquefied once the heat transfer provides enough overheat. There is also a diffusive melting with mass transfer. Here there is a mass transfer from carbon-rich hot metal to low-carbon metal(steel scrap). Overall the primary mechanism was the heat transfer, given that the carbon content was balanced or the temperature exceeds the liquidus temperature (overheat).[41]

2.1.7 Pellet, composition and results

Some of the pellets used in this master thesis were made in the Ph.D. work by S. Lobo, so there is already some data on the composition and effect of the different pre-reduction methods. [42] A qualitative point analysis of the pellets can be seen further down in the materials section in figure 3.1. From S. Lobo's Ph.D. it was proposed an oxidation and reduction pathway for the ilmenite pellets. This pathway can be seen in figure 2.3. Here the proposed path is divided into multiple steps. Simplified the first stage is the reduction of Fe^{3+} to Fe^{2+}, the second step is the reduction of Fe^{2+} to Fe, and the third step is the reduction of TiO_2 to lower Ti-oxides. The first step is shown to be happening rapidly, while the second and third steps are a bit more sensitive to the experimental factors. The factors discussed in the Ph.D. were gas composition, temperature, and chemical composition. [42]

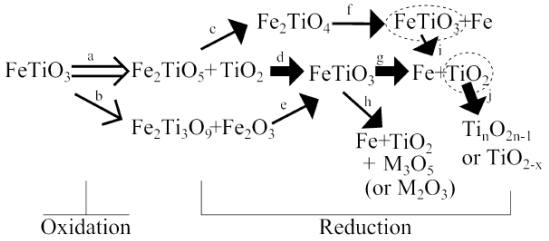

Figure 2.3: Proposed oxidation and reduction pathway taken from S.Lobo's Ph.D. [42]

An explanation to how one can see how the first step is a lot more rapid than the next two can be seen in figure 2.4 below. Here it is seen that the pellet reduces rapidly at the start before it slows down. This reduction mechanism is what is considered the first step, the reduction of Fe^{3+} to Fe^{2+}. The graphs can be used to see when all the Fe_2O_3 has been reduced, which is seen when the steep slope stops and starts rounding off. The resulting/remaining FeO takes longer to reduce to Fe and is thereby a much slower process. It is also seen in this graph that Hydrogen as a reduction agent significantly decreases the conversion time. Meaning that carbon is a slower conversion agent than hydrogen. It is also seen that the conversion degree for G6 is over 1, this implies that the Ti in the ilmenite also has started to reduce.

	G1	G2	G3	G4	G5	G6
Hydrogen content (vol.-%)	0	20	40	60	80	100

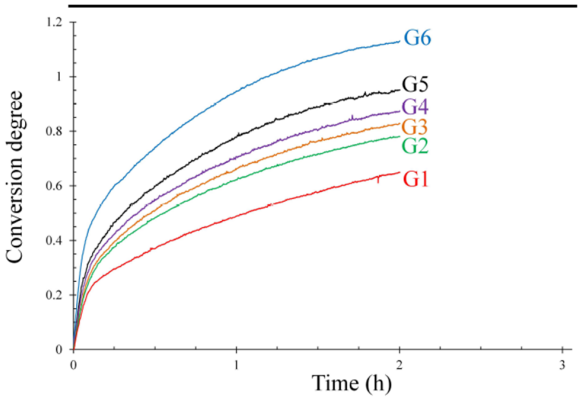

Figure 2.4: Conversion degree plots of the different G series experiments taken from S.Lobo's Ph.D. [42]

2.1.8 The shrinking core model (SCM)

A shrinking core model (SCM) can be used when wanting to describe what happens to a pellet during reduction. In the book chemical reaction engineering the process of SCM for spherical particles of unchanging size has been visualized in 5 steps.[43]

- **Step 1:**
  Diffusion of a gaseous reactant (A) to the surface of the solid particle through the gas film surrounding the particle.
- **Step 2:**
  Diffusion of gaseous reactant to the unreacted core (B) through the reaction interface (C).
- **Step 3:**
  The gaseous reactant (A) react with the unreacted core surface (B) creating a gas product (D) and more reaction interface (C).
- **Step 4:**
  Diffusion of gas product (D) to the surface of the solid particle through the reaction interface (C)
- **Step 5:**
  Diffusion of gas product (D) to the main body of fluid through the gas film.

A basic chemical reaction to better explain the overall reaction taking place can be seen in equation 2.7 below. Here the letters seen in the steps above are inserted.

$$\mathrm{A(g) + B(s) \rightleftharpoons C(s) + D(g)} \tag{2.7}$$

All these proposed steps can be seen visualized in figure 2.5. It is possible for some of these steps to not exist in some situations. An example is if there are no gaseous products (D) formed, meaning there would not be any steps 4 or 5. For these cases, the step with the highest resistance is considered rate-controlling.

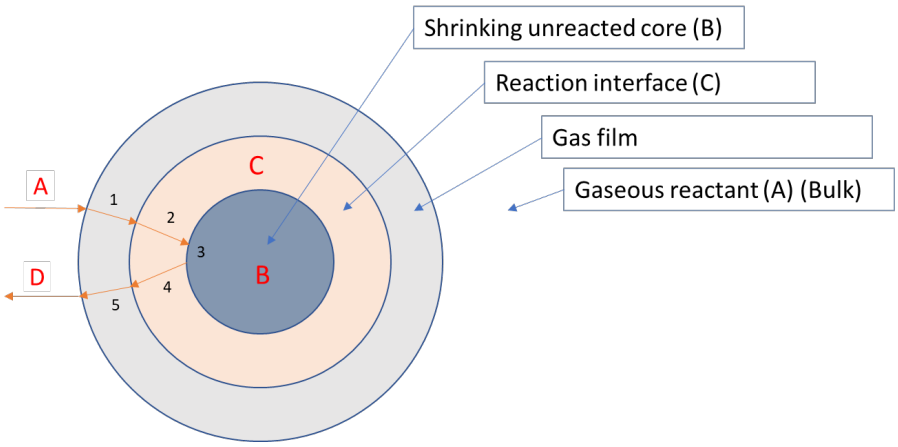

Figure 2.5: Shrinking core model with rate limiting steps indicated. Redrawn from S. Lobo and Chemical Reaction Engineering [42, 43]

There are a few assumptions needed to make this model valid, some of the main ones being the ability for diffusion of gases through the respective layers, remaining a constant shape (i.e. spherical), the gas accumulation in pores is considered negligible, isothermal particle, and constant total pressure throughout the particle. It is also important that the topochemical interface is well-defined. This is the case for most solid-fluid reactions. [42] For ilmenite reduction a schematic with the shrinking core model was created by S. Lobo, seen below in figure 2.6. In this figure it is assumed Ti only reduces after metallic iron is formed. When looking at the stability of TiO_2 compared to iron oxides this seems like an acceptable assumption. This stability can be seen in the phase diagrams and systems section later, more specifically in figure 2.8 .

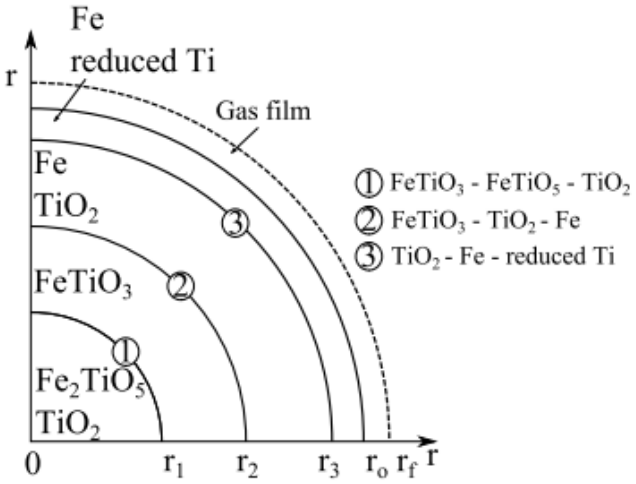

Figure 2.6: Shrinking core model for a reduction of oxidized ilmenite. Image taken from S. Lobo. [42, 43]

For the shrinking core model of ilmenite seen in figure 2.6 there are three "reaction points". These three reductions are as follows, $Fe_2TiO_5 + TiO_2 \longrightarrow FeTiO_3$, $FeTiO_3 \longrightarrow Fe + TiO_2$, and TiO_2 to a reduced Ti phase.

2.1.9 Post treatment of ilmenite pellets

As mentioned earlier some of the pellets used in this master thesis originate from earlier work done by S. Lobo. [42] It was also conducted more research on high-temperature heating of the pellets in a project work done by T. van Kaam. [44] The high-temperature heating of the pellets reduced in CO,

H_2, or a mixture of the two, was conducted in the Resina furnace which is similar to the one used in this master thesis. The figure 2.7 below shows an experimental setup for the Resina furnace, in the setup for T. van Kaam there is no dropping mechanism for pellets seen in this figure, and the crucible with the melt is changed for a crucible with pellets. The furnace is similar to TF2 in this master thesis in regards to atmosphere control, having an Argon atmosphere. The pellets in the crucible were also put on top of a BN substrate to limit/remove a reaction with the outer crucible. This crucible is alumina. The high temperatures the experiments were run at is as follows, 1300 °C, 1400 °C, 1500 °C, and 1600 °C. EPMA (Electron Probe Micro Analyser), XRD, and LECO analysis were done of the pellets after the heating to high temperatures. Some of the main findings of this research were the phase change of the rutile to a pseudobrookite (M_3O_5) phase with increasing temperature. The iron also seemed to agglomerate at increasing temperatures, especially at the edges of the pellets. There were a difference found in the melting behavior of the pellets, This melting was done at 1600 °C. The G1 pellet was completely melted, G6 showed little signs of melting, and G3 was in between these. This was believed to be due to the differing conversion degrees of the pellets. 65%, 83%, and 113% are G1, G3, and G6 subsequently.[44]

There was also some previous work done for this thesis in the form of a project study. [20] This project study is similar to parts of this study in the way that it is looking at the interface between pellet and slag melt, using the Resina furnace setup seen in figure 2.7. One of the other main outcomes of this project study was the development of the setup used in this master thesis. There was also laid a foundation in the exploration of different compositions of high titania slag and viable crucible materials. The project concluded with Molybdenum crucibles being the most viable, while the BN-coated SiC crucible was usable with some obvious drawbacks in the form of the reaction with the slag melt.[20]

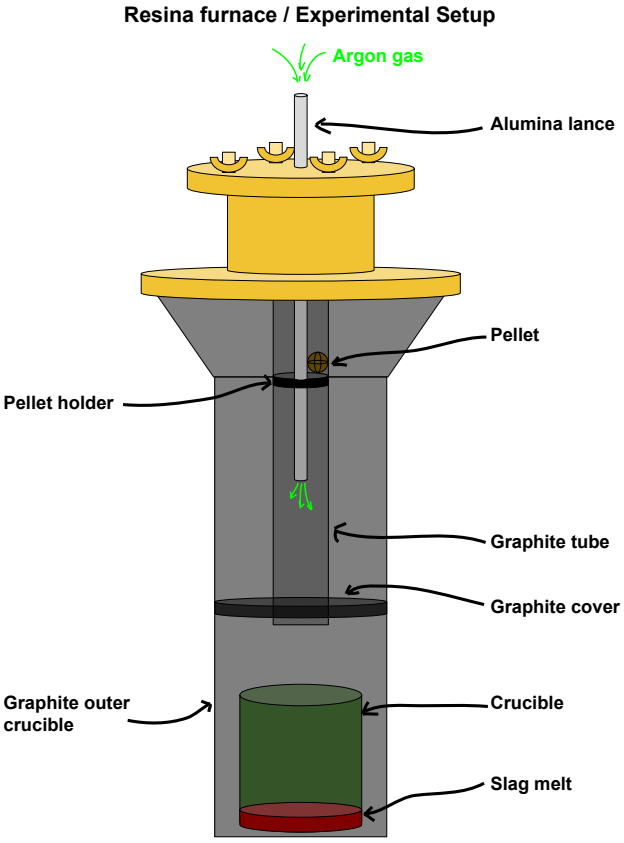

Figure 2.7: Experimental setup for the Resina furnace used in the project work. [20]

2.2 Phase diagrams and systems

In this section, relevant systems and phase diagrams related to this master thesis will be explored. A few phase diagrams found in the literature will be shown and compared to phase diagrams created by Factsage.

Factsage is a program that computes chemical thermodynamic data for different systems. The systems created are based on mathematical models and are verified by experimental data. Factsage has been developed for over 20 years and is one of the largest programs of its kind. [45] The program is able to calculate multi-phase and multi-component equilibrium, giving it the ability to create tertiary-phase diagrams.

2.2.1 Ilmenite (M_2O_3) and Pseudobrookite (M_3O_5)

K. Borowiec and T. Rosenqvist have done studies on the phase relations and oxygen potentials of Fe–Ti–Mg–O and Fe–Fe_2O_3–TiO_2 systems. [46, 47] In these studies there were defined phase diagrams for M_2O_3 and M_3O_5 phases. These were respectively Ti_2O_3–Fe_2O_3 and Ti_3O_5–Fe_2TiO_5. Figure 2.8 shows the phase diagrams suggested in the study. These figures are taken from S. Lobo's Ph.D. because some of the phases on the phase diagram in the original paper were written with quite a small font size. [47]

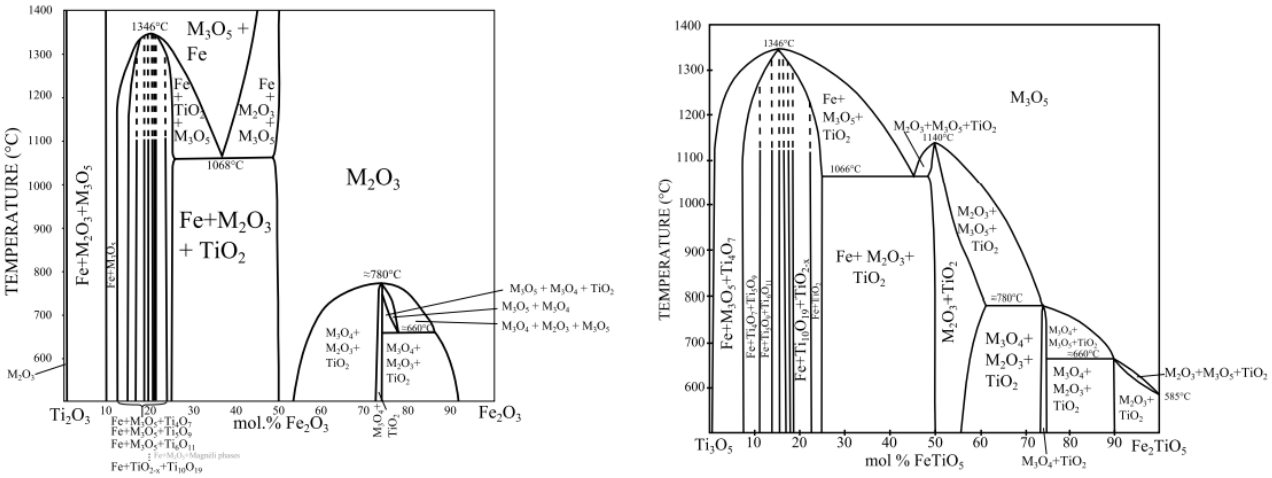

Figure 2.8: Ti_2O_3–Fe_2O_3 (left figure) and Ti_3O_5–Fe_2TiO_5 (right figure) phase diagrams as suggested in Borowiec [47], These diagrams are taken from S. Lobo's Ph.D. where they were redrawn by him.[42]

As seen in the phase diagrams in figure 2.8, for low amounts of Fe a full solid solution is only possible above 1346 °C. Temperature and the iron to titanium ratio are both important parameters in the determining the stable phases present, as seen in the phase diagram. The stability of the phases increases with increasing amounts of iron present. In K. Borowiec's and T. Rosenqvist's studies, it was shown that for the iron-rich region (above 50 wt% Fe_2O_3) there is complete solubility for Fe_2O_3 and $FeTiO_3$ when the temperature exceeds 780 °C.

2.2.2 TiO_2-FeO system

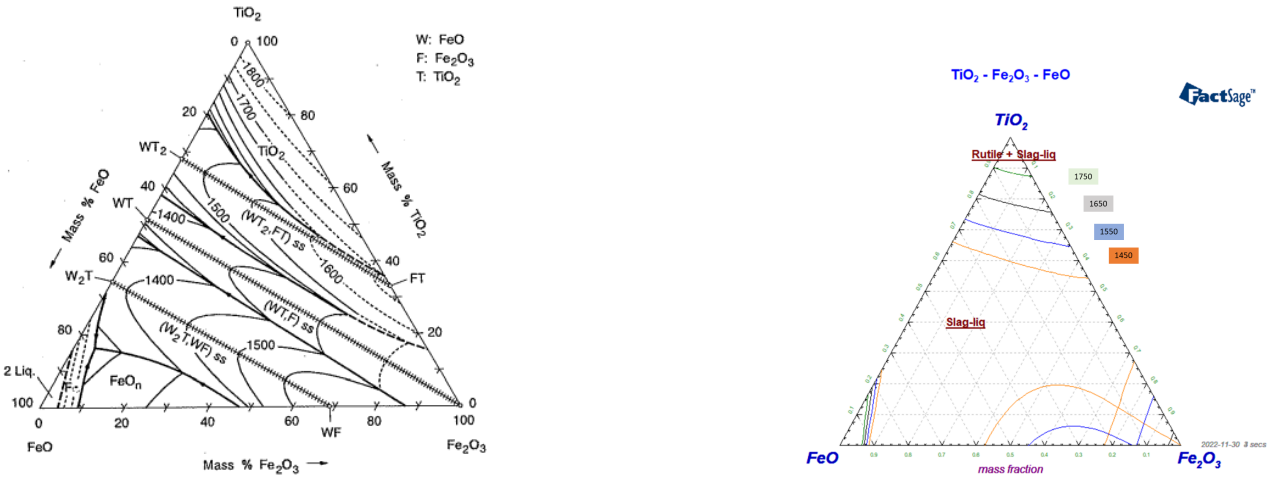

Figure 2.9: Ternary diagram of the TiO2-FeO-Fe2O3 system on the left taken from the slag atlas.[48] Ternary diagram of the TiO2-FeO-Fe2O3 system made using factsage on the right.[20]

The ternary phase diagrams seen in figure 2.9 show what Factsage has calculated compared to what was calculated in the slag atlas.[48] The interesting parts of these diagrams are in the top part of the triangles, meaning the parts with high amounts of TiO_2. These diagrams can be used as a basis to find out the melting point of different slag compositions. In the case of a high titania slag, more than 80 wt% TiO_2, the melting point is over $\sim$ 1650 °C. This melting point is further evident when looking at the binary phase diagram in figure 2.10.

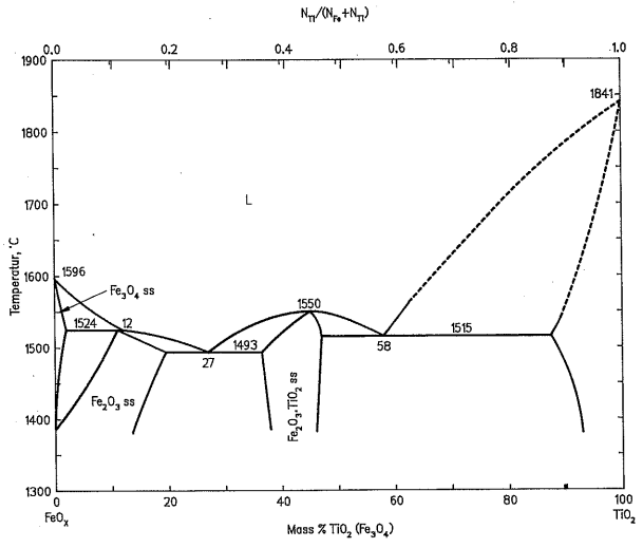

Figure 2.10: Binary phase diagram of FeOx-TiO_2 taken from the slag atlas [48].

The Fe-Ti-O ternary system is a complex system with quite a bit of differing literature. A. H. Webster and F.H. Bright had an early study in 1961, looking at the stability regions of M_2O_3, M_3O_4, and M_3O_5. [49] These investigations varied the oxygen partial pressure at 1200 °C. They concluded with the pseudobrookite series being a complete solid solution at this temperature. In 1999 research done by S. Itoh it was put forward some phase diagrams for the Ti-Fe-O system at 1173 K, 1273 K, and 1373 K. [50] The phase diagram for 1173 K can be seen in figure 2.11. The experimental method consists of samples being placed in a CO-CO_2 gas mixture while the mass changes were being measured. The

measurements stopped when the sample and the mixture reached equilibrium.

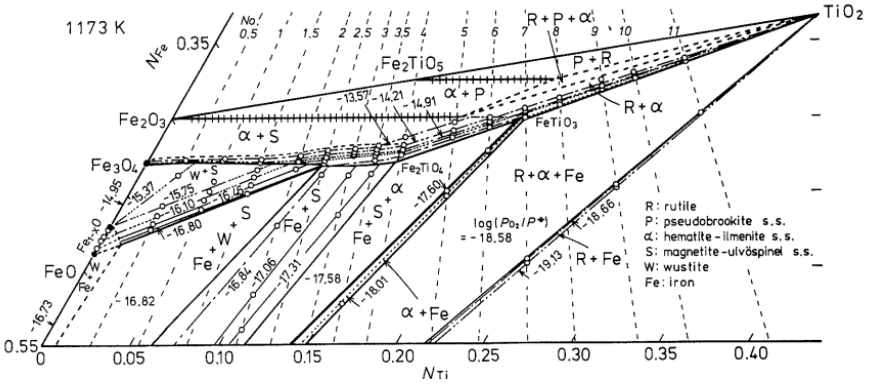

Figure 2.11: Phase diagram of the Ti-Fe-O ternary system and isobars of oxygen at 900 °C. Taken from S. Itoh. [50] The dotted lines represent a decrease/increase in oxygen content.

Going back to K. Borowiec and T. Rosenqvist, in their study they also put forward a phase diagram at 950 °C for the Fe-Ti-O system. This phase diagram can be seen in figure 2.12. This diagram has an additional composition, the Ti_3O_5 compound. The phase diagram explains the behavior of ilmenite reduction/oxidation, meaning the phases formed. Using initial composition data of the ilmenite concentrate it is possible to more accurately see what phases get formed. In other words, the reduction path can be seen to vary with the initial composition of the sample.

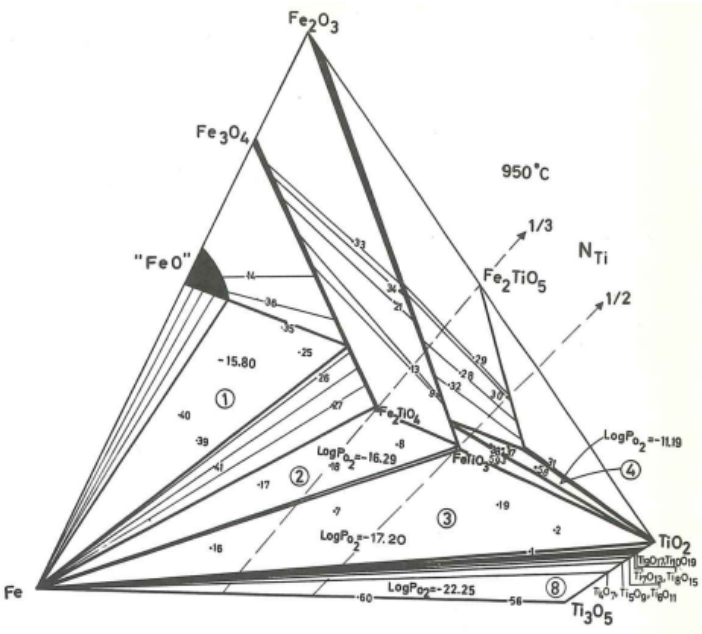

Figure 2.12: Phase diagram at 950 °C for a $Fe-Fe_2O_3-TiO_2$ system. Taken from K. Borowiec and T. Rosenqvist [46]

2.2.3 TiO_2-FeO-CaO system

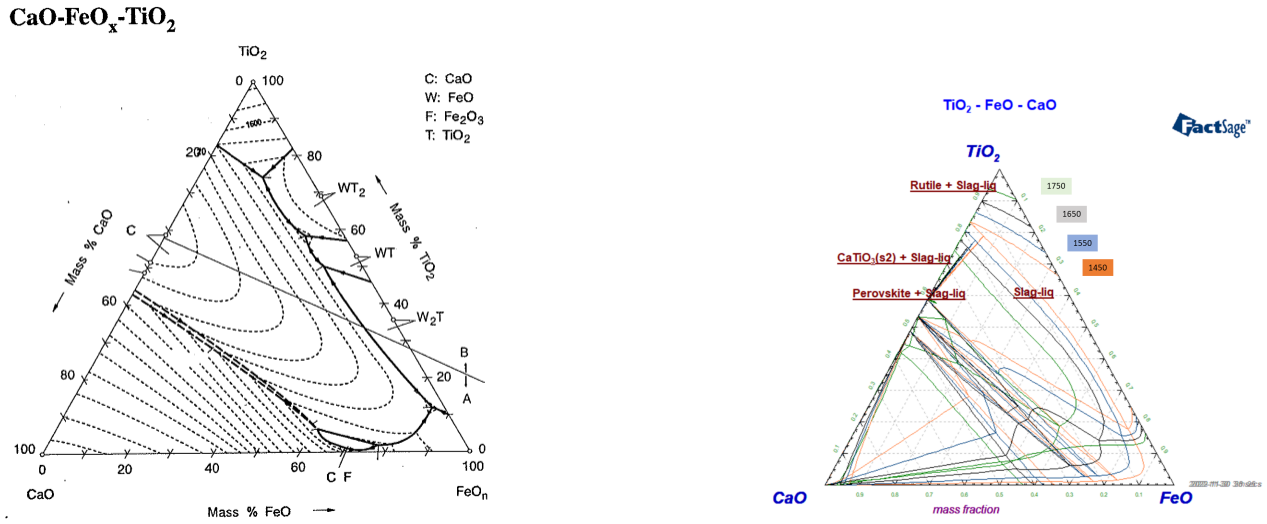

Figure 2.13: Ternary diagram of the TiO_2-FeO_x-CaO system on the left taken from the slag atlas.[48] Ternary diagram of the $TiO_2-FeO-CaO$ system made using factsage on the right.[20]

The TiO_2-FeO_x-CaO system shows a small increase in CaO content in a composition with high TiO_2 wt% greatly decreases the melting temperature of the slag composition. This is most easily seen in the ternary diagram created by factsage.

2.2.4 TiO_2-FeO-SiC-C systems

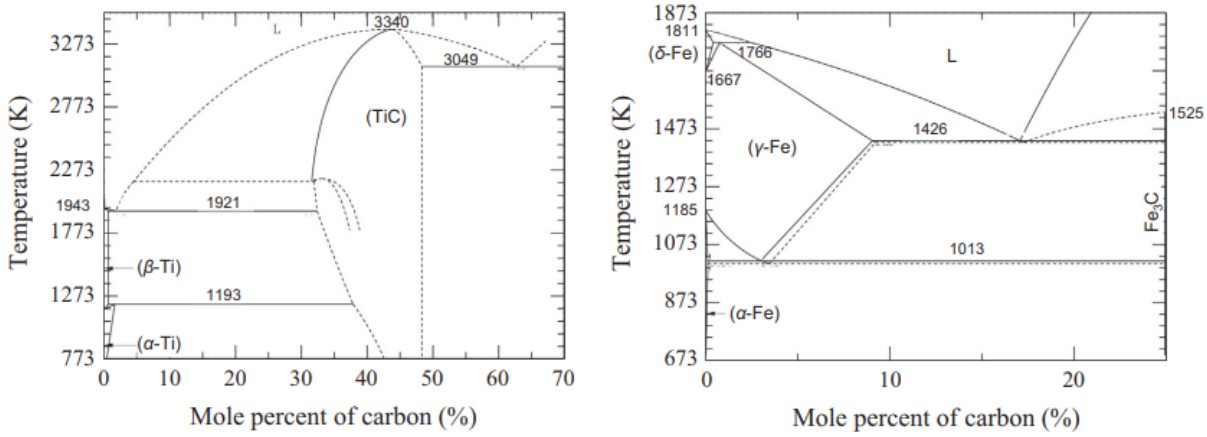

Figure 2.14: Binary phase diagram for Ti-C to the left and Fe-C to the right. Taken from Narumi et al. [51]

The phase diagrams above in figure 2.14 is taken from a thermodynamic evaluation study looking at the C-Fe-Si and C-Ti-Si systems. [51] It is seen that with increasing carbon content, the creation of a TiC phase is possible. In the study of Narumi et al. there was made some ternary diagrams of these systems. Mostly used to look at how the liquidus is affected by the different systems. It was found that the C-Ti-Si had a limiting effect on the liquidus region compared to C-Fe-Si. [51]

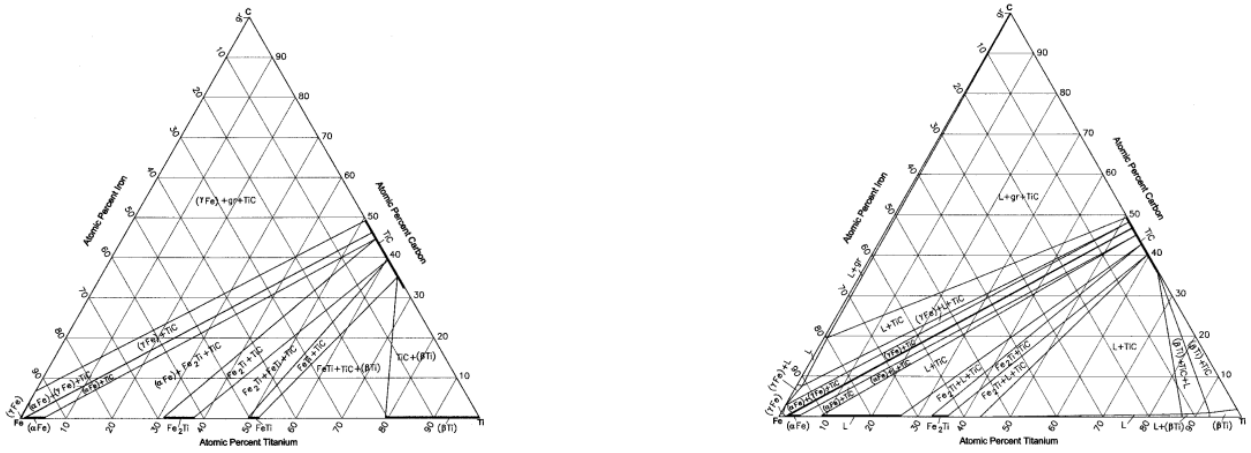

Figure 2.15: Ternary diagrams of the Ti−Fe−C system. The left at 1000°C and the right at 1400 °C. These were recreated in a paper by V.Raghavan from work done by S. Jonsson.[52, 53]

In the phase diagrams seen in figure 2.15 above, the interesting area to look in for this thesis is the bottom right of the triangle. This is the phases for a concentration of a high amount of Ti. Seen from these corners a very tiny amount of carbon is needed for a TiC phase to be formed. These ternary diagrams are resulting from S. Jonasson thermodynamic calculations of the Fe-Ti-C system.[52]

3 Method and Materials

3.1 Materials

3.1.1 Slag composition and preparation

The slag used in the experiments is made using pure oxides and metals. Due to a lack of availability of pure FeO an alternate mixture of Fe_2O_3 and Fe is used. The calculations for this mixture can be seen below.

$$\begin{aligned} Fe_2O_3 + Fe &\longrightarrow 3\,FeO \\ Fe_2O_3 &= 159.69 g/mol \\ Fe &= 55.85 g/mol \\ FeO &= 71.84 g/mol \\ \%Fe = 100\% * 55.85/(3 * 71.84) &= 25.914\% \\ \%Fe_2O_3 = 100\% - 25.914\% &= 74.086\% \end{aligned} \tag{3.1}$$

Using this calculation it is possible to figure out how much Fe and Fe_2O_3 is needed to get the equivalent FeO amount.

Table 3.1: A calculation used to make 10g slag.

Composition (wt%):	TiO2	Fe	Fe2O3	CaO	total weight:
85%TiO2+10%FeO+5%CaO	8.5	0.2591	0.7409	0.5	10g

3.1.2 Pellet composition and preparation

Experiment	Location in pellet	Analysis number	Ti	Fe	Mg	O	Ca	V	Al	Cr	Si	Mn
G1	edge	1	3.12	94.90	0.11	1.73	0.00	0.05	0.00	0.02	0.07	0.00
		2	3.27	94.47	0.17	2.01	0.00	0.05	0.01	0.00	0.00	0.02
		3	32.38	1.09	4.88	60.77	0.02	0.49	0.13	0.06	0.14	0.04
		4	21.03	8.51	11.89	57.13	0.03	0.34	0.07	0.18	0.03	0.79
	core	5	21.39	16.97	3.61	57.50	0.01	0.28	0.06	0.03	0.01	0.16
		6	19.26	19.83	3.70	56.74	0.01	0.25	0.01	0.02	0.05	0.12
G3	core	7	21.42	16.21	4.20	57.36	0.02	0.26	0.24	0.06	0.04	0.19
		8	1.03	5.78	9.06	56.11	0.00	0.03	27.51	0.45	0.00	0.04
		9	34.31	1.99	0.27	63.00	0.02	0.30	0.06	0.02	0.00	0.02
		10	21.96	15.86	4.20	57.19	0.03	0.33	0.15	0.07	0.05	0.16
	edge	11	35.34	0.62	0.26	63.19	0.01	0.31	0.07	0.04	0.15	0.01
		12	30.80	1.92	6.98	58.62	0.00	0.46	0.48	0.18	0.02	0.55
G4	edge	13	35.11	0.51	0.10	63.68	0.09	0.33	0.06	0.02	0.10	0.00
		14	28.46	5.13	6.02	59.24	0.07	0.34	0.37	0.11	0.01	0.24
	core	15	22.04	16.59	3.94	56.88	0.02	0.28	0.05	0.04	0.00	0.17
		16	22.37	16.11	3.91	56.88	0.01	0.30	0.19	0.08	0.00	0.14
		17	31.55	7.07	1.12	59.68	0.02	0.34	0.13	0.02	0.00	0.08
G6	edge	18	28.94	2.07	8.29	59.10	0.02	0.74	0.55	0.10	0.05	0.14
		19	34.67	0.62	0.11	64.08	0.01	0.36	0.04	0.04	0.06	0.01
		20	34.30	0.51	0.51	64.16	0.02	0.35	0.05	0.01	0.10	0.00
		21	21.73	8.92	10.04	57.14	0.08	0.41	0.17	0.12	0.00	1.38
	core	22	34.75	0.70	0.01	64.07	0.00	0.38	0.05	0.02	0.03	0.00
		23	33.74	1.75	0.05	63.94	0.02	0.35	0.07	0.05	0.04	0.01

Figure 3.1: A qualitative point analysis of the pellets used in this master thesis. Taken from S. Lobo's work in his PhD. [42]

The pellets obtained from S. Lobo's work are too big to be used in the dropping mechanism of the tube furnace. [42] A way to circumvent this is to crush the pellets into smaller pieces. This means the pellet dropped would be turned into smaller pellet pieces. An example of how this looks can be seen in figure 3.2. The conversion degree and reduction agent of the pellet can be seen in figure 2.4. The main points being G1 = 100% CO, G3 = 40% H2 + 60% CO, and G6 = 100% H2. The resulting conversion degrees are 65% for the G1 pellets, 83% for the G3 pellets, and 113% for the G6 pellets. All these pellets were run for 2 hours, hence the differing conversion degrees.

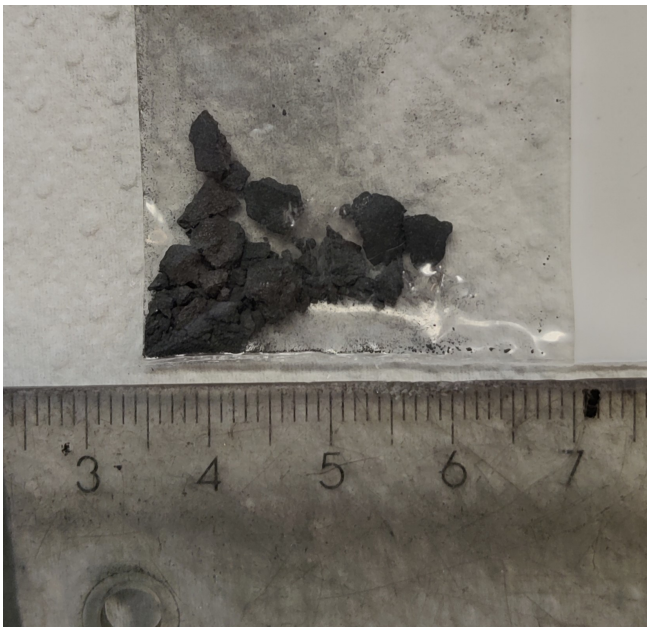

Figure 3.2: A picture of the crushed pellet pieces that will be dropped into the slag melt.

For the H-series experiments, new pellets were made from scratch using ilmenite raw material. These were made so the pellets did not have to be crushed, meaning in theory it would be possible to look at a whole pellet instead of just pieces. The resulting pellets were two batches reduced with CO and H_2 respectively. A1 is reduced with CO and A2 is reduced with Hydrogen. These pellets have a smaller diameter and are possible to use without crushing in the TF2. The composition of the ilmenite raw material can be seen in table 3.2.

Table 3.2: Composition of raw ilmenite as seen from chemical analysis.

XRF (wt%)														Wet Chemical Analysis (wt%)	
MgO	Al_2O_3	SiO_2	CaO	TiO_2	V_2O_5	Cr_2O_3	MnO	P_2O_5	Nb	Zn	ZrO_2	FeO	Fe	Fe_2O_3	FeO
0.6	0.56	0.13	0	53.46	0.308	0.156	1.02	0.025	0.058	0.0139	0.158	39.37	30.61	22.4	19.2

3.1.3 Crucibles

The crucibles used were made of SSiC (sintered silicon carbide) and molybdenum. The SiC crucible was coated with a layer of BN to try to mitigate the reaction between the slag and the crucible. This was the method explored in the preceding project work.[20] Two layers of coating are applied, and between each application, the crucibles and coating were fired at 300 °C for 1 hour. This is to make the paint coating dry more quickly. The molybdenum crucible is made with a purity of above 99 wt% Mo.

3.2 Method

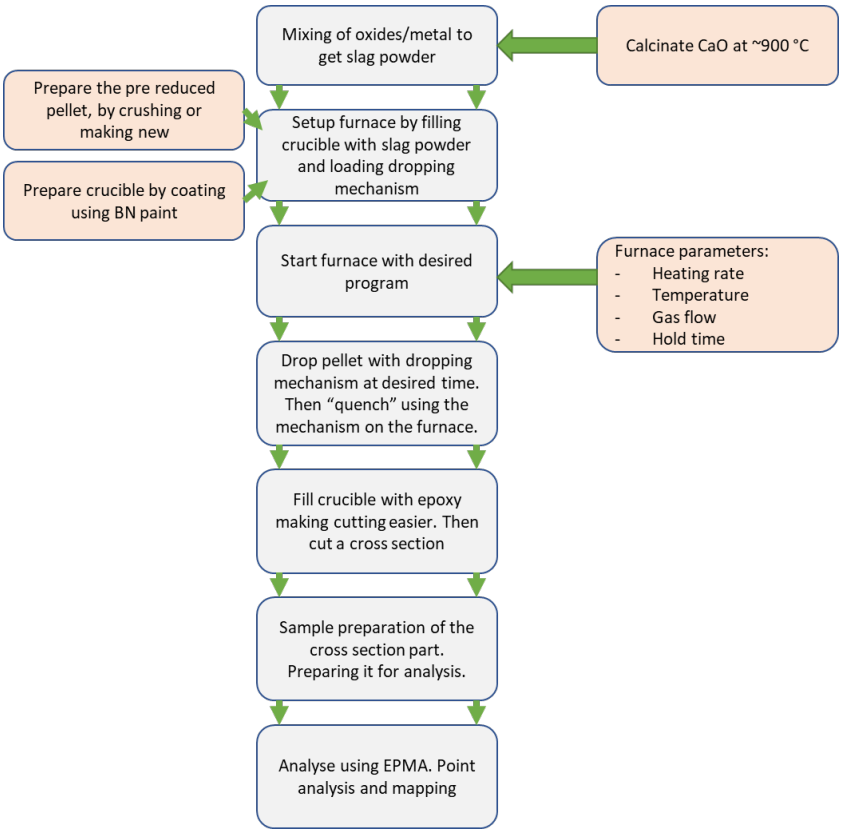

Figure 3.3: A simplified step by step of the experimental method.

The experimental method can be seen in simple terms in figure 3.3 above. The main steps will be explained in greater detail below.

3.2.1 Making of pre-reduced ilmenite pellets

The pellets are made using a rotating pelletizer. A fine powder of ilmenite is inserted into the rotating pelletizer, then the powder inside is sprayed with water. This starts the formation of spherical pellets. These pellets grow when the rotating pelletizer is fed more powder and water. Once the pellets reach a certain size, the largest pellets are scoped out and sieved. These sieves are used to get the desired size pellets. The sieve size used in this master thesis was 9 mm. The pellets that were too big in the sieving were crushed and the ones that were too small were inserted back into the pelletizer with the crushed ones. The ones that fit in the sieves are the product of this process.

To be able to pelletize the ilmenite a fine powder is needed. This is achieved by crushing the ilmenite to a particle size of more than 50 wt% smaller than 25 μm. This crushing was done using a ring mill. The ring mill is a machine that utilizes rotations. Here the sample that needs crushing gets inserted in a bowl together with a puck. The controllable parameters are rpm (rotations per minute) and time. For the creation of these pellets, a program of 1100 rpm for 5 minutes was sufficient to make the powder size small enough.

The next step after the pellets are created is drying. This is done in a muffle furnace overnight at 110 °C to remove excess H_2O. This removal is necessary to limit cracking in the next step, which is the oxidation step. Here the pellets are heated to 850 °C for 2 hours in an oxidizing atmosphere

(in air) using a muffle furnace. This oxidizes the pellets and hardens them in preparation for the reduction step.

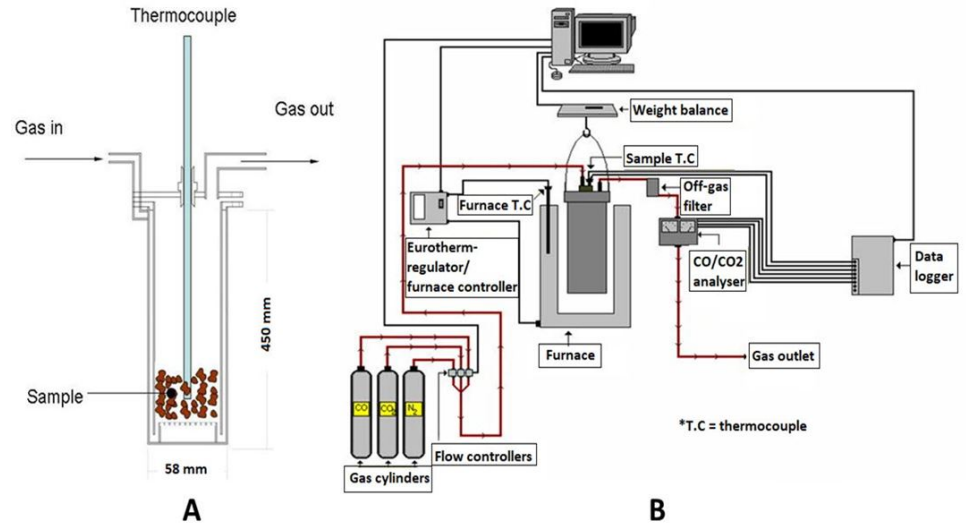

Figure 3.4: Schematic setup of the DisVaDri furnace taken from the SINTEF website.[54]

The last step is the reduction step, using CO and hydrogen as reducing agents. This is done in the DisVaDri furnace. The DisVaDri furnace is a thermogravimetric furnace able to analyze the reaction rate of ores.[54] The parameters used in the reduction was, 1 l/min argon gas during heating then 5 l/min CO/H2 at target temperature. The target temperature was 900 °C. The CO-reduced pellets were reduced for 3 hours. The H2-reduced pellets were reduced till they had the same reduction degree as the CO pellets. In this case, the hydrogen reduction went on for a little over 20 minutes. An image of how the resulting pellets look after reduction is shown in figure 3.5.

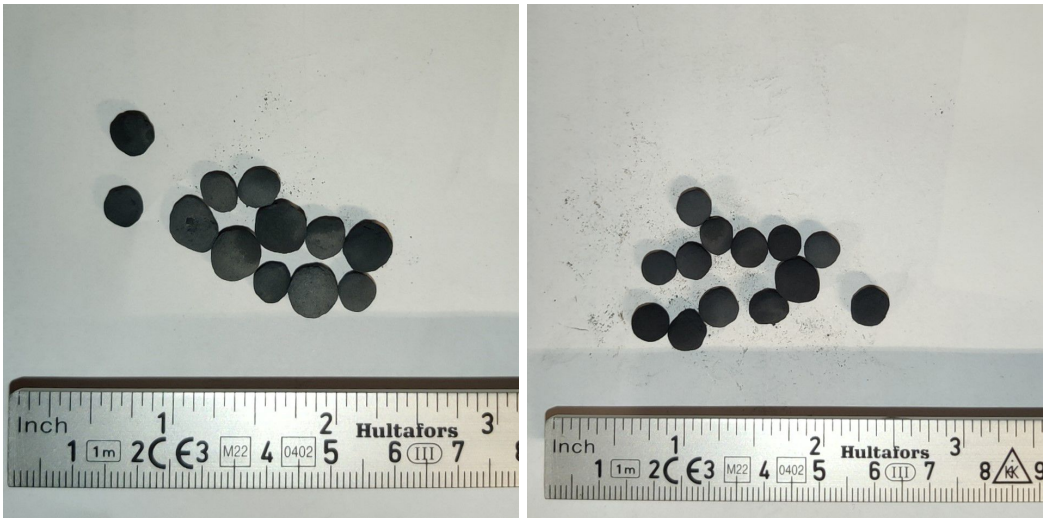

Figure 3.5: Image of the pellets with ruler, left most is CO reduced and right most is H_2 reduced.

Conversion degree calculation

Once the pellets have been reduced in the DisVaDri furnace the conversion degree can be calculated. To calculate the conversion degree it is important to look at the mass loss of the pellets during reduction. It can be assumed that during the oxidation of the pellets, all the Fe in the pellet has oxidized to trivalent iron Fe^{3+}. Meaning $m^O_{oxidised\ ilmenite}$ is just containing $m^O_{Fe^{3+}}$. The amount of

Fe^{3+} can be found by doing a chemical analysis of the ilmenite raw material.
The equation for $m^O_{oxidised\ ilmenite}$ can be seen below:

$$m^O_{oxidised\ ilmenite} = m^O_{Fe^{2+}} + m^O_{Fe^{3+}} \tag{3.2}$$

The equation for $m^O_{Fe^{2+}}$ can be seen below:

$$m^O_{Fe^{2+}} = wt\%FeO * m_{start} * \frac{16}{16 + 55.85} \tag{3.3}$$

The equation for $m^O_{Fe^{3+}}$ can be seen below:

$$m^O_{Fe^{3+}} = wt\%Fe_2O_3 * m_{start} * \frac{3 * 16}{3 * 16 + 2 * 55.85} \tag{3.4}$$

In this equation m_{start} is the amount of material before the reduction takes place. Finally using these equations it can be put together with Δm, the amount of mass reduced, to calculate the conversion degree Z.

$$Z = \frac{\Delta m}{m^O_{oxidised\ ilmenite}} \tag{3.5}$$

3.2.2 Tube Furnace 2 (TF2)

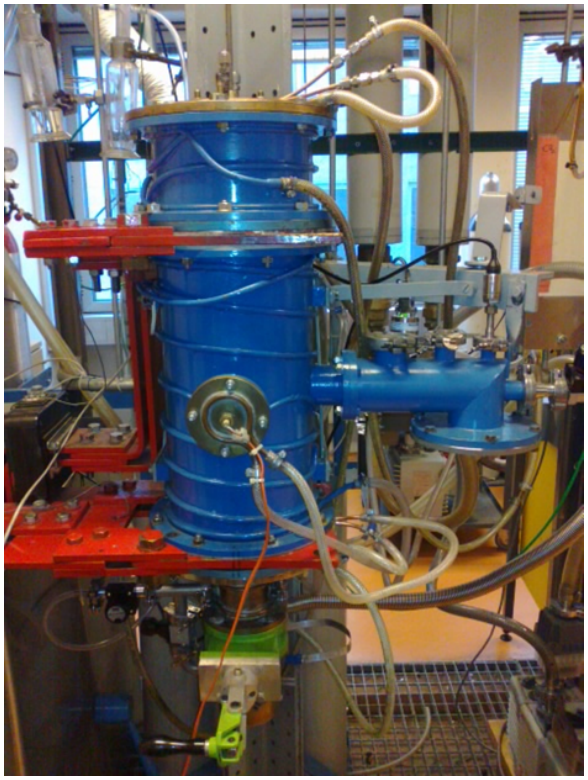

Figure 3.6: A picture of the Tube furnace 2. taken from [55]

The graphite tube furnace shortened to TF2, is a furnace at NTNU with a controllable atmosphere, a possible crucible size of 42 mm, and a temperature limit up to 1600 °C. Possibly higher, but it depends on the temperature limit of the used thermocouple. The controllable atmosphere can not be an oxidizing atmosphere because of a molybdenum support tube and a graphite heating element, since it would oxidize these parts. Meaning an inert atmosphere has to be used in the experiments. [55]

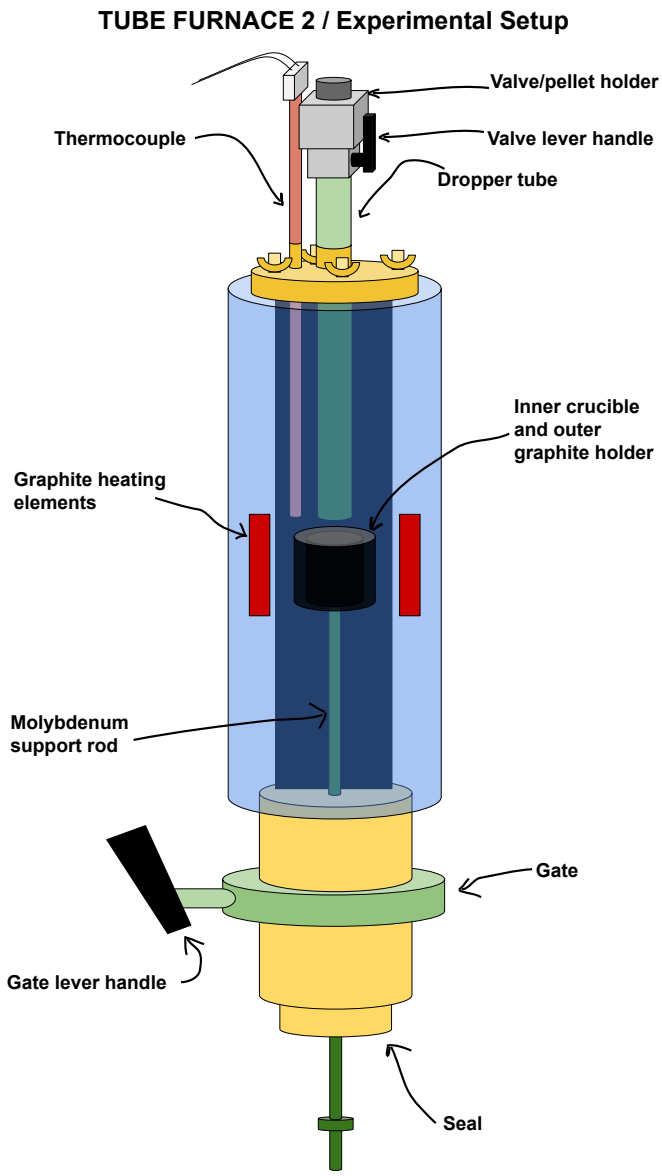

Figure 3.7: A schematic drawing of the TF2 (Tube Furnace 2), showing the different parts.

A schematic of the experimental setup used in this master thesis can be seen in figure 3.7. With the main asset being the dropping mechanism created. The dropping mechanism consists of a chamber with a valve and a dropper tube. This dropper tube has an inner diameter of 1cm. The dropper tube/valve contraption is mounted higher up when the experiment is set up. This is because we want to limit the possibility of pellets melting to the side of the molybdenum wall during dropping. The way the mechanism works is when the pellet inside the chamber is due to being dropped, the dropper tube/valve contraption is pushed down till it is ca 1 cm above the crucible. Meaning it is "cold" compared to the melt. After the contraption is pushed down the valve can be opened, and the pellet/pellets fall into the melt.

To start an experiment using the TF2 the furnace has to be set up as seen in figure 3.7. Here you insert the pellet/pellet parts into the valve chamber and mount the valve and dropper tube on the furnace. The thermocouple needs to be inserted into the furnace down from the top. To find the spot where the highest and most stable temperature is, a graph is used. This is found in a book in the lab, this graph is created from experimental data. In this master thesis, the temperature gradient was not calibrated meaning there is a possibility for error when using the graph. How large of an error has to

be discussed. The crucible position is just below the thermocouple position. Before the crucible can be inserted the slag/powder is put into the crucible. A picture of the efficient heating graph can be seen below in figure 3.8.

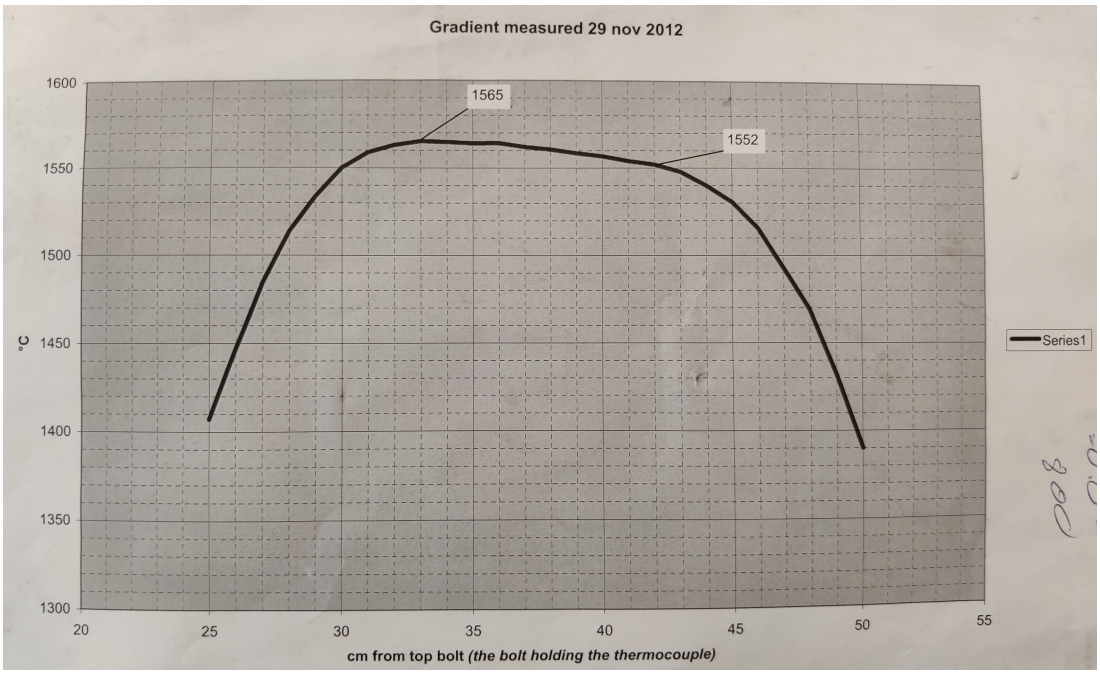

Figure 3.8: A graph showing where the optimal heating in the tube furnace 2 is. Taken from a folder by the furnace.

Once the spot is found for the crucible and thermocouple in the furnace, they are placed in their respective spots. The pre-experiment purging can now be done. This is to remove the oxidizing atmosphere in the furnace and replace it with an inert atmosphere. This atmosphere is Argon. Three purging cycles are done to ensure minimal possibilities of an oxidizing atmosphere. After the purge, the furnace is ready to start the program. This program is made on the computer, with parameters such as heating rate, temperature set points and run furnace run time. Since the drop is a manual effort, adding additional time at maximum temperature is an idea to ensure the drop happens similarly for each experiment. This is because the dropper tube/valve can sometimes be a bit tough to push down, and may take a bit longer than expected. The furnace can be turned off manually by pressing the red button at the power supply, This is much easier to control than using the program on the computer, and the time before quench is much more accurate and similar for all the experiments. A picture showing one of the programs used in this master thesis can be seen below in figure 3.9. The figure shows the temperature where the thermocouple is located from start to finish, however, once the quench happens the crucible is pulled down to a cooler area where the temperature is not measured. Therefore the cooling rate of the graph seen in figure 3.9 is not the one the crucible experiences.

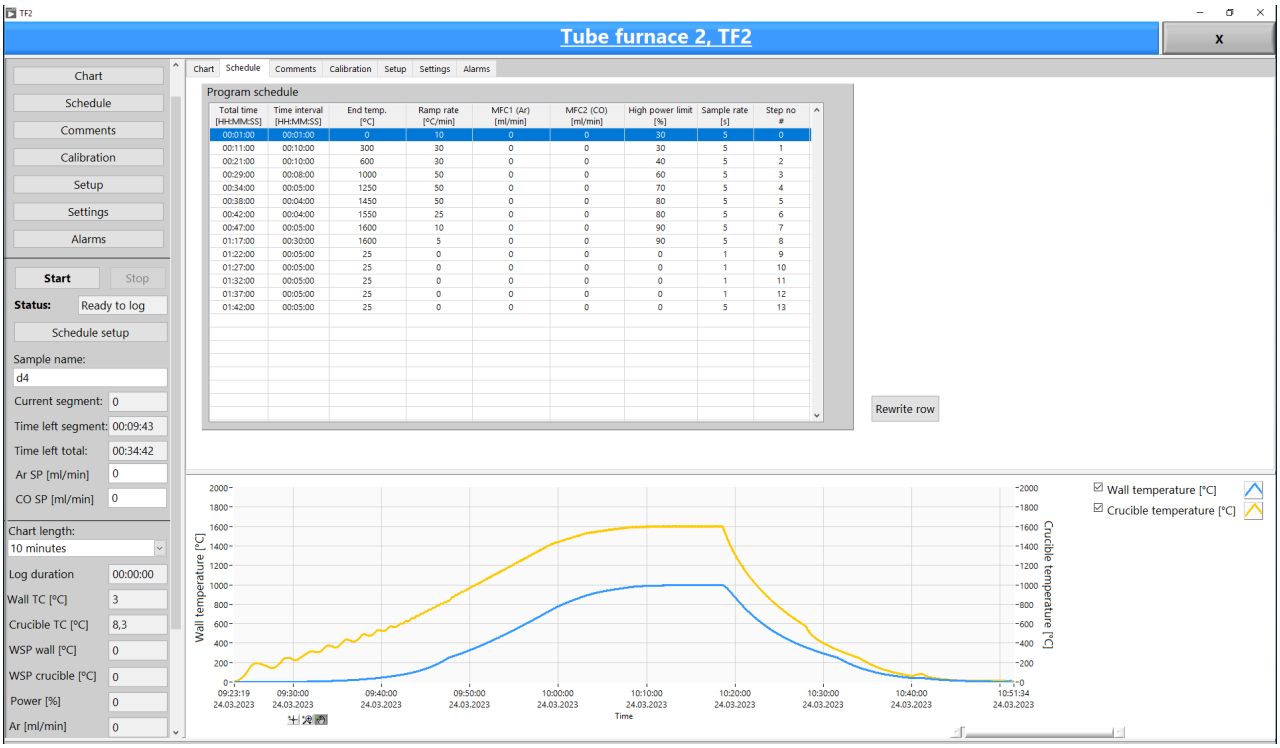

Figure 3.9: A picture of the program and runtime of one of the experiments run on the TF2.

When the program is ready for a drop, the dropper tube/valve is pushed down to the crucible (step 1). Using a timer on the computer or on a phone, the time after the drop is measured. The drop happens when the valve is opened (step 2-3). Once the desired time is reached the furnace is turned off, and the molybdenum support tube is pulled down using gloves (step 4-5). The steps correspond to figure 3.10. This means the crucible gets pulled down to the cooling zone. This cooling area is still warm, but much colder than the heating zone found using the graph in figure 3.8. The sample is then done and can be removed from the furnace after it has cooled down and been purged, to get rid of the off gasses and the inert argon gas.

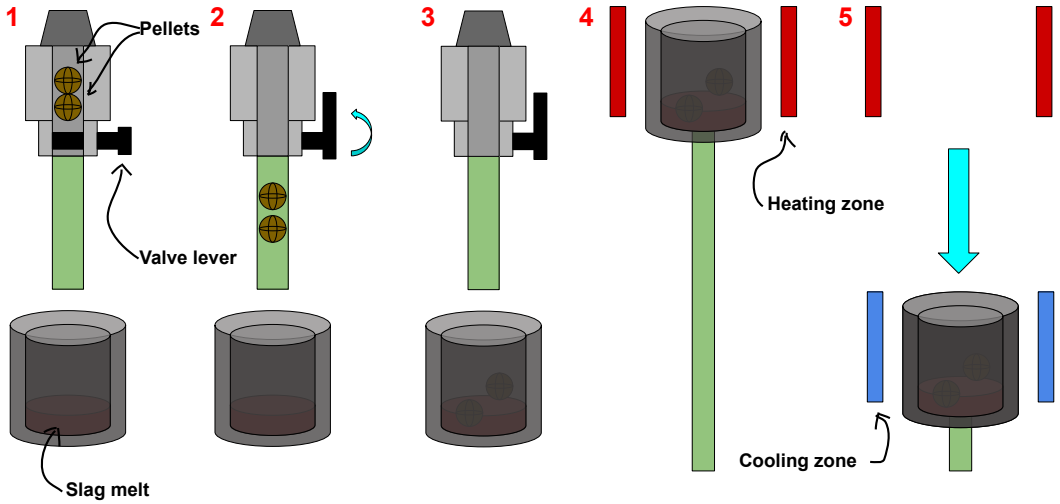

Figure 3.10: A schematic showing a simplified step by step how the dropping works.

3.2.3 Sample preparation for analysis

The sample preparation for Electron probe microanalysis (EPMA) starts with filling the crucibles we get after the TF2 step with epoxy. The crucibles are filled so that the next step, the cutting step, does not just break the crucible. It is filled to add stability during cutting. The crucible is cut at the cross-section, and then one part of the cross-section is cut into a smaller piece. This part is the part that is going to be looked at in EPMA. To get it ready for the EPMA, it has to be polished. It is cast with more epoxy in a sample holder. After the cast has solidified it is ready for the polishing step. the sample is polished using struers tegramin-30. This machine can be programmed depending on what is desired. The program used in this master thesis consists of 4 steps, the steps 1,2,3, and 4 are 220,9,3 and 1 µm sequentially. Step 1 uses water, while the final three use DiaPro. DiaPro is diamond particles in water. Between each of these steps, the samples are cleaned in an ultrasonic bath. After the final step, the samples are almost ready to be looked at in EPMA. They first need to be coated in a carbon layer on the surface of the sample, and an aluminum coating around the round sample. A picture of how these samples look after preparation can be seen in figure 3.11.

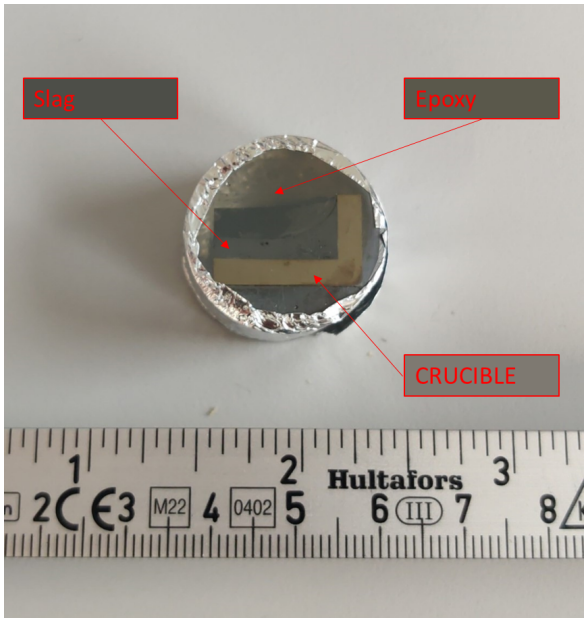

Figure 3.11: Picture of sample cast in epoxy and ready for analysis in EPMA.

3.2.4 Electron Probe Micro Analyser (EPMA)

For the analysis, the JEOL JXA-8500F Electron Probe Micro Analyzer (EPMA) is used. This EPMA combines high SEM (Scanning Electron Microscopy) resolution and high-quality X-ray analysis of sub-micron areas. It has high detection sensitivity of trace elements, high accuracy of quantitative analysis, high resolving power for adjacent x-ray spectra, and high accuracy of light element analysis. [56]

Some of the features used a lot in this master thesis are the mapping and point analysis functions. Mapping is a method of making a picture with the intensity of the chosen element over an area. Then doing this mapping with a few different elements, it is possible to compare and get an idea of which phases/element combinations are present in the sample. The other feature is point analysis, here a point on the sample is chosen and analyzed using X-ray. The point analysis tells how much of each phase/element is present in the measurement. These phases/elements are decided on the computer system before the analysis. Examples of both of these will soon follow in the results part.

3.3 List of experiments

The experiment series that was decided to be run in this master thesis was put together in such a way that it would be in tune with the aims and scope. It was also necessary to look at the available resources for these experiments, meaning the availability of crucibles, pellets, and slag oxides. There were quite a few SiC crucibles available making this a good choice for the main bulk of the experiments. The pellet types G1, G3, and G6 are thoroughly researched in other works and are thereby a good choice for experiments. It was acquired two Mo crucibles that fit the furnace, and it was discussed how to best use these in this master. It ended up being desired to test the Mo crucibles using pellets specially created for use in the TF2, Meaning smaller diameter size. There were made two batches of pellets, A1 and A2. They were reduced with 100% CO and 100% H_2 respectively.

The slag amount seen in the three tables following can be seen put to 10g exactly. This is not necessarily the case and there could be an error of around 0.2 g, due to some of the powder being stuck in the bag it is contained in before it is inserted into the crucible. The time before quench also has an error, however, this one is not too big, just around 1-2 seconds. All the experiments listed below are run using the TF2.

Table 3.3: Experimental matrix of 9 experiments using the different pellets G1, G3 and G6 in SiC crucible.

ID	Pellet	Pellet amount	Slag Composition (wt%)	Slag amount	Crucible	Coating	Maximum T*	Time BQ**
D1	G1	0.88 g	85wt%TiO_2-10wt%FeO-5wt%CaO	10 g	SiC	BN	1650 °C	0 min
D2	G1	0.92 g	85wt%TiO_2-10wt%FeO-5wt%CaO	10 g	SiC	BN	1600 °C	1 min
D3	G1	0.94 g	85wt%TiO_2-10wt%FeO-5wt%CaO	10 g	SiC	BN	1600 °C	3 min
E1	G3	0.87 g	85wt%TiO_2-10wt%FeO-5wt%CaO	10 g	SiC	BN	1650 °C	0 min
E2	G3	0.88 g	85wt%TiO_2-10wt%FeO-5wt%CaO	10 g	SiC	BN	1600 °C	1 min
E3	G3	0.93 g	85wt%TiO_2-10wt%FeO-5wt%CaO	10 g	SiC	BN	1600 °C	3 min
F1	G6	0.9 g	85wt%TiO_2-10wt%FeO-5wt%CaO	10 g	SiC	BN	1650 °C	0 min
F2	G6	0.87 g	85wt%TiO_2-10wt%FeO-5wt%CaO	10 g	SiC	BN	1600 °C	1 min
F3	G6	0.91 g	85wt%TiO_2-10wt%FeO-5wt%CaO	10 g	SiC	BN	1600 °C	3 min

* Maximum temperature refers to the temperature the furnace is run at to melt the slag.

** Time BQ = Time before quench, it refers to the time after the pellet is dropped before the sample is quenched.

Table 3.3 above a matrix of the nine first melting experiments done can be seen with their corresponding parameters. Here it is seen D1, E1, and F1 have a temperature of 1650 °C. It was the plan to run all the experiments at this temperature, however, the thermocouples used in the furnace ended up breaking/cracking. Due to this, the temperature was changed to 1600 °C for the remaining experiments.

Table 3.4: Experimental matrix of D4, E4, and F4. All at 1600 °C with different pellets.

ID	Pellet	Pellet amount	Slag Composition (wt%)	Slag amount	Crucible	Coating	Maximum T*	Time BQ**
D4	G1	0.9 g	85wt%TiO_2-10wt%FeO-5wt%CaO	10 g	SiC	BN	1600	0
E4	G3	0.91g	85wt%TiO_2-10wt%FeO-5wt%CaO	10 g	SiC	BN	1600	0
F4	G6	0.95g	85wt%TiO_2-10wt%FeO-5wt%CaO	10 g	SiC	BN	1600	0

* Maximum temperature refers to the temperature the furnace is run at to melt the slag.

** Time BQ = Time before quench, it refers to the time after the pellet is dropped before the sample is quenched.

Table 3.4 shows experiments D4, E4, and F4 with the same parameters as D1, E1, and F1. The only difference is the temperature of 1600 °C instead of 1650 °C.

Table 3.5: Experimental matrix of H series. Pellets A1 and A2 with a Molybdenum crucible.

ID	Pellet	Pellet amount	Slag Composition (wt%)	Slag amount	Crucible	Maximum T*	Time BQ**
H1	A1 (CO)	-	85wt%TiO_2-10wt%FeO-5wt%CaO	10 g	Molybdenum	1600	0
H2	A2 (H2)	-	85wt%TiO_2-10wt%FeO-5wt%CaO	10 g	Molybdenum	1600	0

* Maximum temperature refers to the temperature the furnace is run at to melt the slag.

** Time BQ = Time before quench, it refers to the time after the pellet is dropped before the sample is quenched.

Table 3.5 shows the experiments done using the Molybdenum crucibles. Here there are created new pellets with a smaller diameter. A1 and A2 respectively.

4 Results

The results will be divided into different sections to make them more intuitive. The first section is from the making of A1 and A2 pellets. The second section will include the macroscopic results of this master thesis. The final section will be the microscopic results, meaning EPMA analysis of the samples. The series are grouped together with the main differences, meaning D-series is pellet G1, E-series is pellet G3, F-series is pellet G6, and H-series is molybdenum crucible/pellets A1/A2. These names given for each of the experiments might be hard to intuitively understand as a reader, each of the experiments has been given an additional and more informative name. This can be explained below using color coding.

Pellet type(Pellet reduction gas in %) - Crucible type - Time after drop till quench in minutes - Temperature in ℃

Example: D1 = G1(100%CO) - SiC - 0min - 1650

Example: E2 = G3(60%CO 40%H_2) - SiC - 1min - 1600

Important notice the D1_1 (G1(100%CO)-SiC-0?min-1650) experiment was supposed to be the D2 (G1(100%CO)-SiC-1min-1600) experiment. However, due to a malfunction and the thermocouple breaking, because of the high temperature, 1650 °C. The drop ended up being done a few seconds after the furnace turned off. Meaning a drop time of minus a few seconds. The temperature for the experiment was too high for the furnace and all the following experiments had to lower the temperature by 50 °C. The experiment is included due to the interesting results it gave, and experiments D4, E4, and F4 were based on these findings, because of the visible pellet parts. The D3 experiment was a failure due to the pellets not dropping. The pellets got jammed in the dropper tube, and due to the findings of E3 and F3 seeming insignificant, the experiment was not redone. Since they had the same parameters just different pellet types.

4.1 A1 and A2 pellets

As mentioned A1 and A2 pellets are the pellets created in this master project. Here A1 is reduced with 100% CO and A2 is reduced with 100% H2. In table 4.1 the amount of pellet reduced can be seen. The calculated conversion degree was calculated using equation 3.5, with the assumption of 100% oxidation of Fe. The wt% Fe_2O_3 in equation 3.4 is calculated using the chemical analysis in table 3.2. Here it is given a Fe amount of 30.61, using this with the assumption of 100% oxidation, the wt% $Fe_2O_3 = 30.61 * \frac{2*55.85+16*3}{2*55.85}$. This gives wt% $Fe_2O_3 = 43.76$ wt%

Table 4.1: Weight change of A1 and A2 pellets during oxidation and reduction steps. Also the calculated conversion degree after reduction.

	pre-oxidation	post-oxidation	pre-reduction	post-reduction	Conversion degree
Weight ilmenite pellets	577.66 g	556.7 g	-	-	-
Weight A1 (CO)	-	-	200.59 g	179.9 g	76 %
Weight A2 (H2)	-	-	200.20 g	184.2 g	61 %

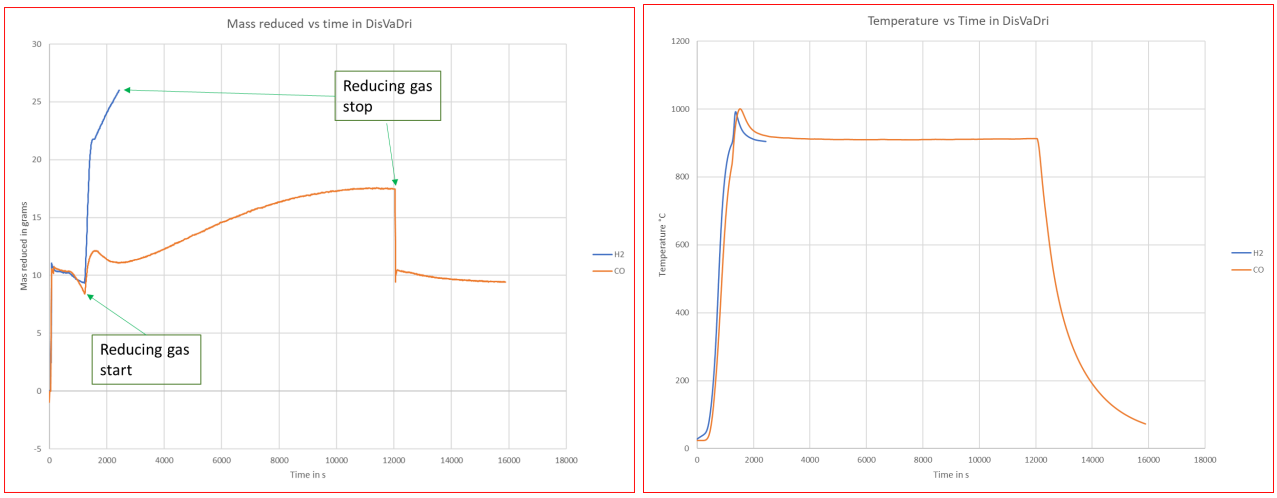

Figure 4.1: The measured mass loss vs time and Temperature vs time in the DisVaDri furnace.

Figure 4.1 shows the program of the reduction for A1 and A2 pellets. Here it is seen the program starts at a ∼10g reduction before the experiments even start. The mass-reduced graph does not correlate with the final mass reduced at all. The correct mass reduced is seen in table 4.1. The reduction gas is introduced just before 2000 s as seen by the sharp increase in mass reduced. The temperature graph shows a big increase in temperature when the reduction gas is introduced. Showing that the first reduction reaction is exothermic. This is seen just before the 2000 s point in the graph.

Table 4.2: Temperature measurements from the crucible during the reductions.

	A1(CO)	A2 (H2)
Furnace set point (°C)	845	845
T(°C) at start of reduction	834.9	898.4
T(°C) maximum during reduction	1000.1	991.9
T(°C) average during reduction	915.1	926.1

Table 4.2 shows the difference in temperature between the H_2 and CO experiments. It is expected for A2 to be lower due to H_2 being a more endothermic reduction. This is seen in the maximum temperature of the reductions, and can almost be seen in figure 4.1 where the trend of the hydrogen temperature seems to stabilize lower than CO. It was cut short due to the experiment being shorter.

4.1.1 Oxidized pellets

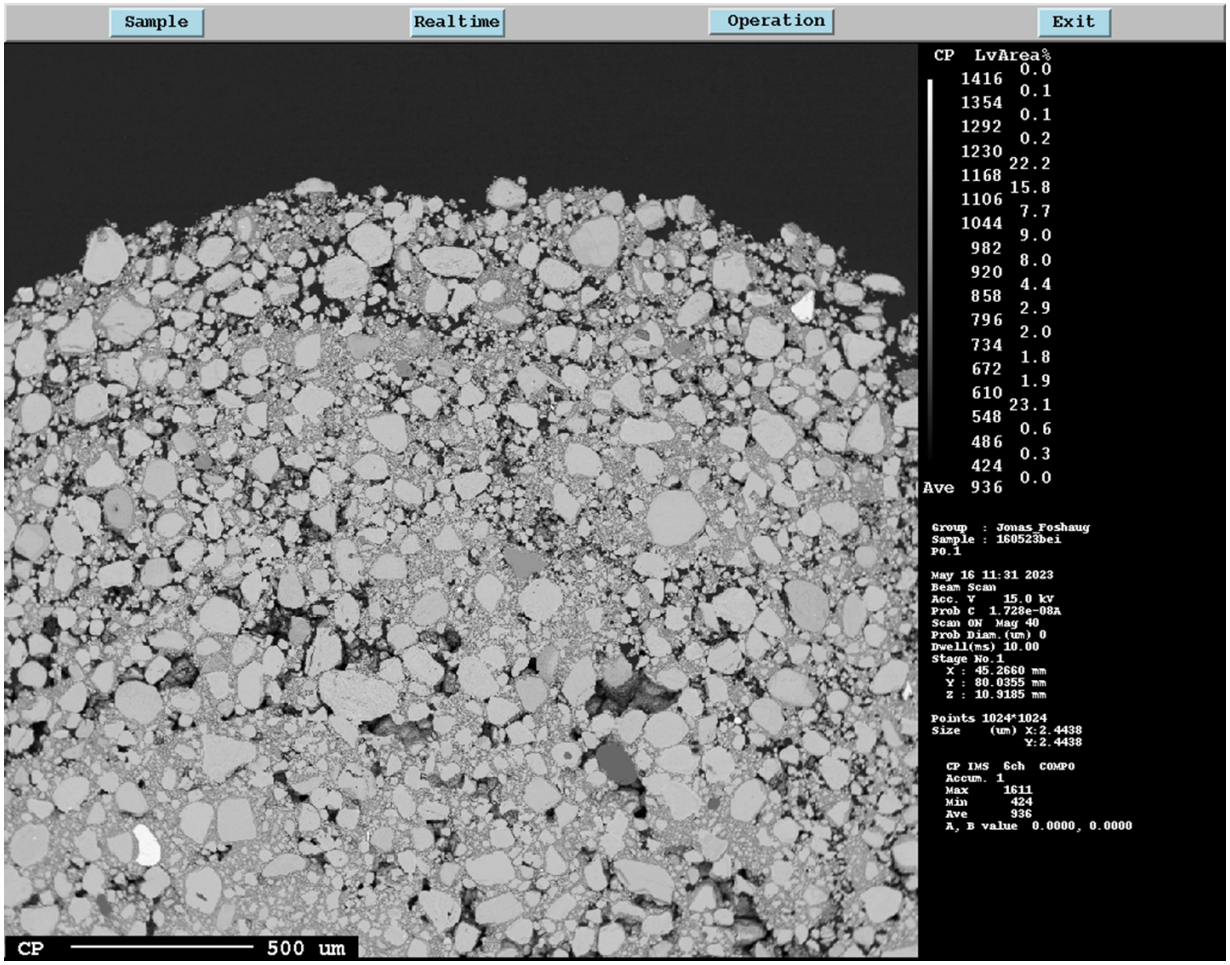

Figure 4.2: An overview EPMA image at 40x zoom for the cross-section of the oxidized pellets. The edge is at the top while the center is roughly seen at the bottom.

In figure 4.2 it is seen a cross-section EPMA image of an oxidized pellet. Here the bottom part of the image is the core while the top part is the edge of the pellet. The pellet is seen to have no metallic phases present, except one in the bottom left corner and one in the top right corner of the image. These metallic phases are not Fe, as will be seen in the point analysis. There are some small grains of darker phases scattered around in the pellet. The pellet seems to be a bit porous, seen from all the black holes between the gray phases. The completely black phases are epoxy applied during preparation.

Point analysis

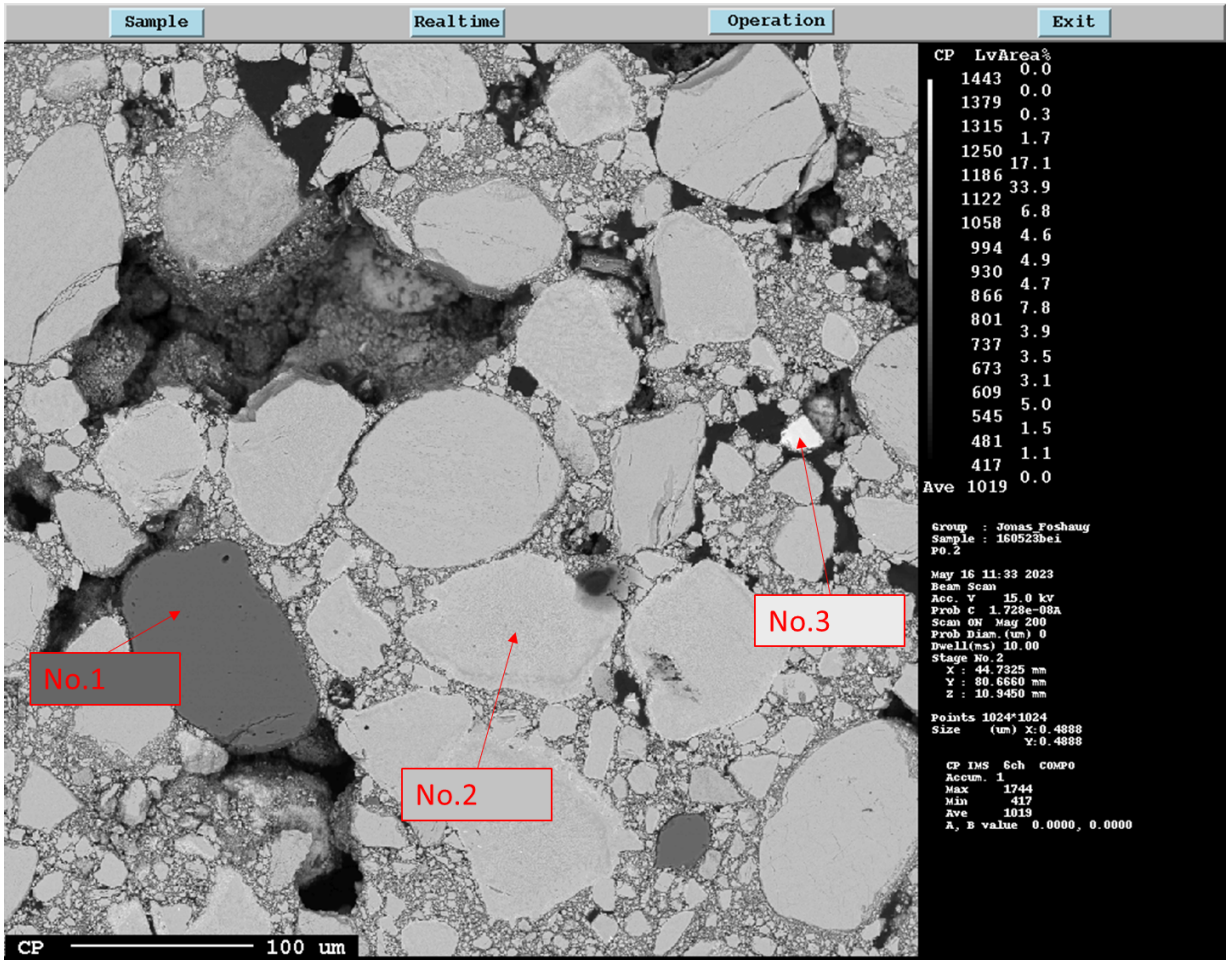

Figure 4.3: EPMA image of the oxidized pellets at 200x zoom. The drawn in numbers correspond to table 4.3 with the point analysis below.

For the point analysis, it was zoomed in at an area with a dark gray phase and a white metallic phase. This is seen in figure 4.3. It was gathered that the darker area No.1 is mainly a SiO_2 phase, while the white metallic area, No.3, consists of Zr. The most abundant area, light gray area No.2, consists of oxidized Fe and oxidized Ti. The composition for these phases is shown in table 4.3. It is not necessarily FeO that is the phase, it would be more logical for it to be Fe_2O_3 because this pellet has been oxidized for 2 hours. But since the analysis only looked for Fe as FeO, the Fe_2O_3 is likely included in this part. This can be verified with analysis methods not done in this master thesis, like XRD (X-ray diffraction).

Table 4.3: Point analysis of different phases of the oxidized pellets. Number 1 is an average point analysis of the dark gray phase. Number 2 is the white zone, while number 3 is the light gray zone. Seen more clearly in figure 4.3.

No.	SiO2	MgO	FeO	CaO	Al2O3	TiO2	ZrO2	Total
1	101.826	0	0.199	0	0	0.343	0	102.368
2	0.094	0.024	36.119	0	0.255	57.418	0	93.91
3	34.152	0.007	0.489	0	0.001	0.376	60.791	95.816

4.1.2 CO reduced pellets (A1)

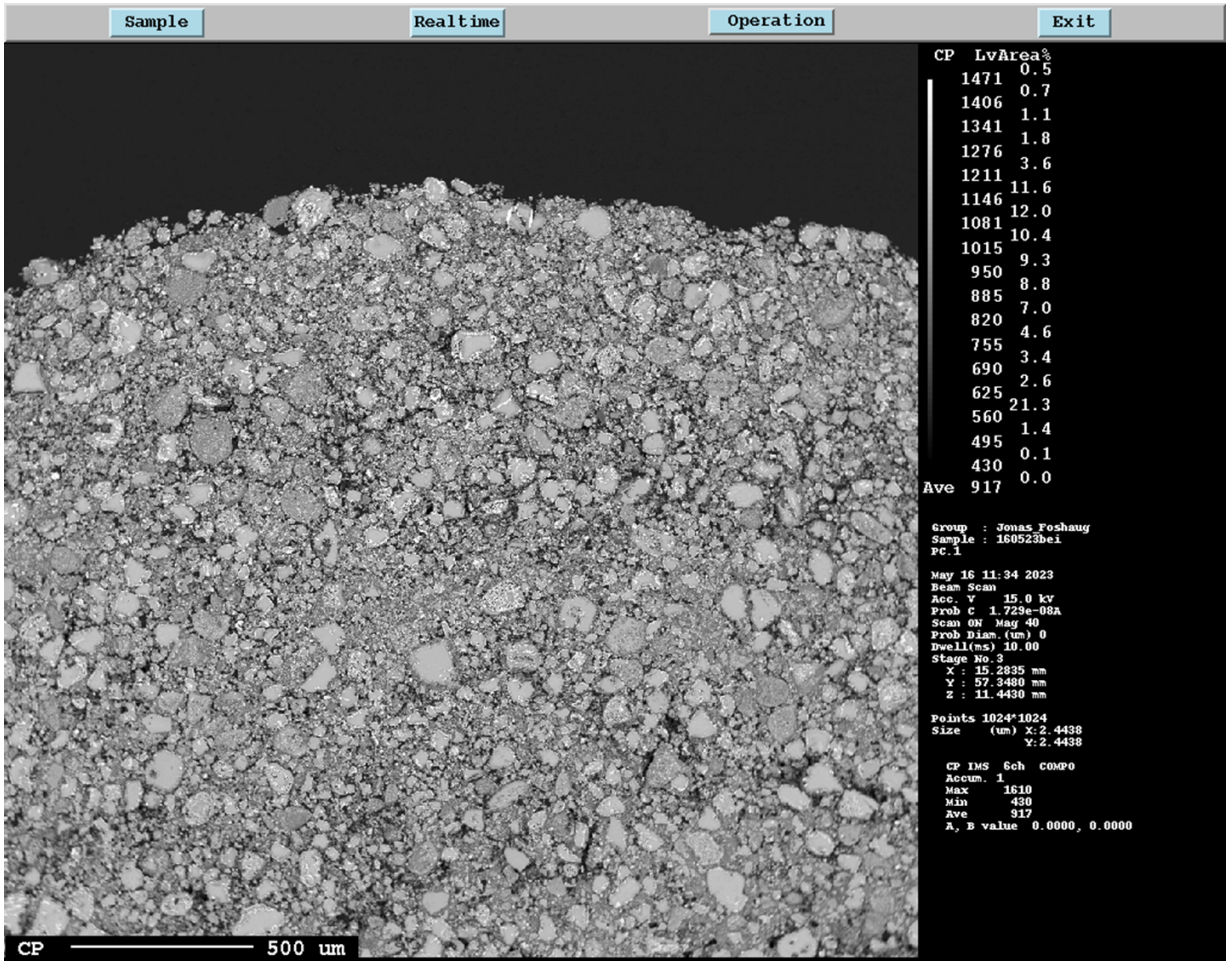

Figure 4.4: An overview EPMA image at 40x zoom for the cross-section of the CO pre-reduced pellets. (A1) The edge is at the top while the center is roughly seen at the bottom.

The image in figure 4.4 show the cross-section of a CO-reduced pre-oxidized pellet. The cross-section shows the pellet to be less porous with fewer big gray phases than the oxidized pellet cross-section. When looking closer at the gray phases there is seen a white metallic iron phase being created around the edges of the gray particles. Seen more closely in figure 4.5 below. This metallic phase shows that a reduction has taken place. This metallic phase is created throughout the whole pellet, meaning the reduction gas has managed to diffuse into the pellet core. There is less diffusion into the light gray particles since the metallic phases are at the edges.

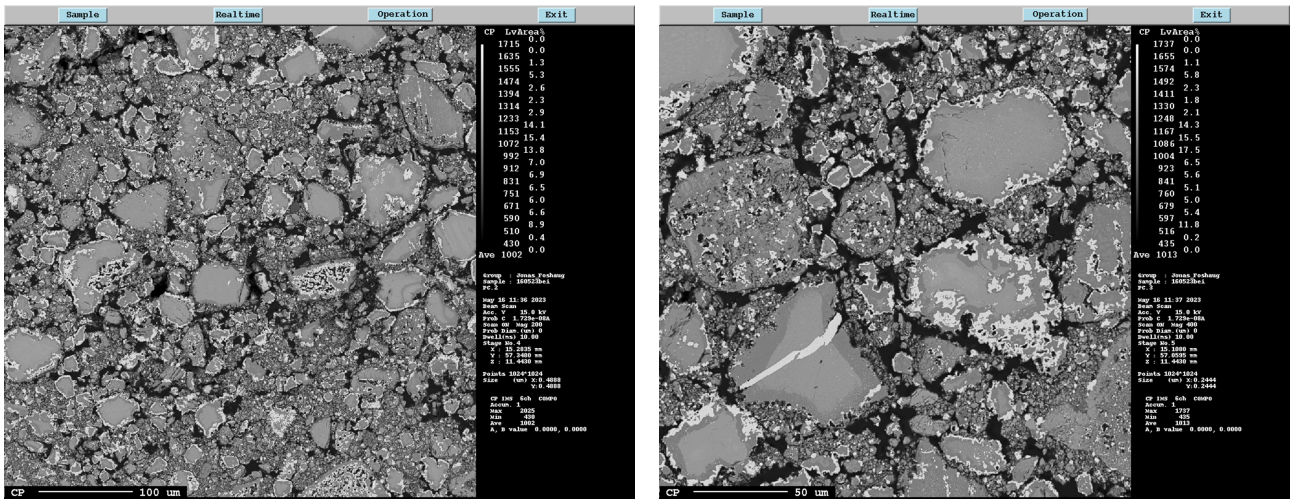

Figure 4.5: Two EPMA images of the CO-reduced pellets. Here the left image is at 200x zoom and the right image is at 400x zoom.

From LOM (light optical microscopy) pictures seen in figure 4.6. Showing what the core looks like compared to the outer edge. Showing what is expected in a simplified Shrinking Core Model. This image is very contrasted to make the interface more clear, with a red dotted line.

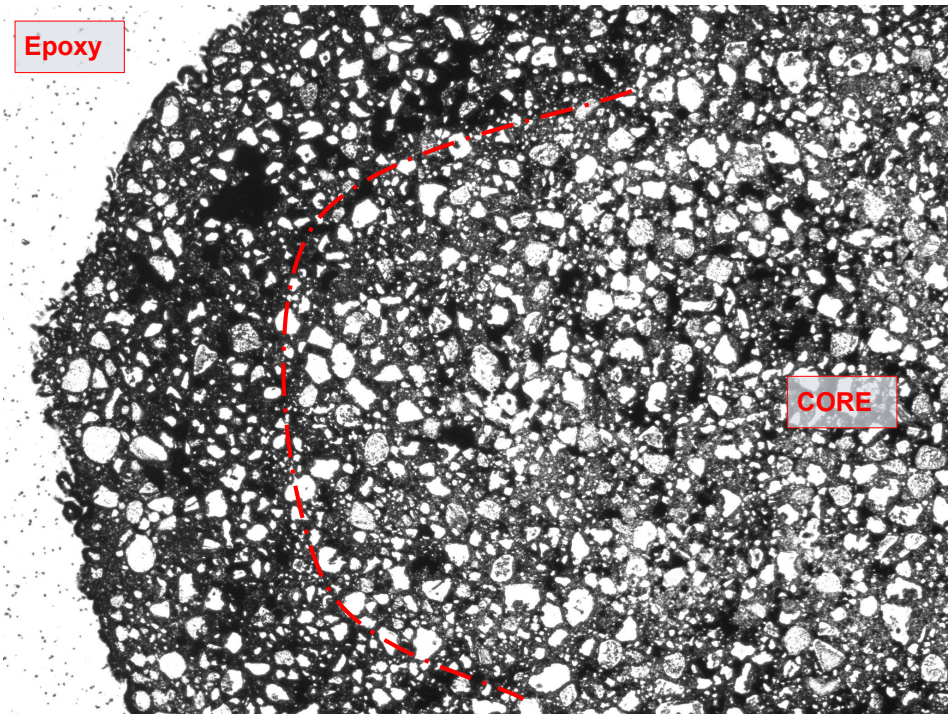

Figure 4.6: LOM image of A1 (CO reduced) showing core and edge.

4.1.3 H2 reduced pellets (A2)

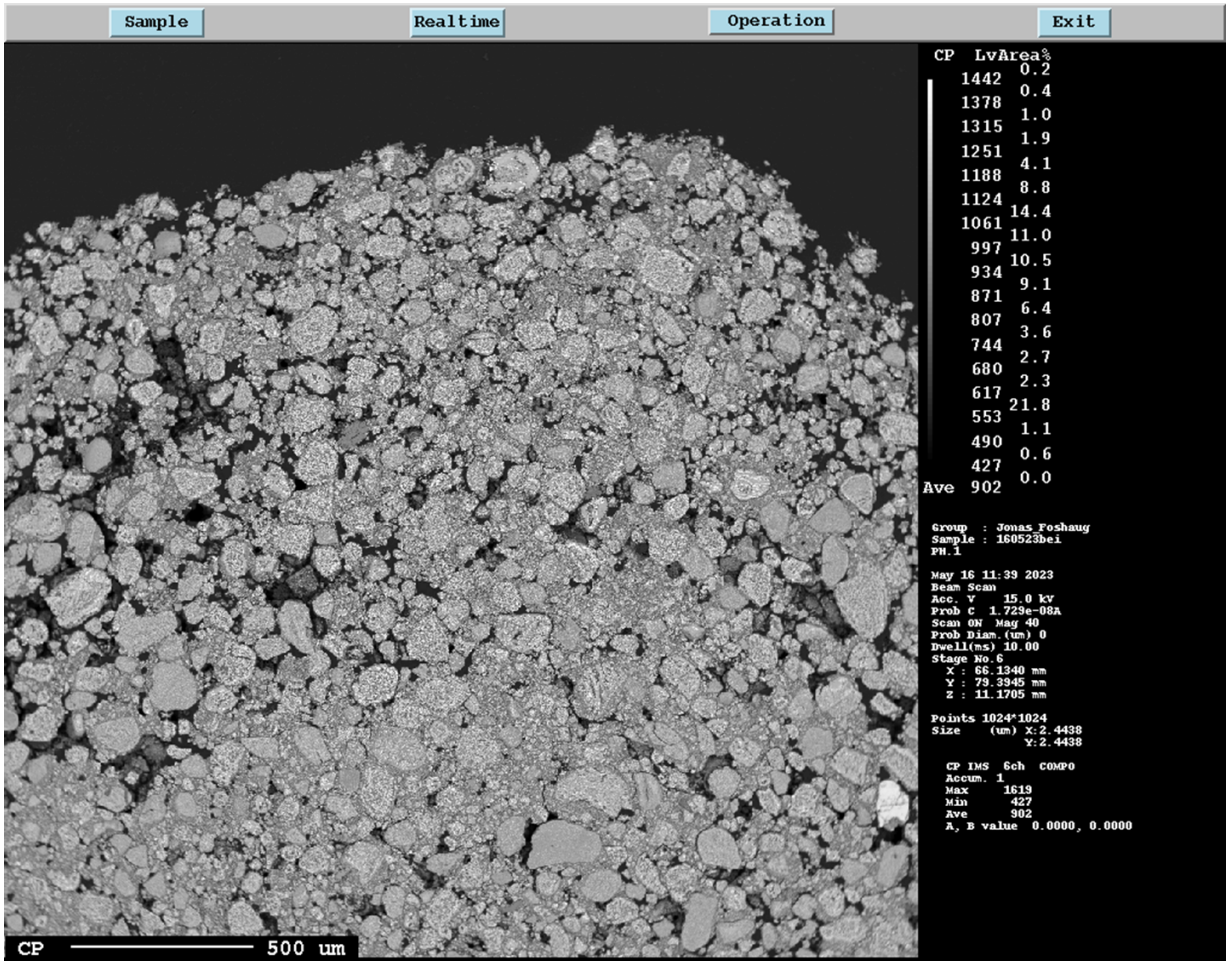

Figure 4.7: An overview EPMA image at 40x zoom for the cross-section of the H_2 pre-reduced pellets. (A2) The edge is at the top while the center is roughly seen at the bottom.

The image in figure 4.7 shows the cross-section of a Hydrogen-reduced pre-oxidized pellet. The cross-section shows the pellet to be similarly porous with a similar amount of big gray phases as the oxidized pellet cross-section. When looking closer at the gray phases they are seen to have metallic iron phases throughout the whole particle. These phases indicate a reduction has taken place. The closer look is seen in the images below in figure 4.8. Here there is a larger diffusion of reduction gas even into the light gray particles when compared to the pellets reduced with CO, because of the metallic phases being present throughout.

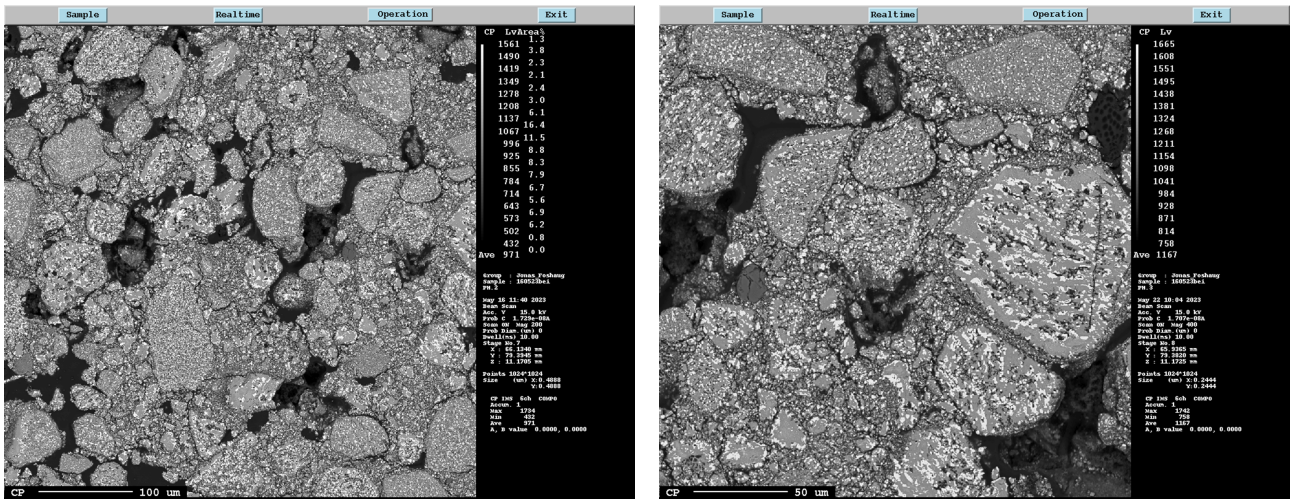

Figure 4.8: Two EPMA images of the H_2-reduced pellets. Here the left image is at 200x zoom and the right image is at 400x zoom.

4.2 Macro pictures

The following figures show the cross-sections of all the melting experiments done. They are grouped in their respective series, and their more informative name can be seen below each image. These pictures were taken using a macro image camera and then stitched together to make the quality acceptable. All crucibles are filled with epoxy before cutting, this is due to the possibility of cracking during cutting. The different phases are marked using color-coded circles to easier understand the images.

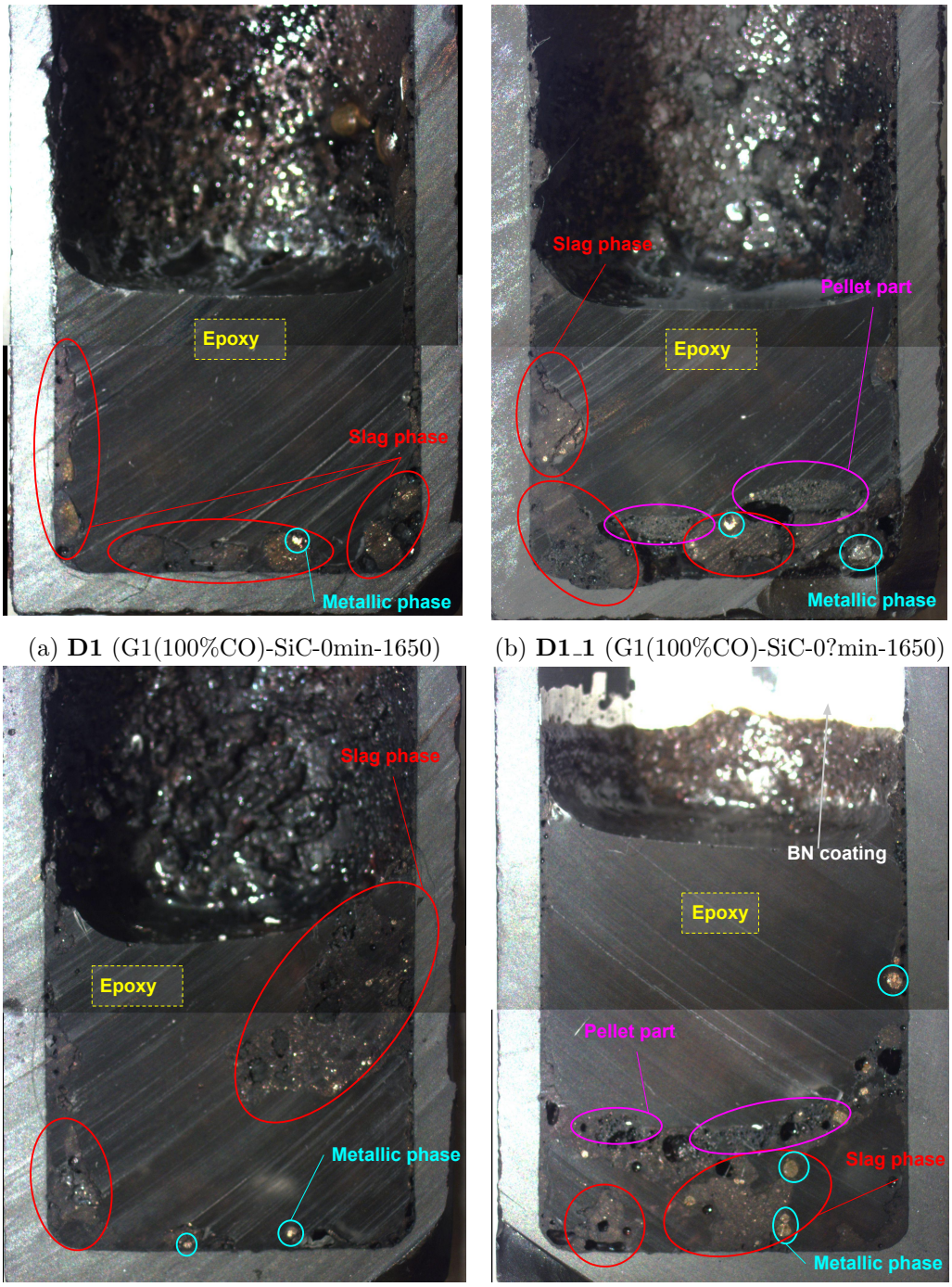

(a) **D1** (G1(100%CO)-SiC-0min-1650) (b) **D1_1** (G1(100%CO)-SiC-0?min-1650)

(c) **D2** (G1(100%CO)-SiC-1min-1600) (d) **D4** (G1(100%CO)-SiC-0min-1600)

Figure 4.9: Cross section of samples from the D-series of experiments. Showing crucible and slag after melting.

Figure 4.9 shows how the slag and pellets have reacted. Here it is seen that in experiments D1_1 and D4 there are still whole visible pellet pieces. The slag also has a very dark/black color and is seen to be climbing upwards in the crucible. Most notably seen in D2 where there is almost no slag at the bottom of the crucible. Big metal phases are also present in all the D series experiments, they are hard to spot and more abundant than the markings indicate. The white on top of D4 is BN coating not covered with slag residue as the other experiments are. In the D1_1 experiment, it is seen a major reaction between slag and crucible. This is seen when looking at the bottom left of the crucible, where a piece of the crucible is corroded away.

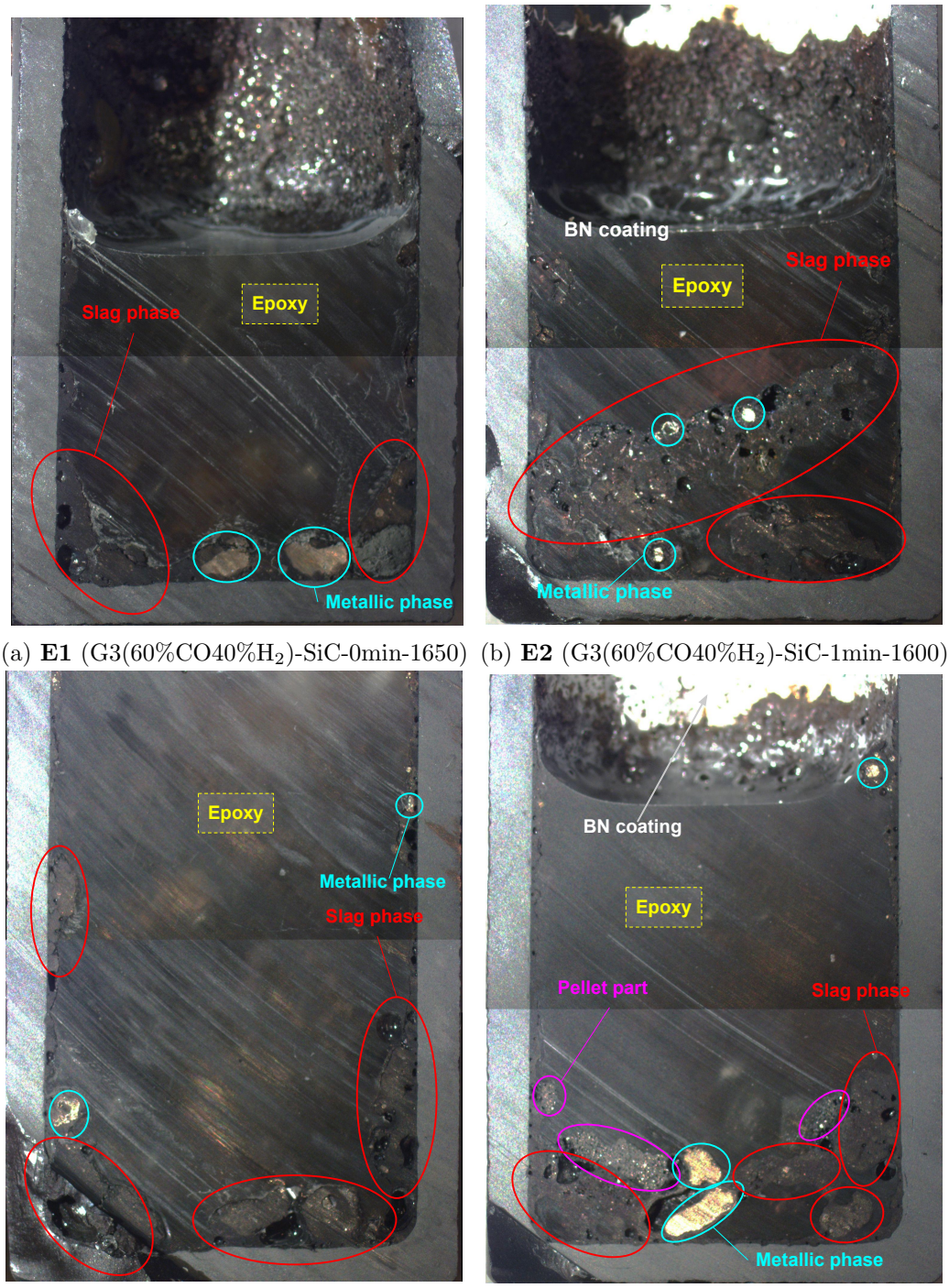

(a) **E1** (G3(60%CO40%H_2)-SiC-0min-1650) (b) **E2** (G3(60%CO40%H_2)-SiC-1min-1600)

(c) **E3** (G3(60%CO40%H_2)-SiC-3min-1600) (d) **E4** (G3(60%CO40%H_2)-SiC-0min-1600)

Figure 4.10: Cross section of samples from the E-series of experiments. Showing crucible and slag after melting.

Similarly to the D series figure 4.10 shows that there are only pellets visibly present in the E4 experiment, meaning there are only non-melted pellets present with faster quenching and lower temperature. There are significant metal phases present in all the experiments, and the slag seems to climb in the crucibles. The white on top of the crucibles in E2 and E4 is BN coating not covered by slag residue.

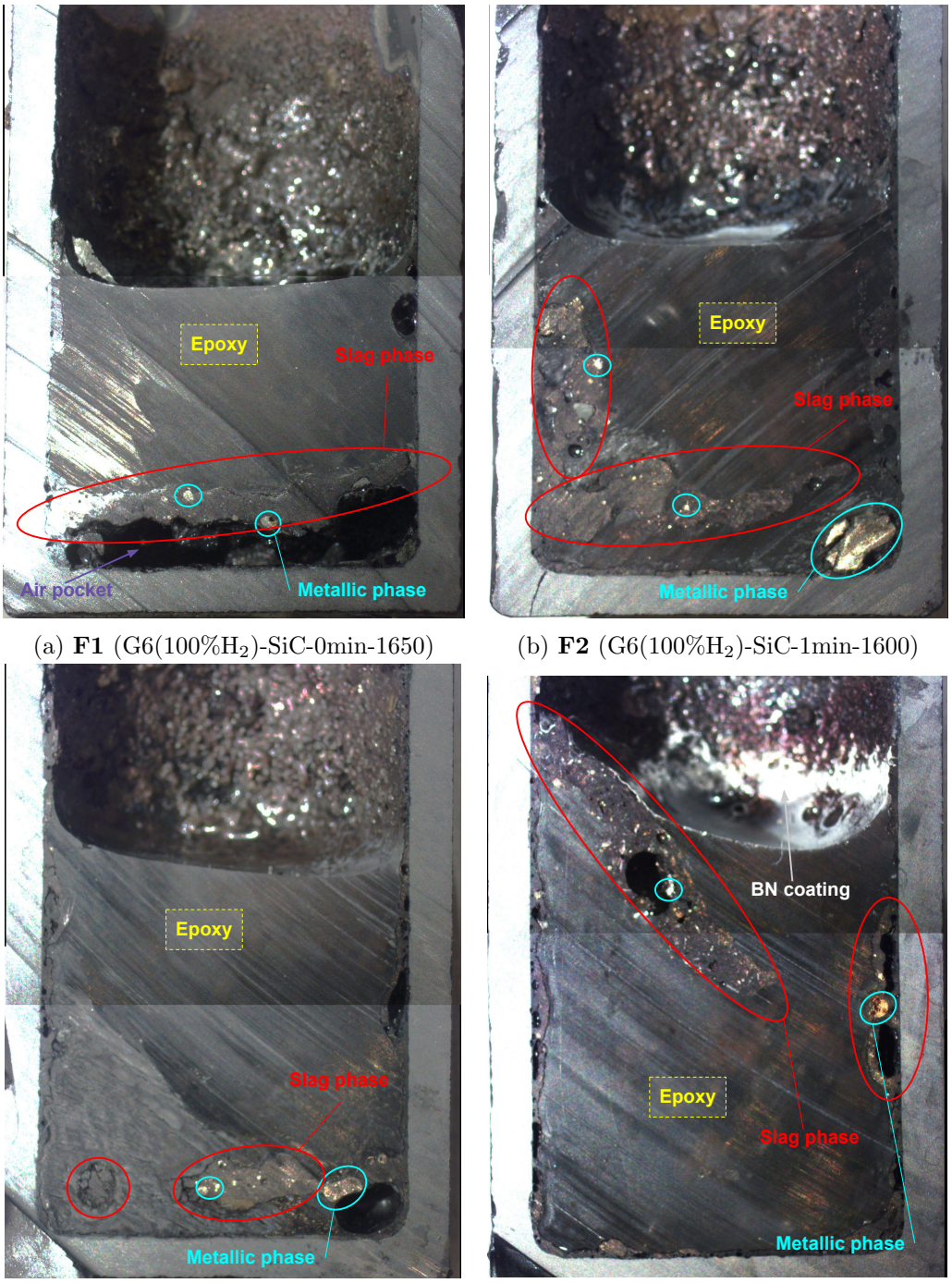

(a) **F1** (G6(100%H_2)-SiC-0min-1650) (b) **F2** (G6(100%H_2)-SiC-1min-1600)

(c) **F3** (G6(100%H_2)-SiC-3min-1600) (d) **F4** (G6(100%H_2)-SiC-0min-1600)

Figure 4.11: Cross section of samples from the F-series of experiments. Showing crucible and slag after melting.

Figure 4.11 shows many of the same aspects seen in D and E series. Slag is climbing in the crucible, this is easily seen in F1 and F4. In F1 there is an air pocket below the slag and in F4 the slag is almost at the top of the crucible. There are also significant metal phases present in all the samples. The pellet is not seen in this cross-section of F4, this is because it was cut out into the sample that was prepared for EPMA. But it was located between the two slag phase rings seen marked in the image. The slag in the samples are all dark/black, and the white on top of the crucibles is the BN coating not covered by slag residue.

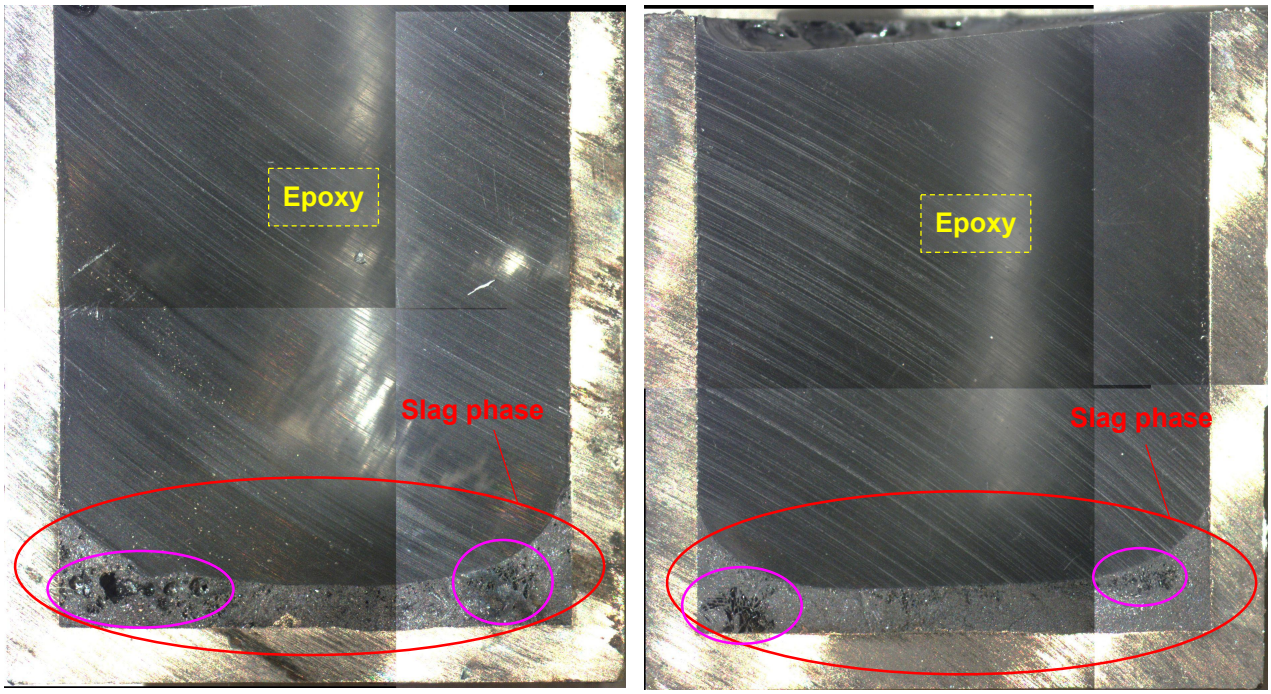

(a) **H1** (A1(100%CO)-Mo-0min-1600) (b) **H2** (A2(100%H_2)-Mo-0min-1600)

Figure 4.12: Cross section of samples from the H-series of experiments. Showing crucible and slag after melting. Pink circles indicate topography differences/holes.

Figure 4.12 shows the cross sections for the Molybdenum experiments. Here there can be seen some different phases marked with purple rings, these were at first considered to be pellet bits but more likely just a mixture of the phase being a different topography and structure. The slag in the molybdenum crucibles does not climb, and the coloration is more of a darker gray than dark/black. The coloration difference is more clear to the naked eye than what is seen in these images, this is due to an auto-focus/contrast function on the camera apparatus.

4.3 D-series EPMA analysis and mapping

Table 4.4: Parameters for the D series experiments.

Identification	Pellet	Slag composition	Crucible	Coating	Temperature	Time BQ*
D1	G1	85wt%TiO_2-10wt%FeO-5wt%CaO	SiC	BN	1650 °C	0 min
D2	G1	85wt%TiO_2-10wt%FeO-5wt%CaO	SiC	BN	1600 °C	1 min
D1_1	G1	85wt%TiO_2-10wt%FeO-5wt%CaO	SiC	BN	1650? °C	0? min
D4	G1	85wt%TiO_2-10wt%FeO-5wt%CaO	SiC	BN	1600 °C	0 min

* Time BQ = Time before quench, it refers to the time after the pellet is dropped before the sample is quenched.

Table 4.4 shows the parameters used for the experiment series D. The main point of D series is the pellet type, G1. These pellets were reduced using 100% CO and achieved a conversion degree of 65%. The amount of pellet for the experiments was around 1 g in weight while the slag was around 10g.

4.3.1 Experiment D1 (G1(100%CO)-SiC-0min-1650)

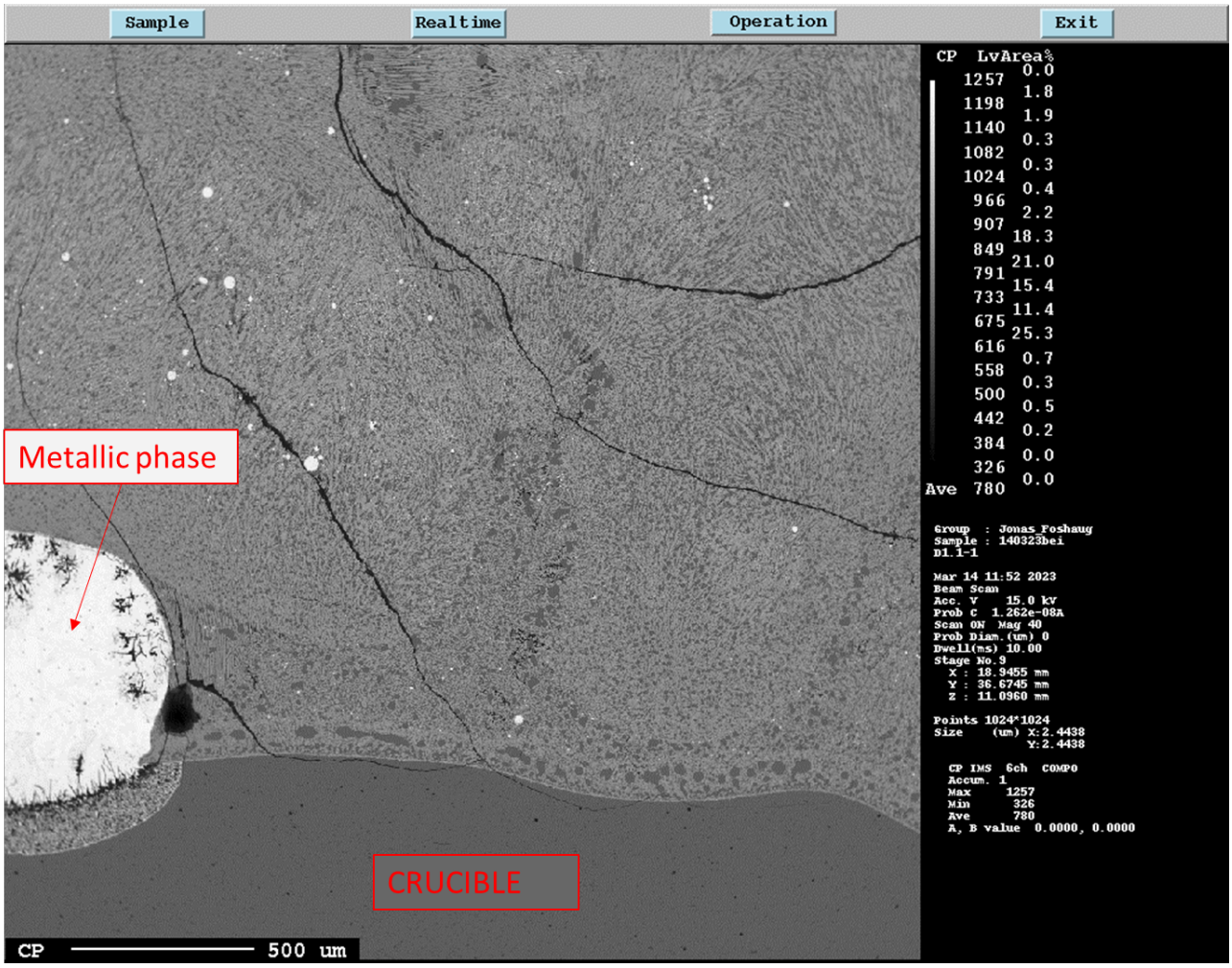

Figure 4.13: An overview EPMA image at 40x zoom of the D1 sample. Here the slag is on top of the crucible floor, and a metallic iron phase has formed.

The EPMA images of experiment D1 in figure 4.13 show the slag on top of the crucible floor. Here it is seen that the slag has reacted with the crucible since the crucible floor is not completely flat. There is also a significant metallic iron particle present, with lesser metallic phases present throughout the slag. The slag does not look very homogeneous in the way that there look to be many different phases present.

Point analysis

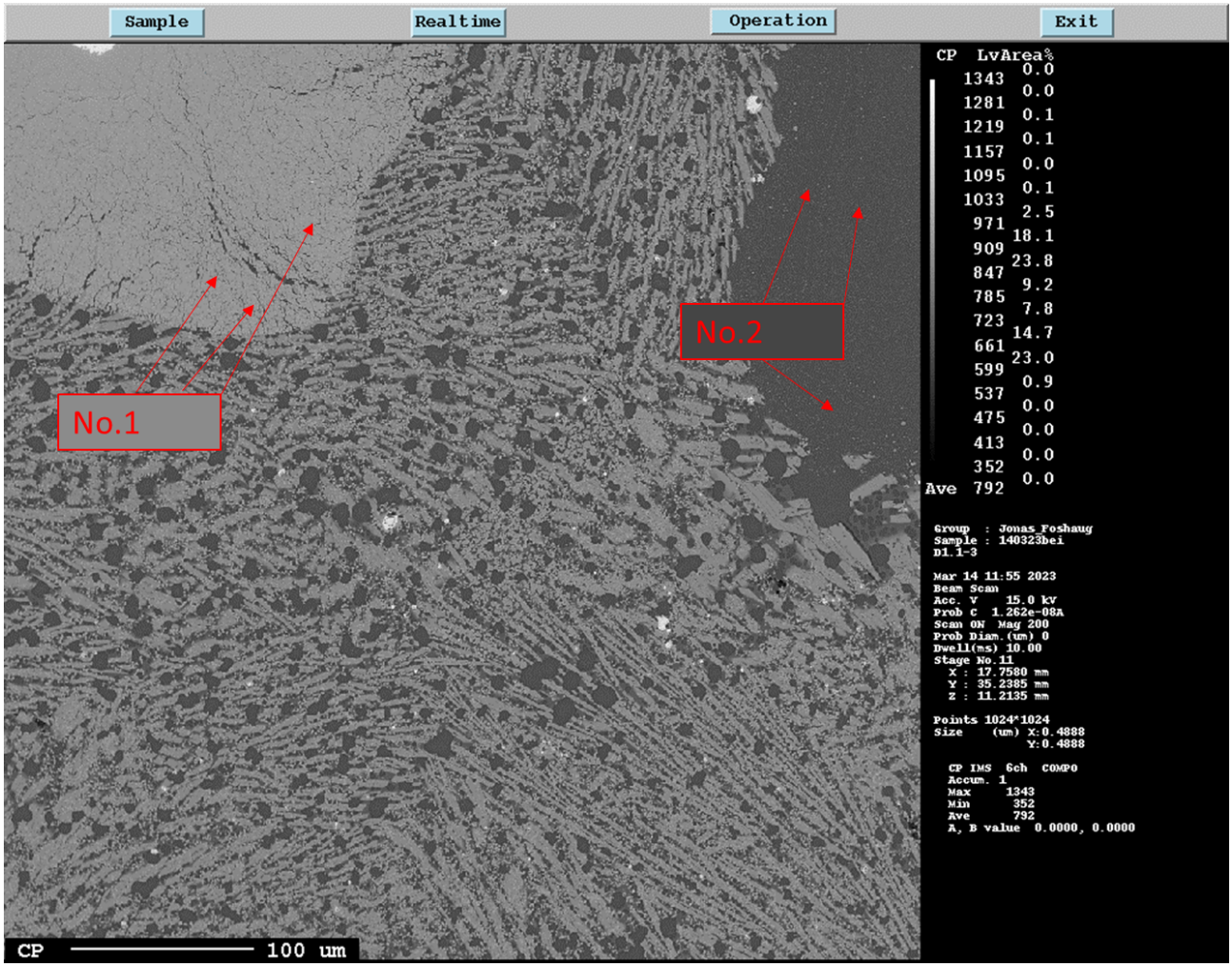

Figure 4.14: EPMA image of D1 at 200x zoom. The drawn in numbers corresponds to table 4.5 with the point analysis below.

Figure 4.14 shows where the point analysis in table 4.5 is taken. There was taken three point analysis of each phase, and the average of these is what is seen in the table. The point analysis shows that the SiC crucible has reacted into the slag sample creating a phase with predominantly SiO_2 in the darker No.2 phase. While the light gray phase consists of TiO_2, however, it might be a Ti carbide phase since the measurement is as high as 133.902 total. Meaning the point analysis is looking for counts of Ti in TiO_2, but instead picks up Ti in TiC. These two big phases are seen more mixed into smaller pieces in the slag, seen below in the same figure.

Table 4.5: Point analysis of different phases on sample D1. Number 1 is an average point analysis of the lightest gray zone. Number 2 is of the darker gray zone. Seen more clearly in figure 4.14

No.	SiO2	MgO	CaO	FeO	Al2O3	TiO2	Total
1	1.461	0.060333	0.454	0.331333	0.156667	131.4387	133.902
2	77.09933	0.012	1.497333	0.079333	1.306	7.996667	87.99067

EPMA mapping

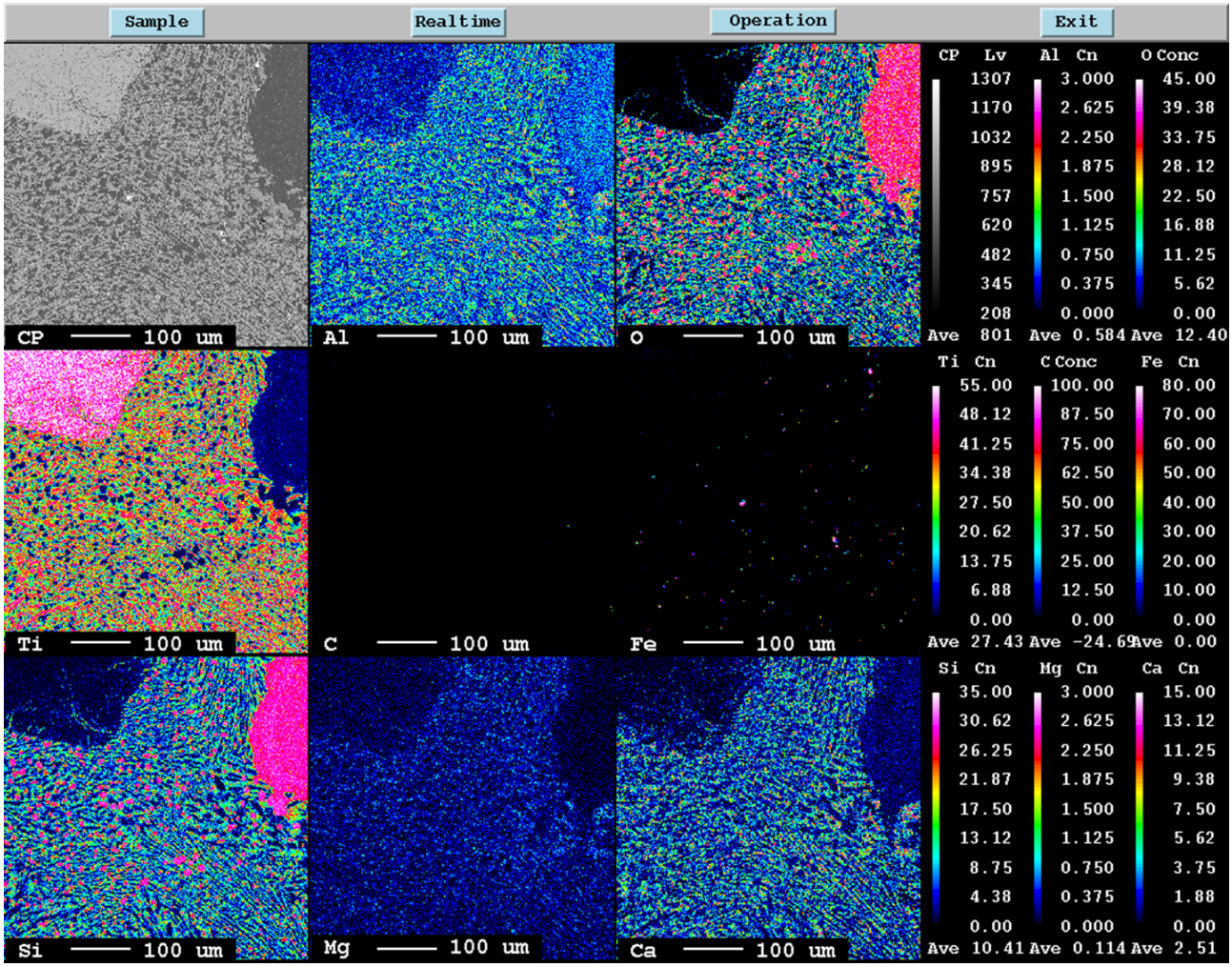

Figure 4.15: EPMA mapping of sample D1, showing the crucible in the bottom left corner of the image.

The mapping seen in figure 4.15 shows the top light gray phase mainly consisting of Ti while the darker top right phase consists of Si and O. The light gray phase is likely TiC, but the C was not picked up in the EPMA mapping. It is also seen that the Fe is dotted about in the white phases and not present throughout the slag.

4.3.2 Experiment D2 (G1(100%CO)-SiC-1min-1600)

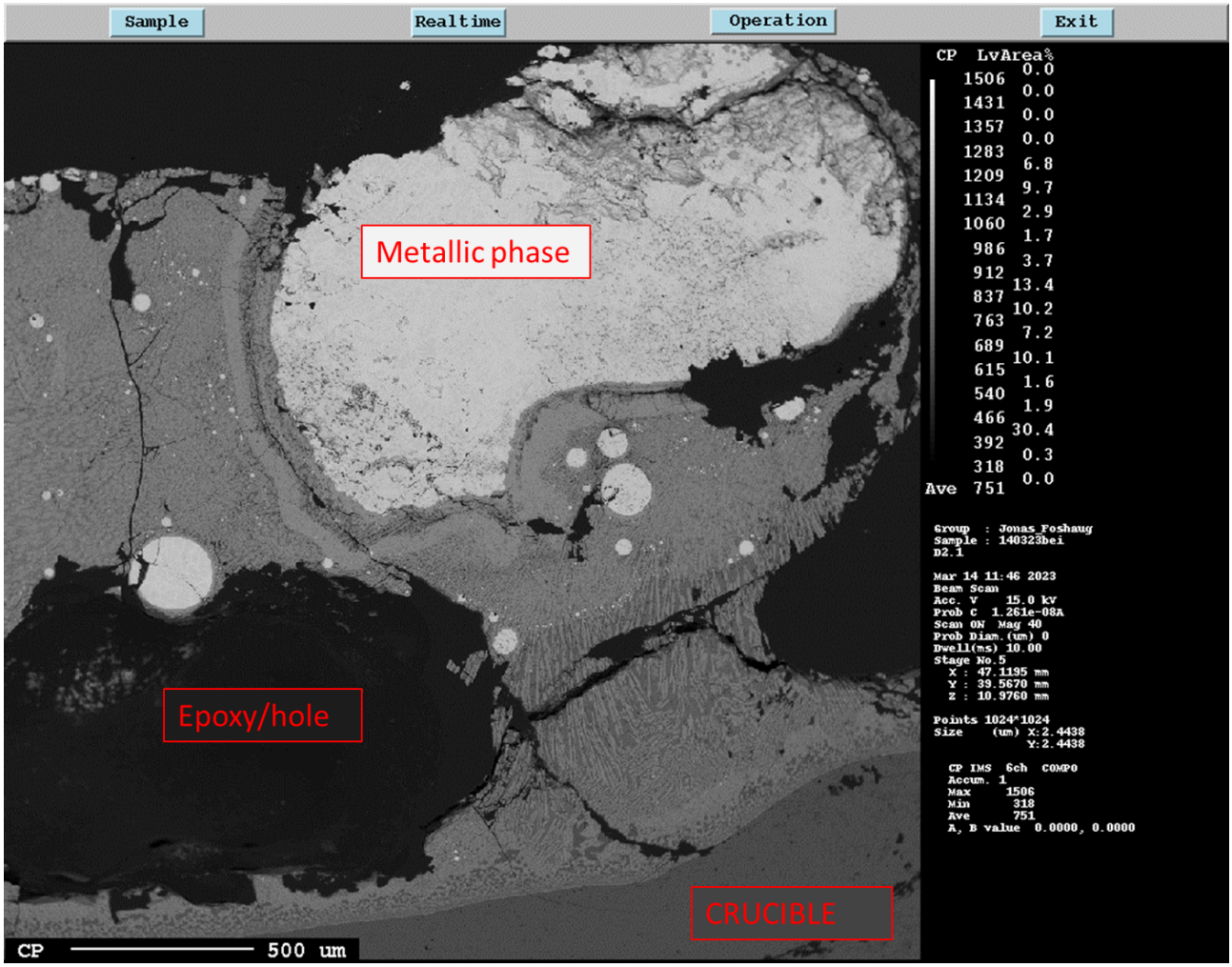

Figure 4.16: An overview EPMA image at 40x zoom of the D2 sample. Here the slag is on top of the crucible floor, and a huge metallic iron phase has formed.

Figure 4.16 shows the slag created in experiment D2 on top of the SiC crucible. In the slag, it has been created a huge metallic iron phase. Around this metallic phase, there is a ring made of a lighter phase, a Ti phase as will be seen in the following analysis.

Point analysis

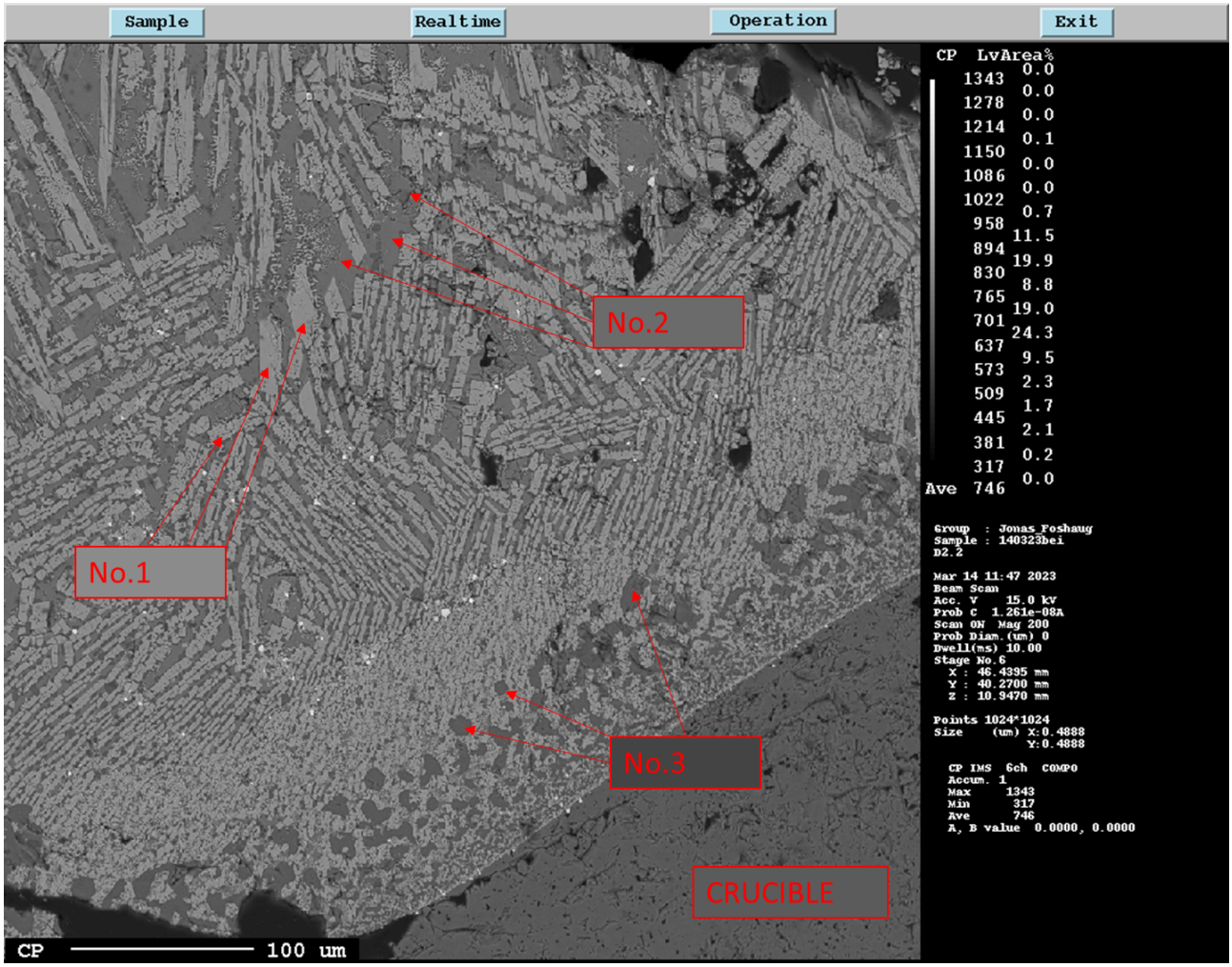

Figure 4.17: EPMA image of D2 at 200x zoom. The drawn in numbers corresponds to table 4.6 with the point analysis below.

The point analysis taken in figure 4.17 shows the different phases found near the crucible boundary. There was taken three point analysis of each point, these corresponds to table 4.6. Here it is seen that the darkest gray No.3 shows a reaction between the SiC crucible and the slag, creating a phase mostly consisting of SiO_2. Phase No.2 is a mixture of a lot of the less-containing elements in the slag, meaning Mg, Ca, and Al. The dominant element here is still Si. The light gray is mostly a Ti phase.

Table 4.6: Point analysis of different phases on sample D2. Number 1 is an average point analysis of the lightest gray zone. Number 2 is of the darker gray zone, while number 3 is from the darkest zone. Seen more clearly in figure 4.17.

No.	SiO2	MgO	CaO	FeO	Al2O3	TiO2	Total
1	0.982333	0.49	0.534333	0.055333	0.271	99.92867	102.2617
2	47.322	6.860667	22.784	0.155667	3.128	11.62	91.87033
3	86.50333	0.594333	1.817667	0.074333	0.620667	5.325333	94.93567

The white metallic phase seen in figure 4.16 is made up of Fe and Si, and when looking closer at this white phase it is seen to be two very similar phases. Two metallic iron phases with a small amount of

Si mixed in. This is seen in figure 4.7, with the corresponding point analysis seen in table 4.7. This implies the SiC from the crucible has reduced the iron in the slag melt to the metallic iron phase.

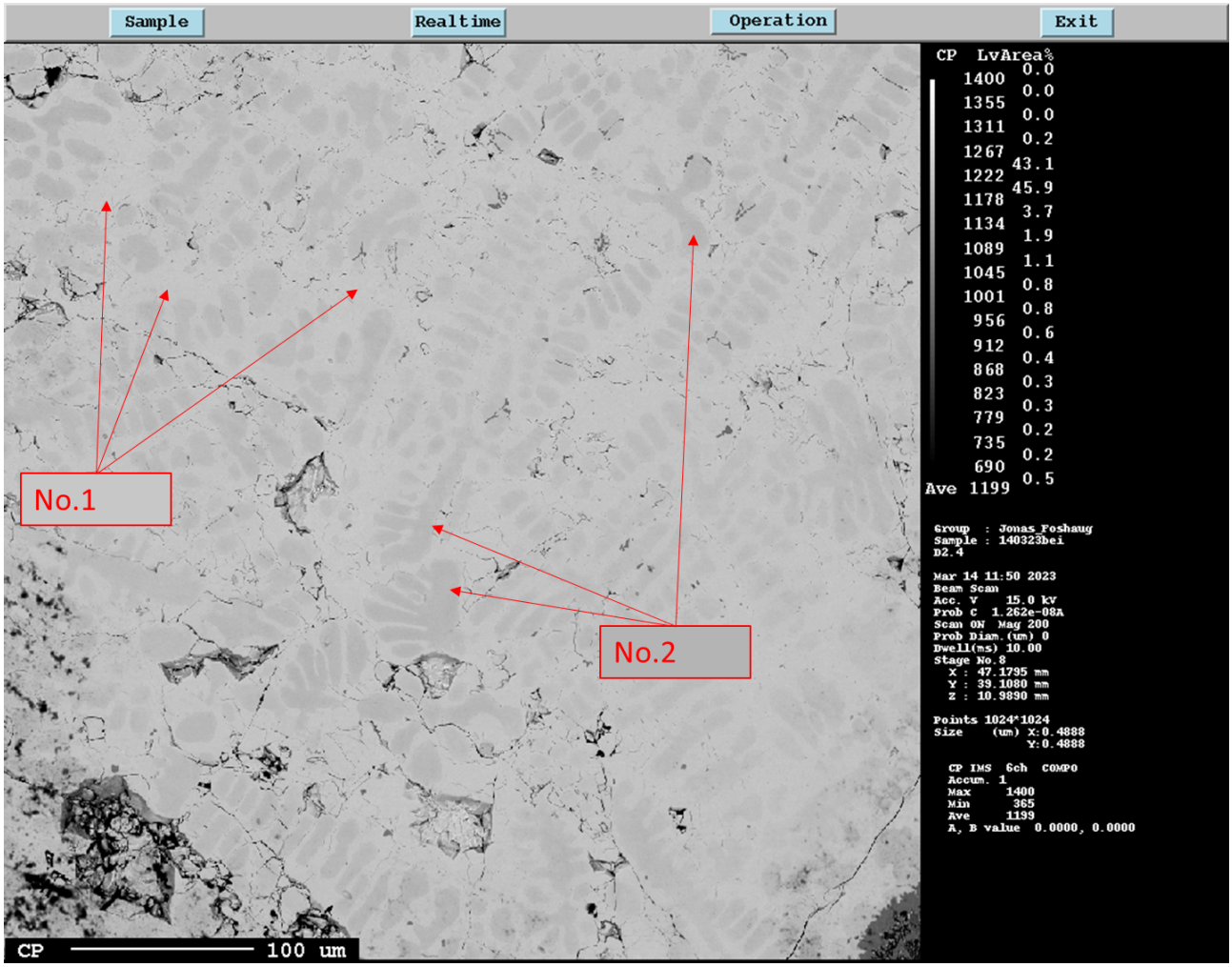

Figure 4.18: EPMA image of D2 at 200x zoom. The drawn in numbers correspond to table 4.7 with the point analysis below.

Table 4.7: Point analysis of different metallic phases on sample D2. Number 1 is an average of point analysis of the lightest zone. Number 2 is of the darker zone. Seen more clearly in figure 4.18.

No.	Si	Ti	Fe	Total
1	7.756667	0.278	86.567	95.80933
2	10.50333	0.021667	88.83833	99.53967

EPMA mapping

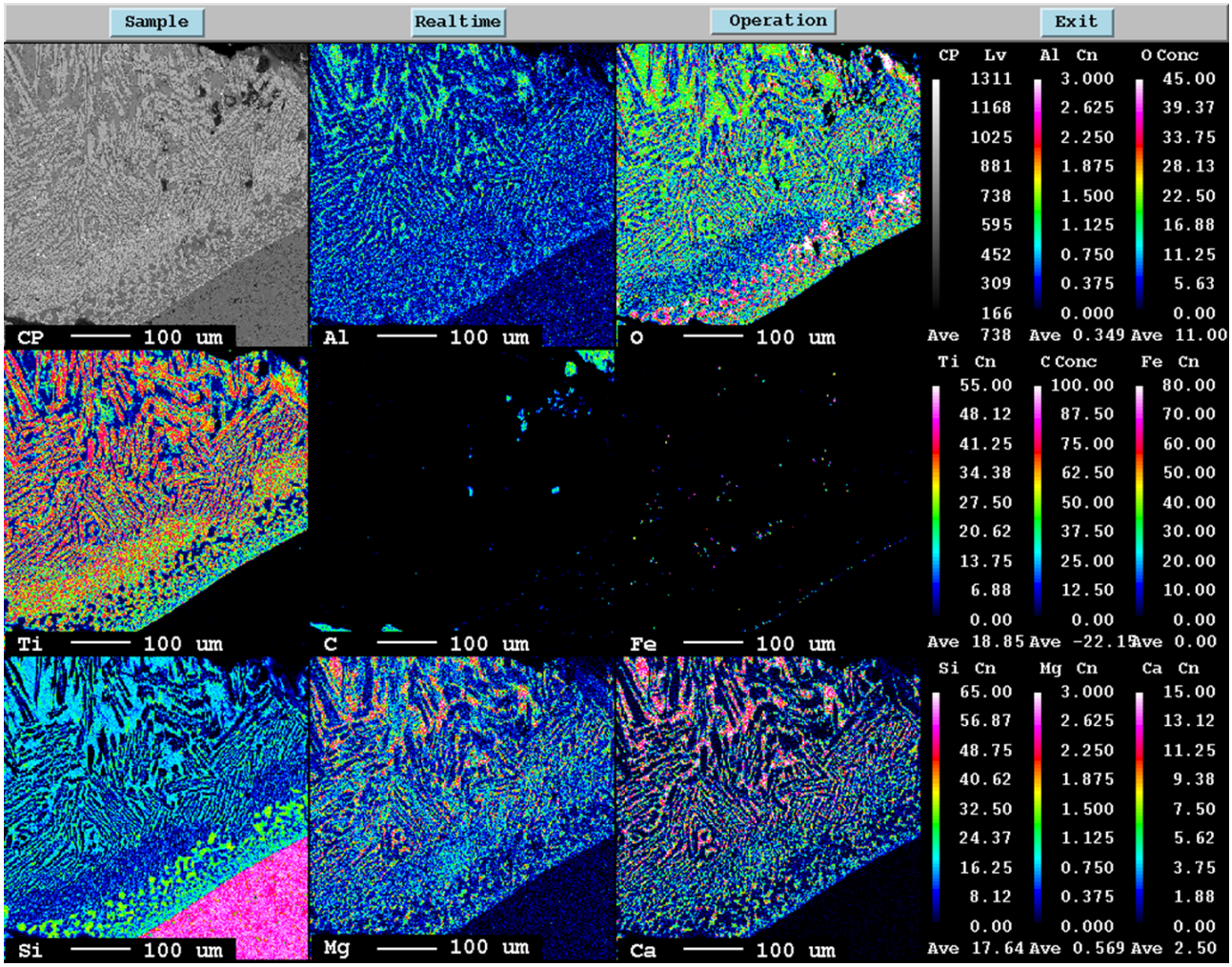

Figure 4.19: EPMA mapping of sample D2, showing the crucible in the bottom right corner of the image.

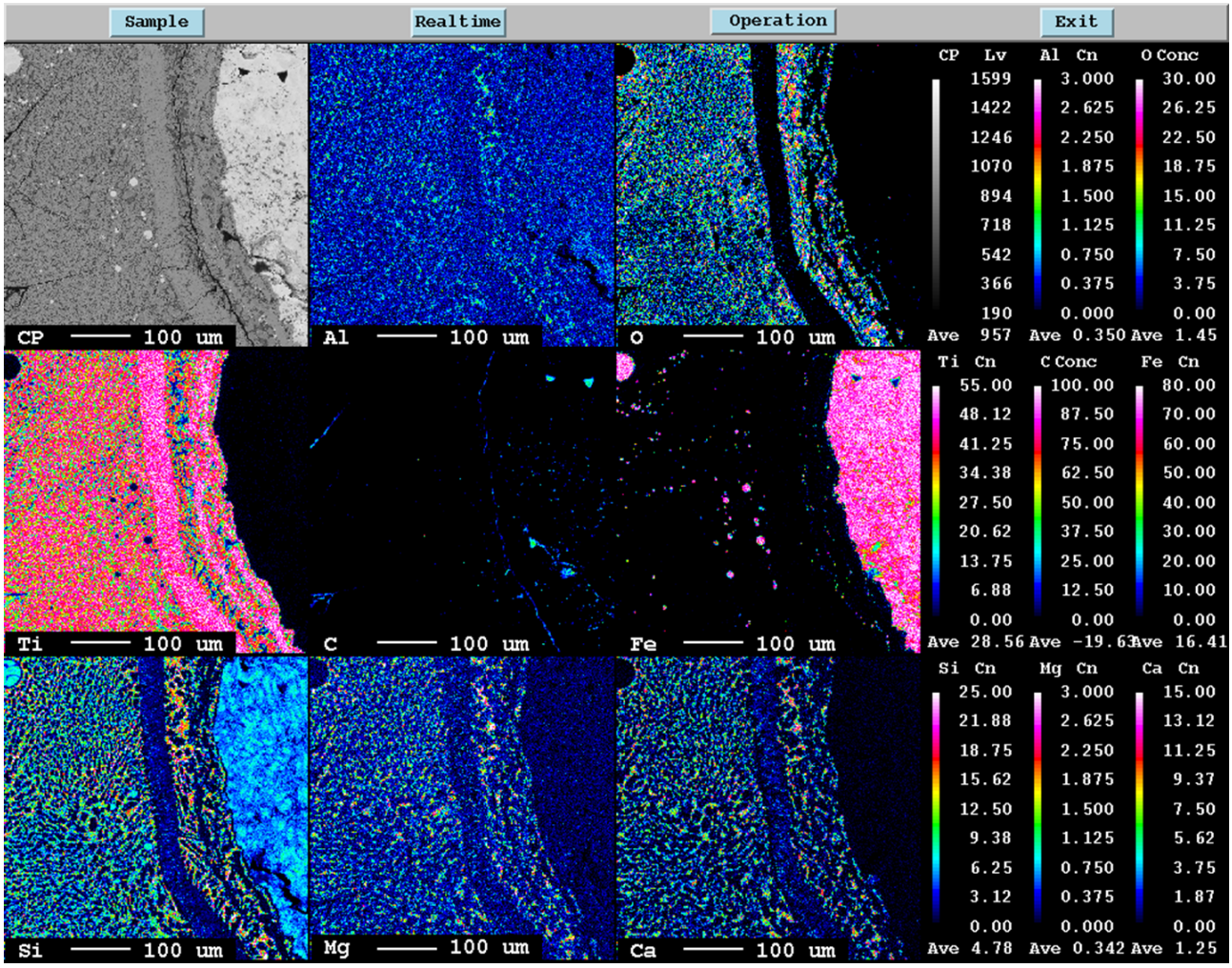

Figure 4.20: EPMA mapping of sample D2, taken from the middle of the sample near the big metal phase.

Figure 4.19 and 4.20 shows two mapping analysis of the D2 sample. One from towards the "center" and one from the crucible border. Figure 4.19 shows how the Fe close to the crucible has diffused towards the border. It is also seen that the Si from the crucible has diffused into the slag, here the Si has reacted with O from the slag and created a Si-oxide phase. This is seen compared to what has happened to the Fe, the Oxygen has diffused towards the crucible. Seen by the lack of oxygen further into the slag from the Si-oxide phase. The light gray phases seem to mainly consist of Ti. The carbon mapping does not pick up any carbon in the SiC crucible in the mapping in figure 4.19. This is something that is the case for all the mappings.

Figure 4.20 is a mapping near the big white metallic iron phase seen in the sample. Around this white phase, there is observed a light gray ring. This ring seems to consist of mainly Ti, it is also seen to be oxygen deprived. The metallic phase is also seen to contain a bit of Si with the Fe.

4.3.3 Experiment D1_1 (G1(100%CO)-SiC-0?min-1650)

Experiment D1_1 is the "failed" experiment. Here the temperature was 1650 °C, however, the drop took place at a bit lower than this due to the furnace being turned off from the malfunction of the thermocouple. The experiment drop was done simply because the crucible is not reusable and once the furnace turned off, the pellet parts might as well be dropped. This gives a negative drop time, This time is very uncertain since it was not measured, it is most likely not more than 20 seconds.

Figure 4.21 shows the EPMA of the slag and a part of the pellet. Here it is seen how the interface between pellet and slag looks before completely reacting together.

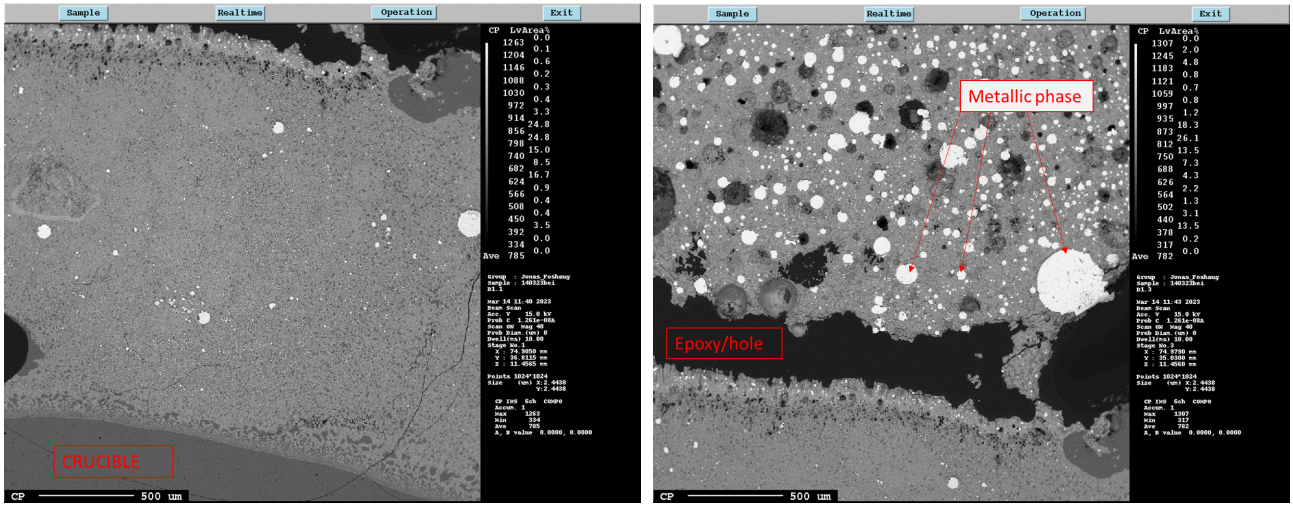

Figure 4.21: Two overview EPMA images at 40x zoom of the D1_1 sample. Here the slag is on top of the crucible floor seen on the left, while the picture to the right is further up in the sample.

Point analysis

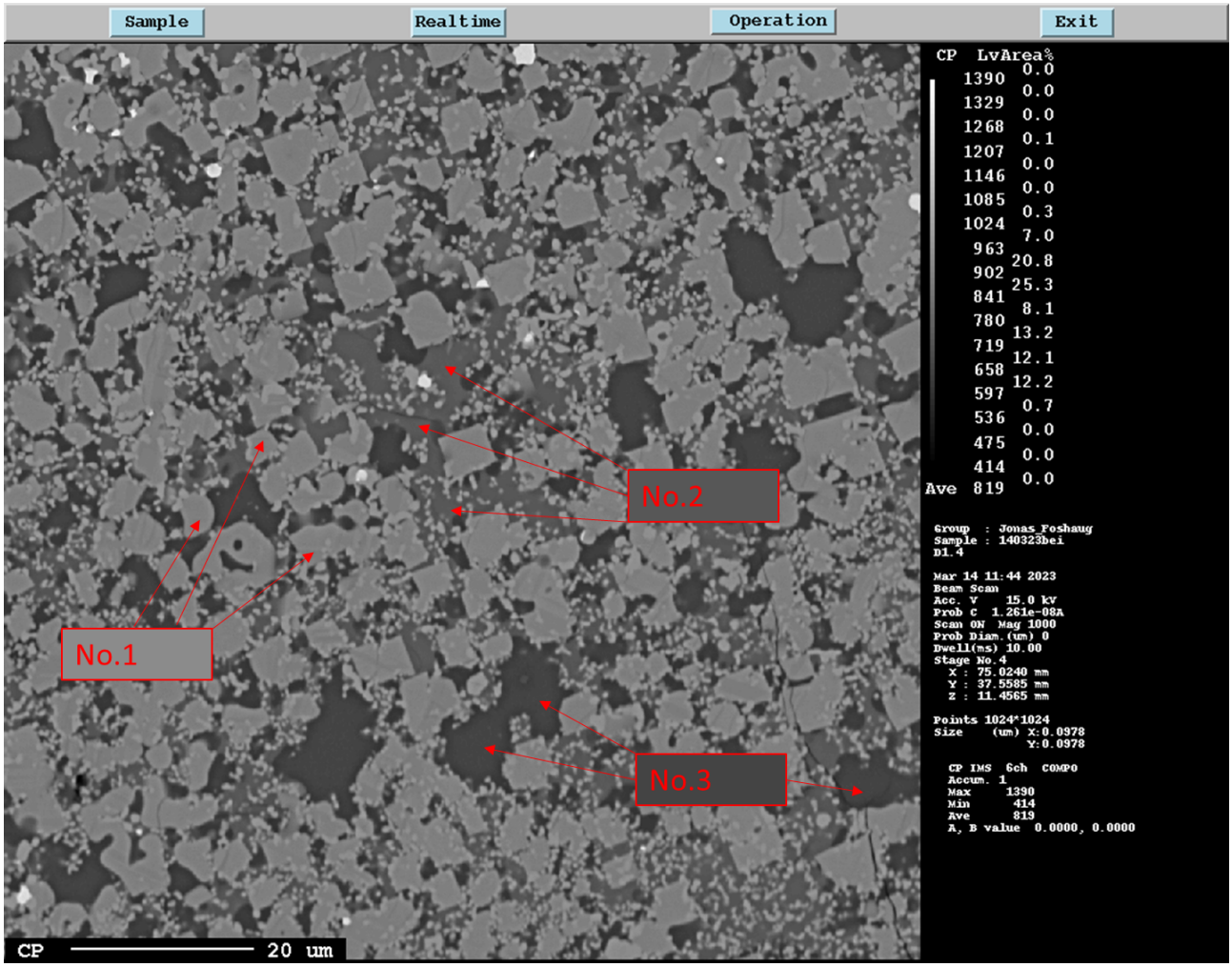

Figure 4.22: EPMA image of D1_1 at 1000x zoom. The drawn in numbers correspond to table 4.8 with the point analysis below.

Point analysis of experiment D1_1 is seen in table 4.8. The point analysis is taken closer to the center of the slag, away from the crucible. These points correspond to what is shown in figure 4.22. The points in the table are the average of three point from each of the phases. The darkest phase No.3 shows mainly SiO_2. The lightest phase No.1 is mainly Ti, and the dark gray phase No.2 is a mixture of Si and different minor elements in the slag. The point analysis shows a substantial amount of FeO in the No.1 and No.2 phases.

Table 4.8: Point analysis of different phases on sample D1_1, all numbers are in mass percentage. Number 1 is an average point analysis of the lightest gray zone. Number 2 is of the darker gray zone, while number 3 is from the darkest zone. Seen more clearly in figure 4.22.

No.	SiO2	MgO	CaO	FeO	Al2O3	TiO2	Total
1	0.959	0	0.087	8.842	0.907333	86.40933	97.20467
2	49.85933	12.946	6.992333	16.88633	4.444333	7.137	98.26533
3	87.03167	0.009	1.188667	0.025	0.513333	7.679667	96.44733

EPMA mapping

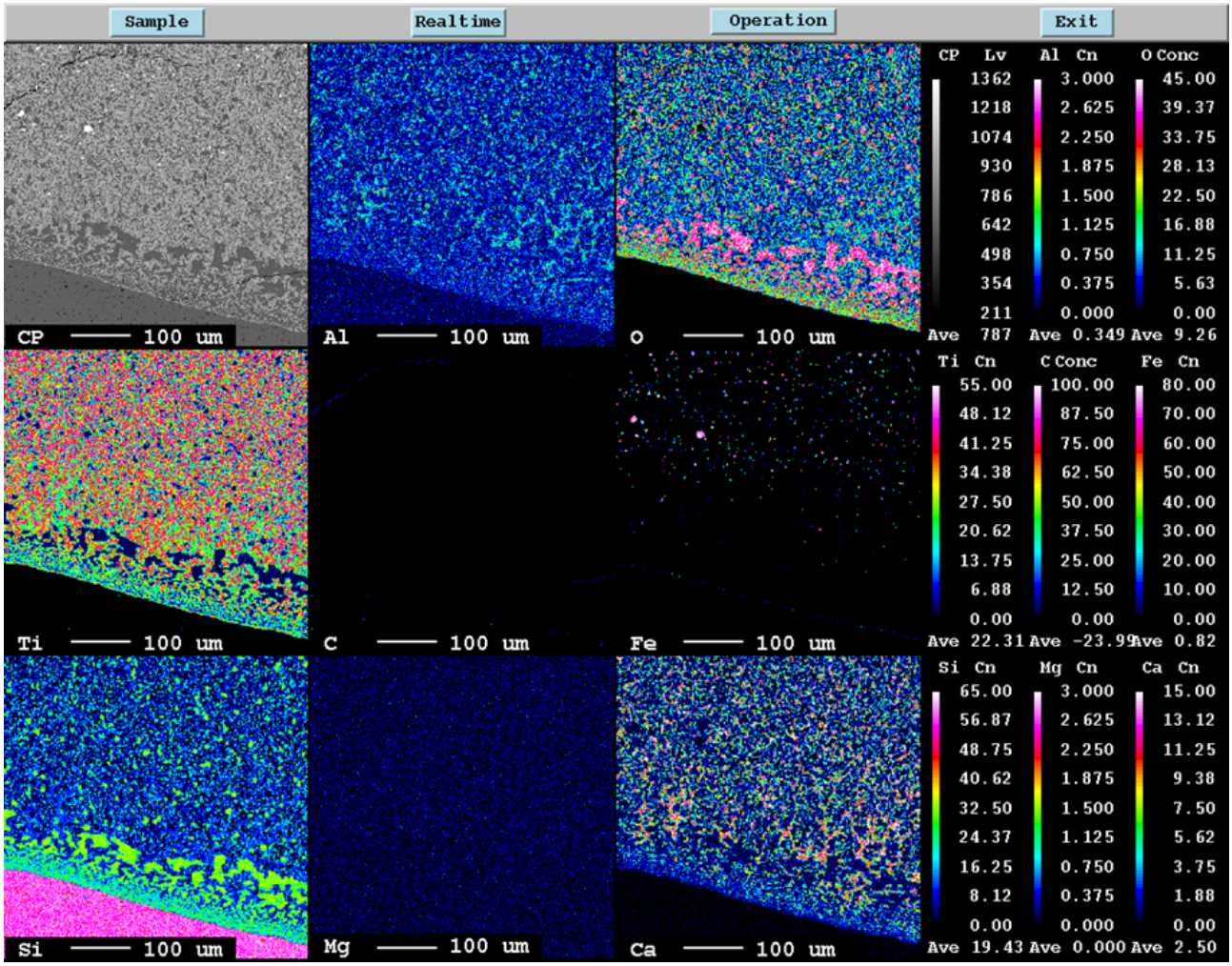

Figure 4.23: EPMA mapping of sample D1_1, taken near the crucible border.

In the mapping of figure 4.23 It can be seen that there is a gathering of Fe at the crucible, this might be a bit difficult to see since it is a dark blue color on a black background. While a little bit into the slag there is a lack of Fe before it gets more homogeneous further into the slag. It is also seen to be no Mg near the crucible, implying no pellet has reacted near the crucible wall since the Mg can only come from the pellet. The SiC crucible is seen to react with the slag creating phases with Si throughout the slag. This is especially the case near the crucible where it can be seen a creation of a SiO_2 phase. The Ca seems to also be a bit more prevalent away from the crucible.

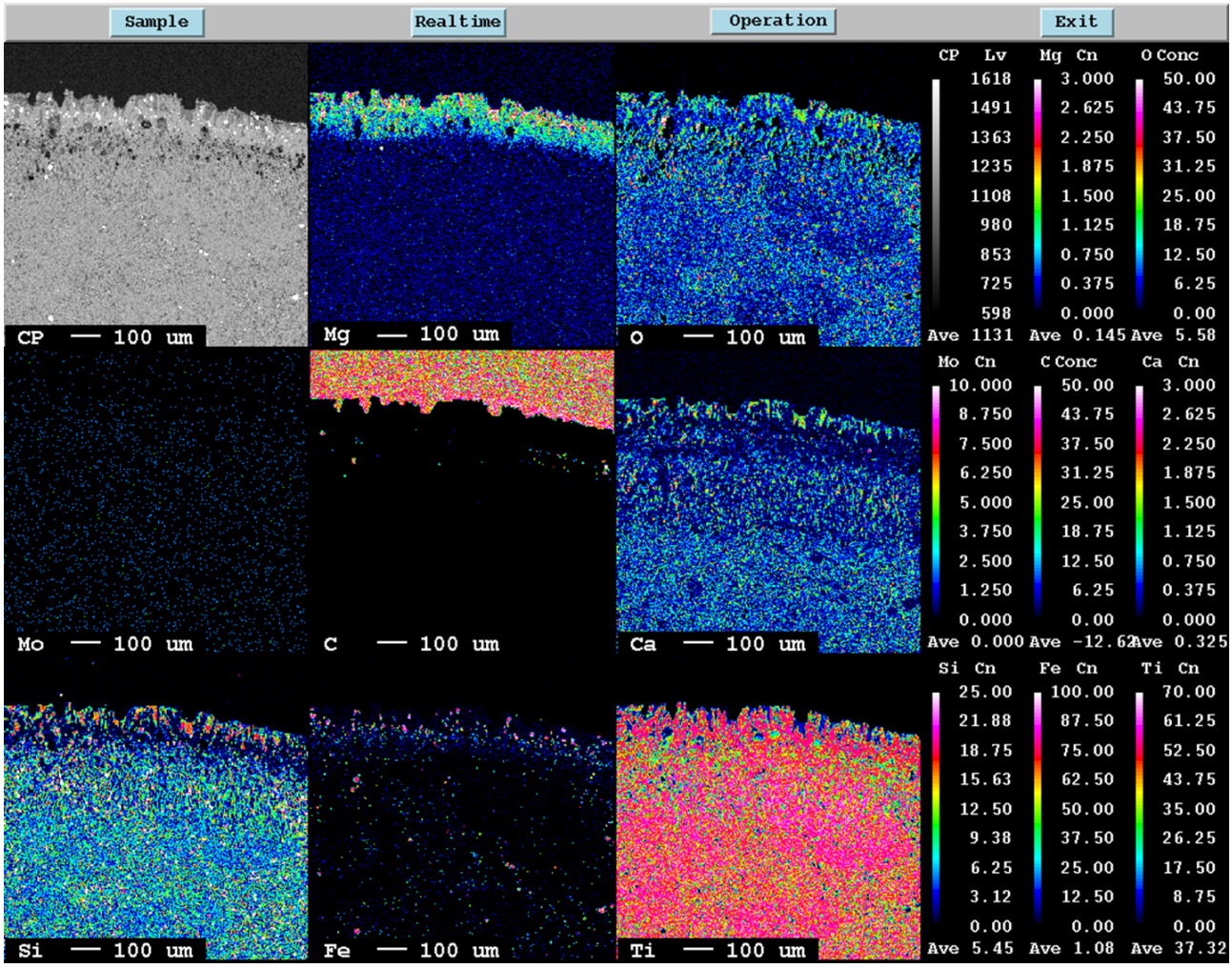

Figure 4.24: EPMA mapping of sample D1_1, taken between the slag and the pellet part.

Mapping of the interface between the pellet and the slag is seen in figure 4.24. The reaction interface is the very top part. Here it is clearly seen a divide in the Mg mapping. The Mg only originates from the pellets. It is seen to slowly react into the slag. The Si can also be seen having small SiO_2 phases in the reaction interface. For both the mappings done for D1_1, the Fe is seen to have more of a phase in the slag not just concentrated in the metallic phases. Meaning the mapping is not completely pitch black around the metallic phases. It is however seen to be pitch black near the crucible meaning it has completely reduced here.

4.3.4 Experiment D4 (G1(100%CO)-SiC-0min-1600)

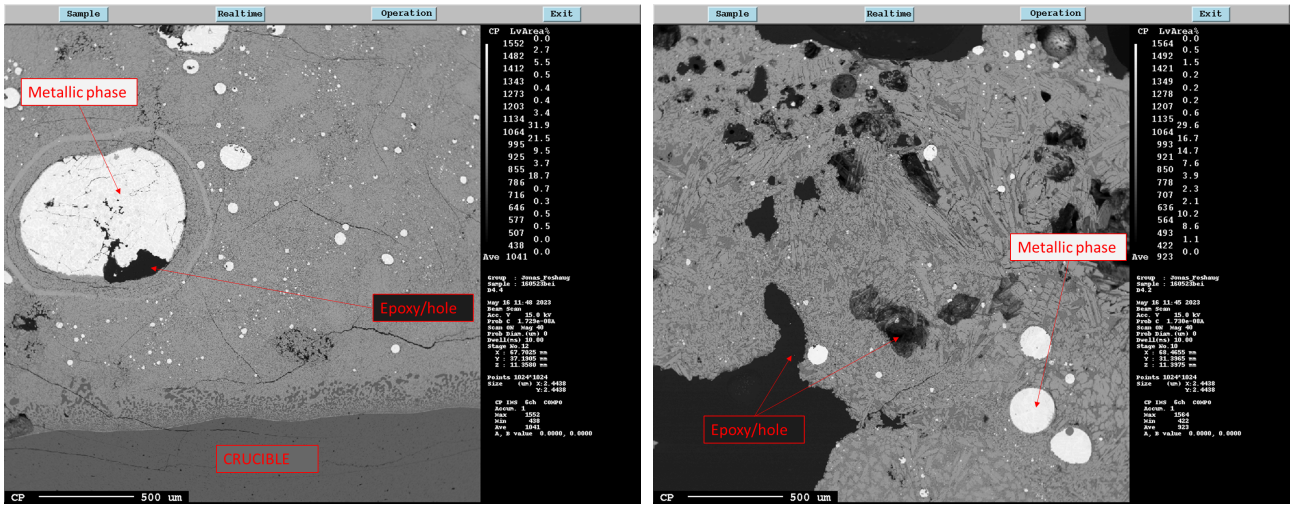

Figure 4.25: Two overview EPMA images at 40x zoom of the D4 sample. Here the slag is on top of the crucible floor seen on the left, while the picture to the right is further up in the sample.

In figure 4.25 it can be seen microstructure changes from the crucible edge to the center of the slag. The structure is more lamellae/plate-like towards the center, seen in the rightmost image, when looking macroscopically at the cross-section of the sample this top part of the left image looks like a pellet piece. There have been created significant metallic phases in experiment D4, the bigger ones have a light gray ring around them. The rugged crucible floor shows a reaction between the slag and the crucible.

Point analysis

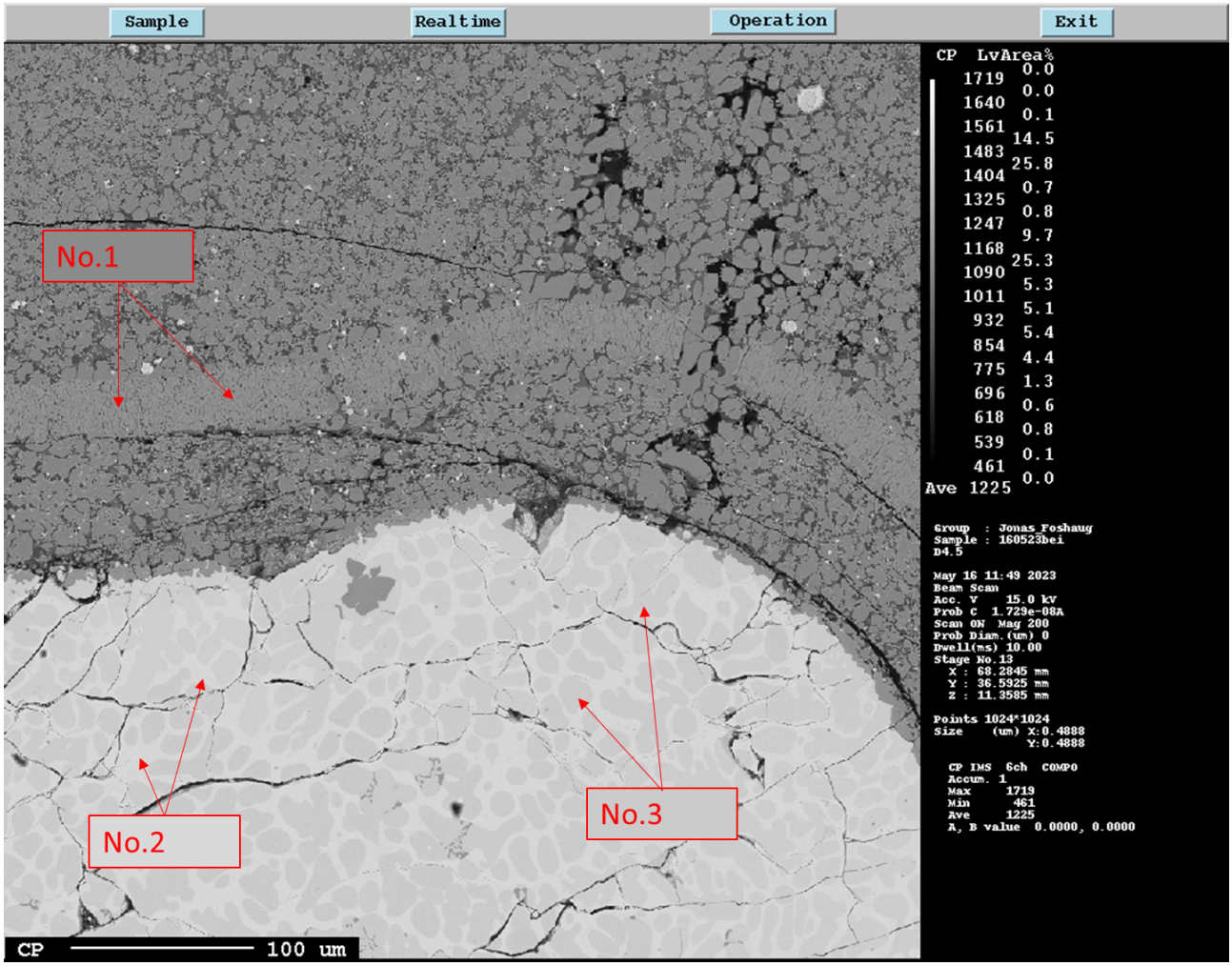

Figure 4.26: EPMA image of D4 at 200x zoom. The drawn in numbers correspond to table 4.9 with the point analysis below.

The point analysis is taken to see what elements the ring around the metallic phase contains. The results seen in table 4.9 show a TiC phase in the ring, while the metallic phase seems to be a Fe phase with some Si. The points in the table can be seen drawn into figure 4.26

Table 4.9: Point analysis of different phases on sample D4. Number 1 is an average point analysis of the gray ring surrounding the metal phase. Number 2 is of the lightest white zone, while number 3 is the grayer white zone. Seen more clearly in figure 4.26.

No.	Si	P	C	Fe	Ti	Total
1	0.3	0.005	15.762	0.184	81.767	98.018
2	5.223	2.858	9.201	83.658	0.736	101.676
3	11.919	0.157	7.386	81.356	0.155	100.973

EPMA mapping

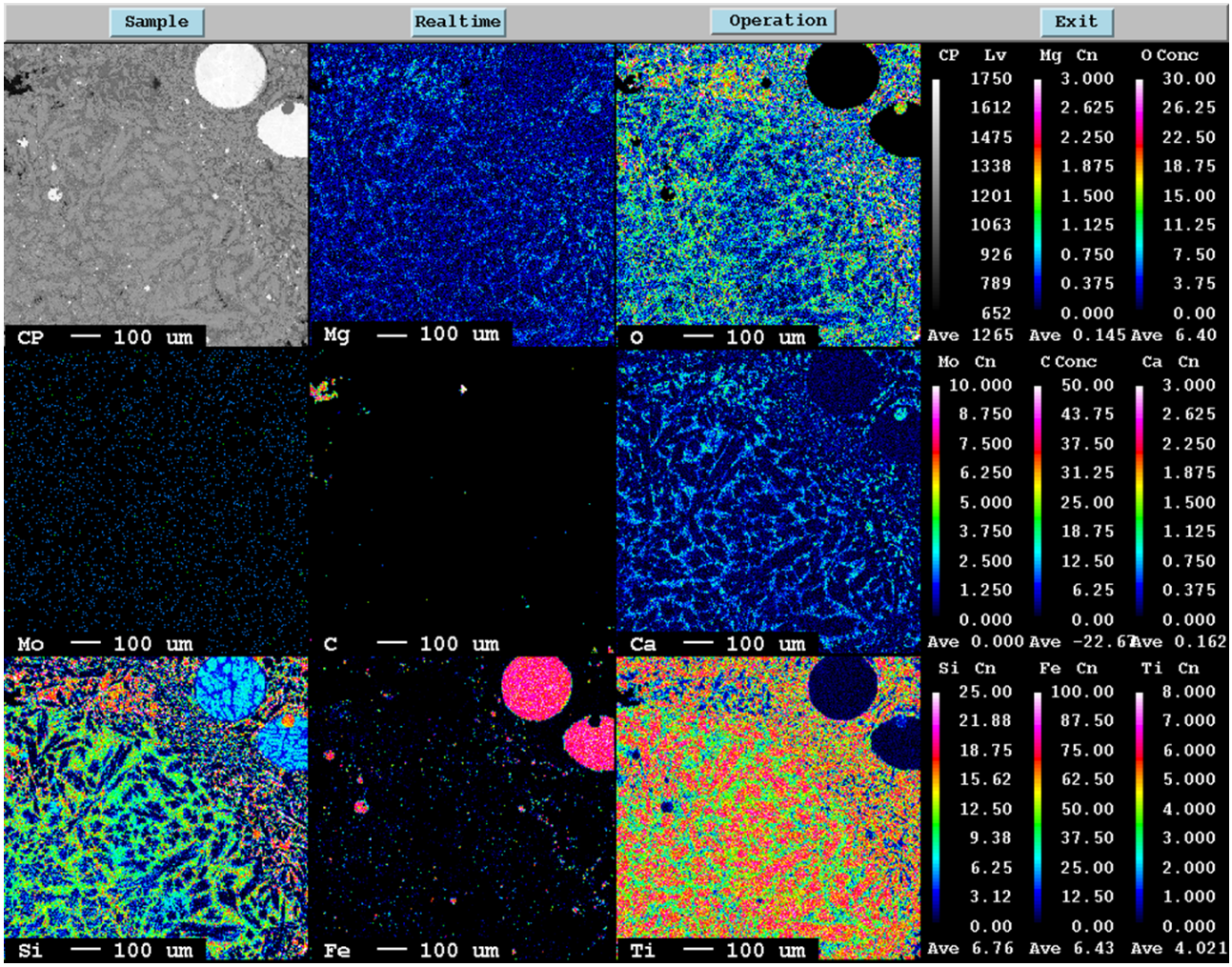

Figure 4.27: EPMA mapping of sample D4, taken in the changing microstructure towards the center of the slag.

The mapping for D4 is taken from the interface between the two microstructures, seen in figure 4.27. The mapping shows the big metallic phases to be Fe with a bit of Si. The Si is also seen to be in larger less concentrated phases at the bottom structure. The Ca follows the Si concentration.

4.3.5 Main findings D-series

Table 4.10: Some of the main findings for the D-series, the experiments using G1 pellets in SiC crucibles.

Findings	**Comments**
Black coloration of the slag	
Climbing of slag in the crucible	High wettability between slag and crucible
A reaction between slag and crucible	Crucibles seen corroded Si seen throughout the slag
Non-melted pellet parts visible in D1_1 and D4	Clear interface between slag and pellet
No pellets visible in D1 and D2	D1 is increased temperature D2 is increased melting time before quench The pellets melt quickly, hard to clearly see pellets
Creation of big metallic iron phases	Gray ring around the bigger ones made of TiC TiC around the edge of the big metallic phase Reduced with the help of the SiC crucible
Si present in the metallic phases near the crucible	Reaction from the crucible
Si also present throughout the slag	

4.4 E-series EPMA analysis and mapping

Table 4.11: Parameters for the E series experiments.

Identification	Pellet	Slag composition	Crucible	Coating	Temperature	Time BQ*
E1	G3	85wt%TiO_2-10wt%FeO-5wt%CaO	SiC	BN	1650 °C	0 min
E2	G3	85wt%TiO_2-10wt%FeO-5wt%CaO	SiC	BN	1600 °C	1 min
E3	G3	85wt%TiO_2-10wt%FeO-5wt%CaO	SiC	BN	1600 °C	3 min
E4	G3	85wt%TiO_2-10wt%FeO-5wt%CaO	SiC	BN	1600 °C	0 min

* Time BQ = Time before quench, it refers to the time after the pellet is dropped before the sample is quenched.

The parameters for the E-series are similar to the ones set for the D series, the difference being the pellet type. Here the G3 pellets are used, these pellets are reduced with both CO and H. 40% Hydrogen and 60% CO, and they achieved a conversion degree of 83%

4.4.1 Experiment E1 (G3(60%CO40%H_2)-SiC-0min-1650)

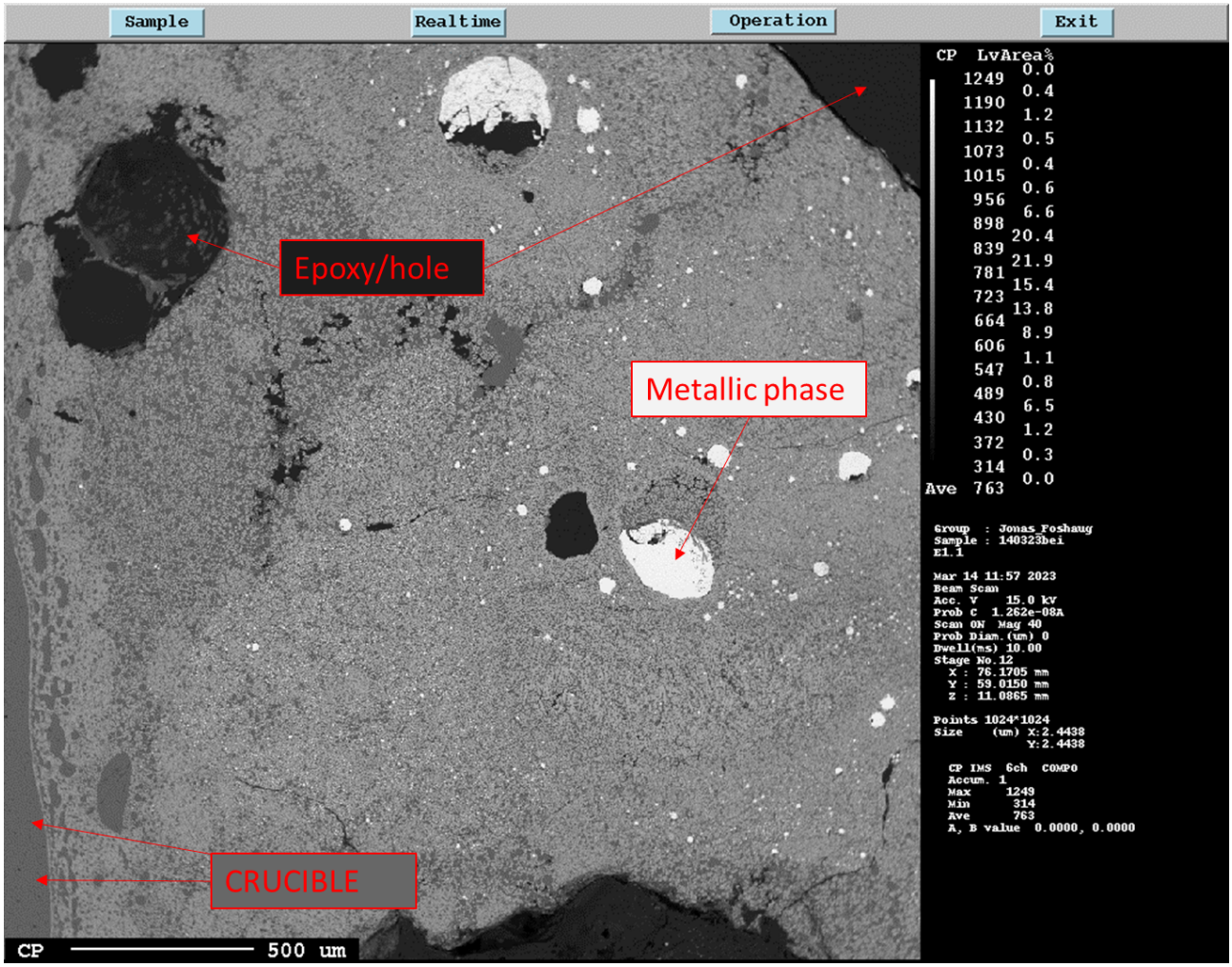

Figure 4.28: An overview EPMA image at 40x zoom of the E1 sample. Here the slag can be seen with the crucible wall to the left.

The slag melt in experiment E1 had climbed in the crucible meaning figure 4.28 shows a sample taken further up in the crucible. The crucible seen to the left is the crucible wall and not the floor. It is seen that this wall has reacted with the slag since the crucible wall is not completely straight. There have been formed big metallic iron phases in the slag, and there seems to be a higher metallic iron concentration away from the crucible. indicating a reduction of iron throughout the slag.

Point analysis

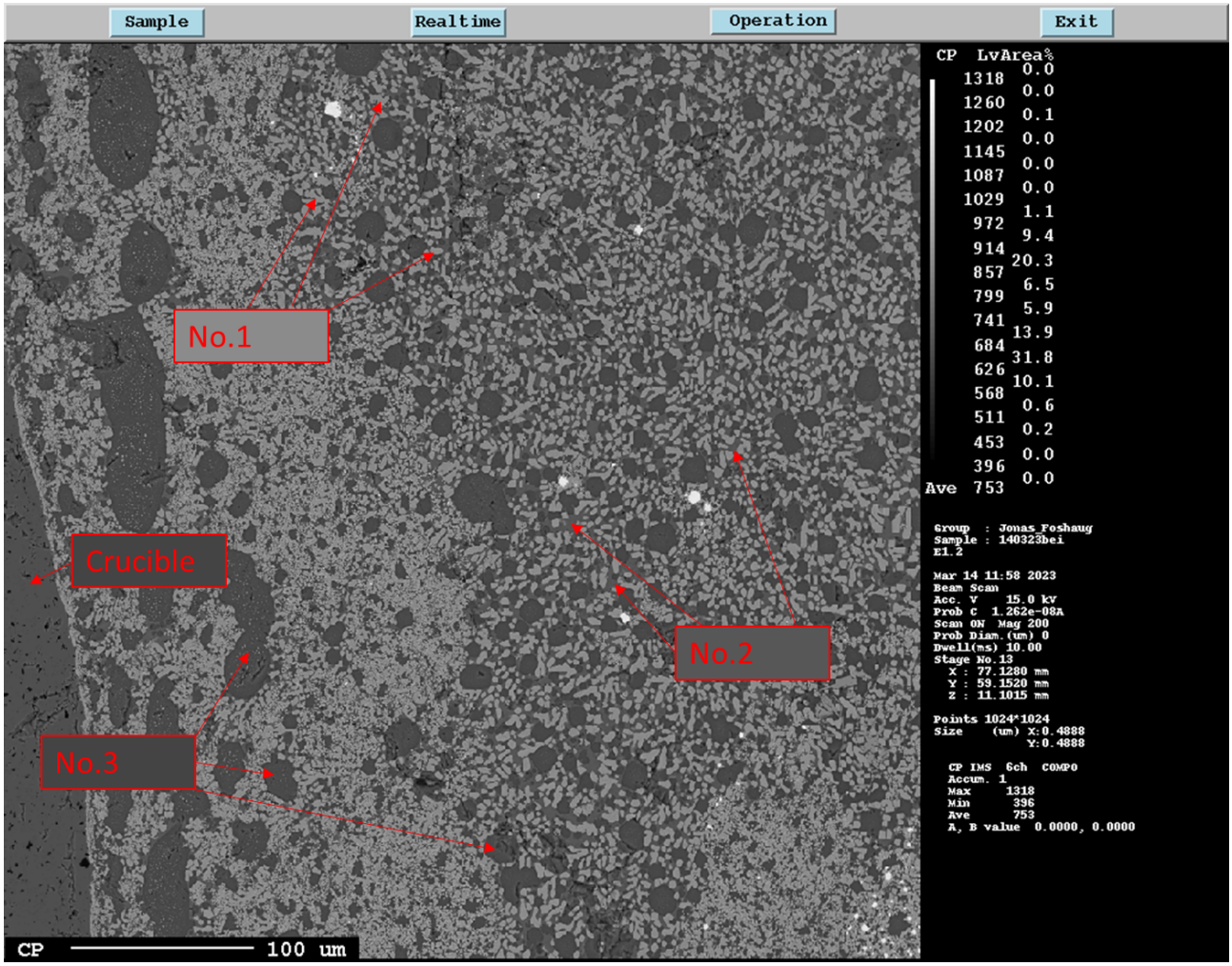

Figure 4.29: EPMA image of E1 at 200x zoom. The drawn in numbers correspond to table 4.12 with the point analysis below.

The point analysis is taken near the crucible border of experiment E1. This is seen in figure 4.13 and 4.12. The light gray No.1 is mainly a Ti phase, and the dark gray No.2 is a mixture of mainly Ca and Si with a bit of Al and Ti. The darkest gray phase is a SiO_2 phase that has come from the crucible. There is almost no FeO in these phases. There are low total values seen in the tables, this might indicate that there is an element/oxide missing in the analysis of the slag phase. It could possibly be a carbide phase.

Table 4.12: Point analysis of different phases on sample E1. Number 1 is an average point analysis of the lightest gray zone. Number 2 is of the darker gray zone, while number 3 is from the darkest zone. Seen more clearly in figure 4.29.

No.	SiO2	MgO	CaO	FeO	Al2O3	TiO2	Total
1	1.830333	0.157	0.881333	0.127333	0.227333	100.2213	103.4447
2	33.84933	0.723333	24.14133	0.092333	7.683	9.563333	76.05267
3	78.03	0.031667	2.004667	0.057333	1.232667	5.802	87.15833

EPMA mapping

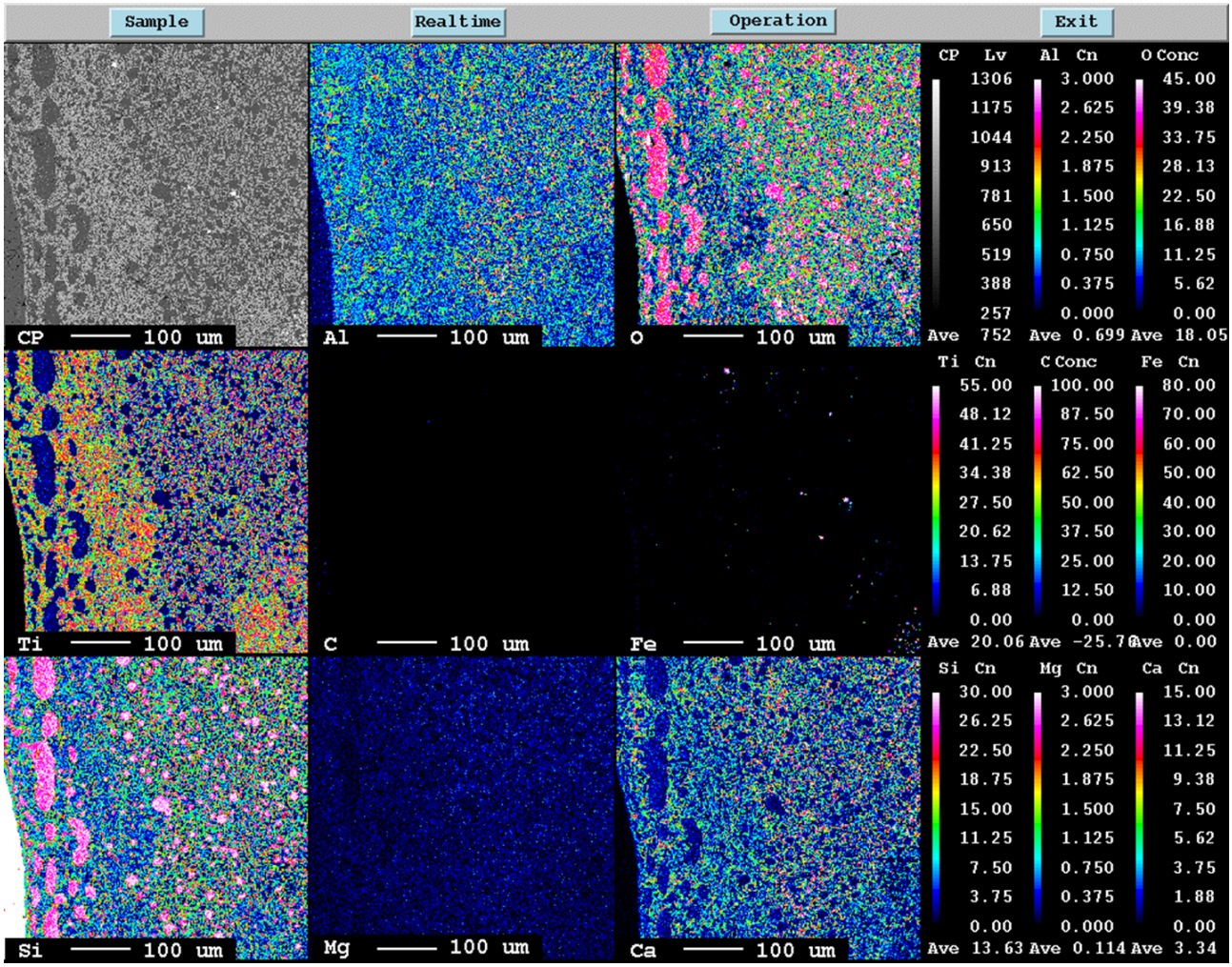

Figure 4.30: EPMA mapping of sample E1, showing the crucible on the left of the image.

The mapping of E1 is taken close to the crucible wall, seen in figure 4.30. The interesting points are a diffusion towards the crucible of the Fe close to the crucible, a SiO_2 phase breaking from the crucible. There is some Mg present further into the slag, indicated by the slight change in color to the right (center) in the picture. Can be argued to be negligible since it is so small when looking at the count of the color for the Mg mapping.

4.4.2 Experiment E2 (G3(60%CO40%H_2)-SiC-1min-1600)

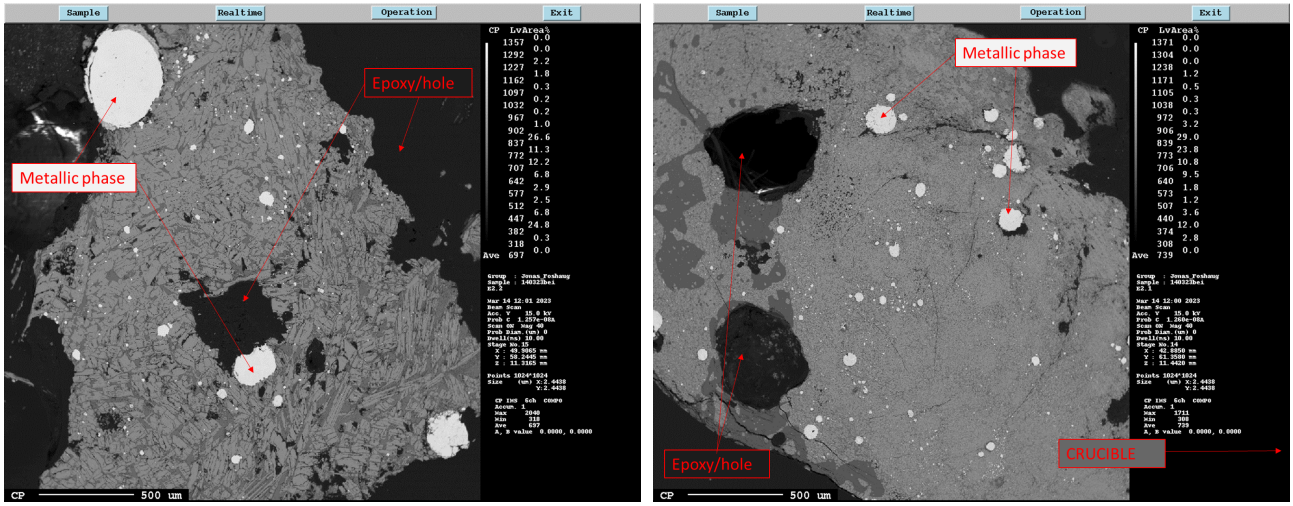

Figure 4.31: Two overview EPMA images at 40x zoom of the E2 sample. Here the crucible floor is further to the right of the right most image. The left image is further into the center of the sample.

The EPMA image for E2 is rotated, meaning the crucible floor is to the right of the images. This can be seen marked in figure 4.31. The left image here is further into the center of the slag. It is seen to be a different mixture of phases further from the crucible floor, seen in the way that the phases in the left image have a more lamellae/plate-like micro-structure. There are huge metallic iron phases created throughout the sample, the white phases in the images.

Point analysis

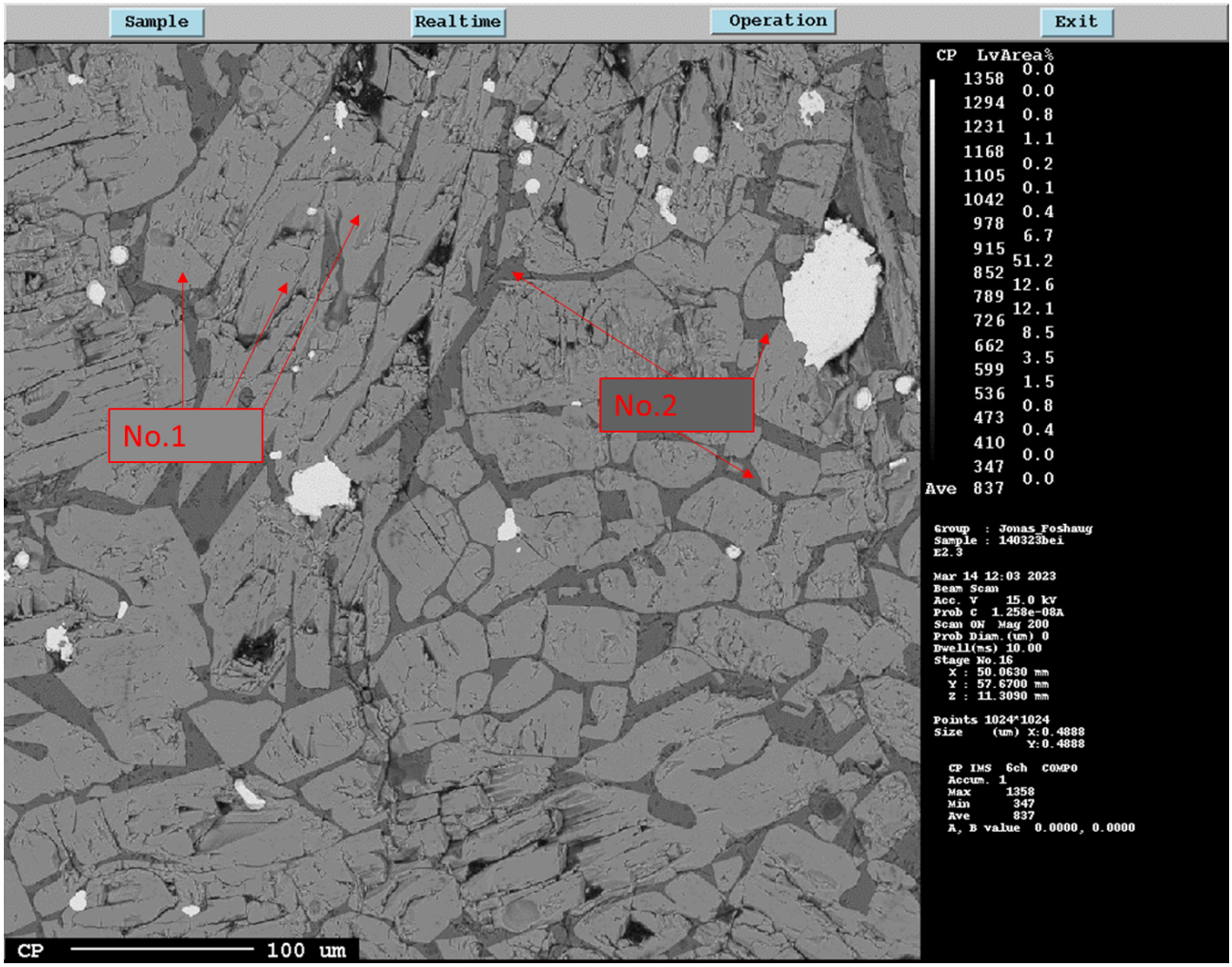

Figure 4.32: EPMA image of E2 at 200x zoom. The drawn in numbers correspond to table 4.13 with the point analysis below.

The point analysis in figure 4.32 shows a point analysis of the part further towards the center of the slag. Meaning the part on the leftmost image in figure 4.31. The points show that the light gray phase mainly contains TiO_2, while the darker gray phase is a mixture of SiO_2 and other elements such as Mg, Ca, and Ti. These points are shown in table 4.13. The point analysis was done for oxide phases, the white metallic phase is a Fe phase, but there is not done an analysis of this.

Table 4.13: Point analysis of different phases on sample E2. Number 1 is an average of point analysis of the lightest gray zone. Number 2 is of the darker gray zone. Seen more clearly in figure 4.32.

No.	SiO2	MgO	CaO	FeO	Al2O3	TiO2	Total
1	0.380667	0.79	0.130667	0.247	0.366333	100.1827	102.0973
2	44.723	6.346333	23.18867	0.805667	2.911	13.35433	91.329

EPMA mapping

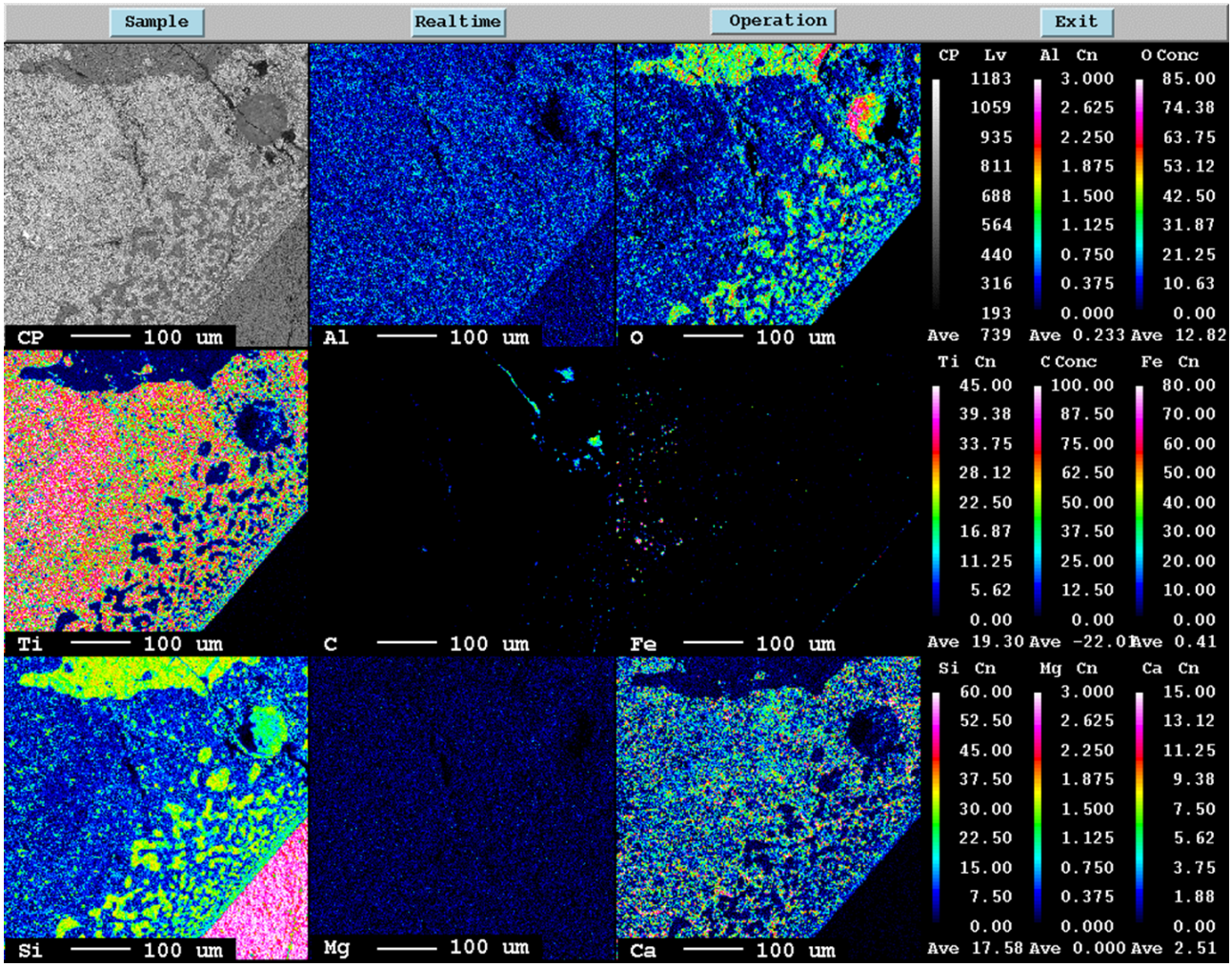

Figure 4.33: EPMA mapping of sample E2, showing the crucible in the bottom right corner of the image.

The mapping for E2 was taken near the crucible border, Seen in figure 4.33. Some interesting findings of this mapping are the diffusion of Fe towards the crucible border. The Mg mapping also shows a lack of Mg near the crucible. There is also seen a major reaction between crucible and slag. The Si from the SiC has reacted with O and created phases in the slag. Shown in the Si mapping.

4.4.3 Experiment E3 (G3(60%CO40%H_2)-SiC-3min-1600)

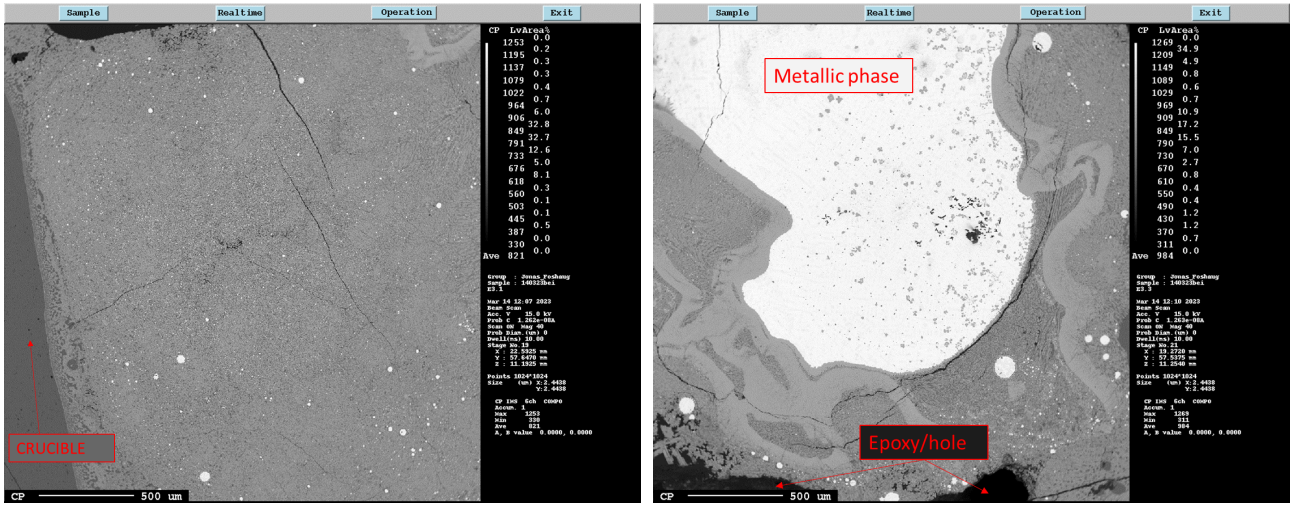

Figure 4.34: Two overview EPMA images at 40x zoom of the E3 sample. Here the crucible floor is seen on the left image. The right image shows a huge metallic phase formed further into the centre of the sample.

The images in figure 4.34 are rotated since the crucible floor is located to the left. In the image, there is seen a massive metallic phase created further to the center of the slag. This metallic phase has a ring around it with a lighter gray color.

Point analysis

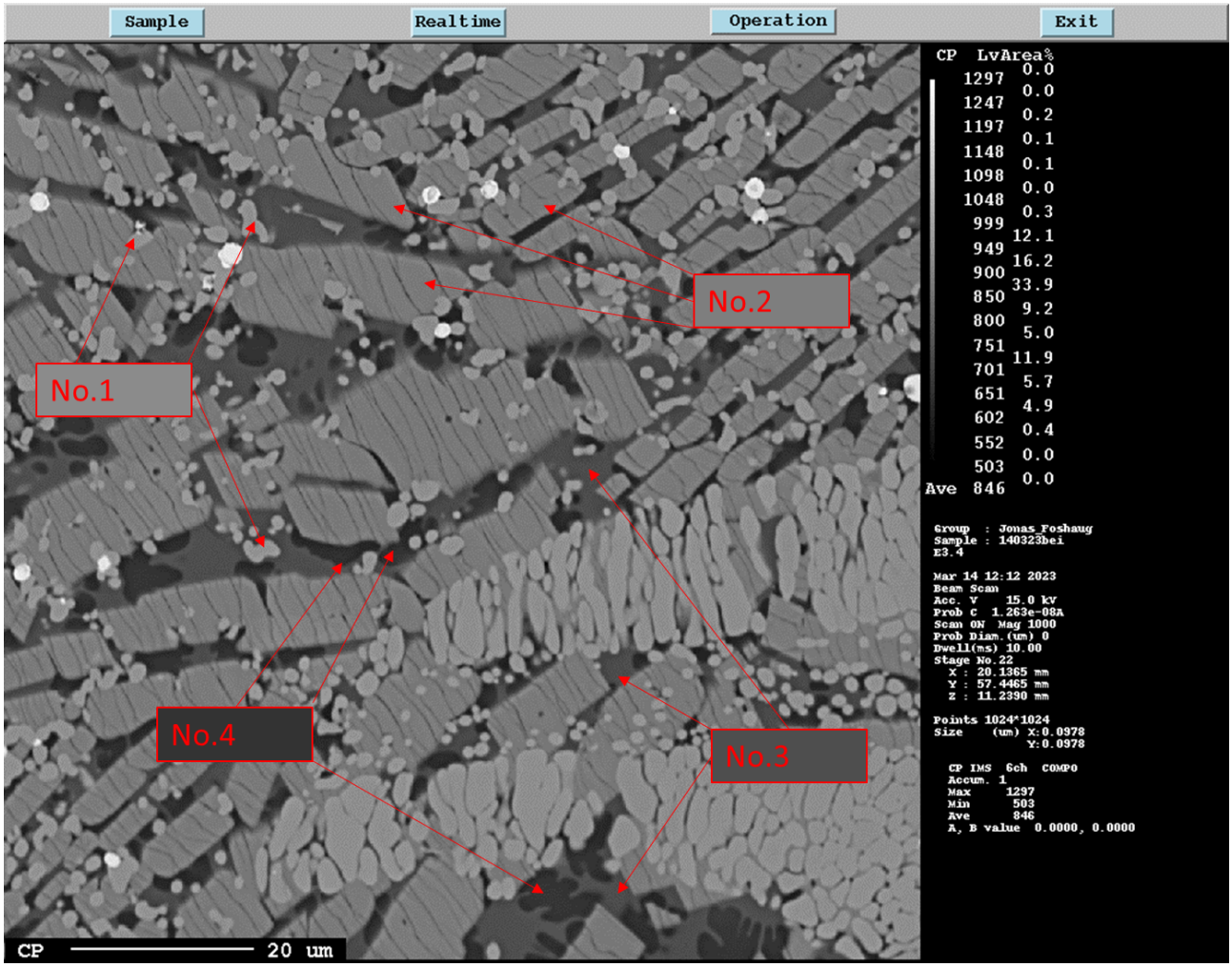

Figure 4.35: EPMA image of E3 at 1000x zoom. The drawn in numbers correspond to table 4.14 with the point analysis below.

Figure 4.35 shows a 1000x magnification of the E3 experiment. Here it is seen 4 different oxide phases, all marked and point analyzed as seen in table 4.14. The lightest phases, No.1 and No.2 show a phase consisting mainly of Ti. No.1 is likely a carbide phase while No.2 is likely an oxide phase. Argued by the total value of 136.0187 for phase No.1. This higher total value argues for it being a carbide phase since the point analysis search for TiO_2, not TiC. Phase No.3 is a mixture between Si, Ca, Mg, Al, and Ti. Phase number 4 consists of SiO_2 and a small amount of Ti. Because of the high magnification, the possibility of contamination from other phases in these point analyses is not negligible.

Table 4.14: Point analysis of different phases on sample E3. Number 1 is an average point analysis of the lightest gray zone. Number 2 is of the darker light gray zone. Number 3 is the darkest gray zone and number 4 is the black zone. Seen more clearly in figure 4.35.

No.	SiO2	MgO	CaO	FeO	Al2O3	TiO2	Total
1	0.292667	0.014	0.43	0.299667	0.042667	134.9397	136.0187
2	0.618667	0.183333	0.394	0.113333	0.277333	100.6013	102.188
3	45.79833	2.495	26.59167	0.091667	3.415333	14.61333	93.00533
4	82.50667	0.148667	1.396667	0.043333	0.507	15.84233	100.4447

EPMA mapping

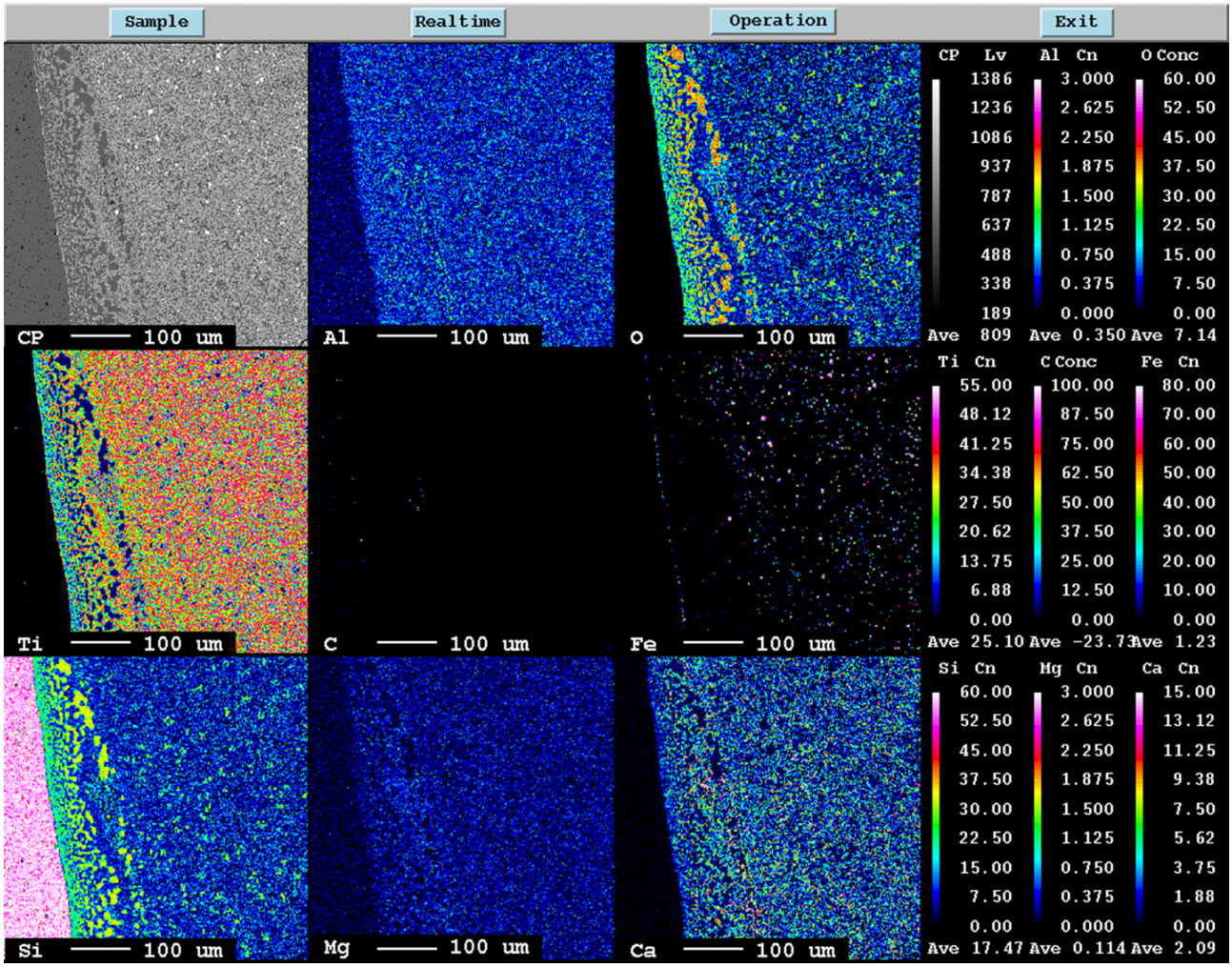

Figure 4.36: EPMA mapping of sample E3, showing the crucible on the left in the image.

The mapping of E3 is taken from the crucible border. Shown in figure 4.36, here the crucible floor is on the left. A reaction between the crucible and the slag is seen in the Si mapping, a SiO_2 phase created near the crucible. The iron can be seen diffusing to the crucible border, with a lack of iron near the crucible before it gets more homogenous further out.

4.4.4 Experiment E4 (G3(60%CO40%H_2)-SiC-0min-1600)

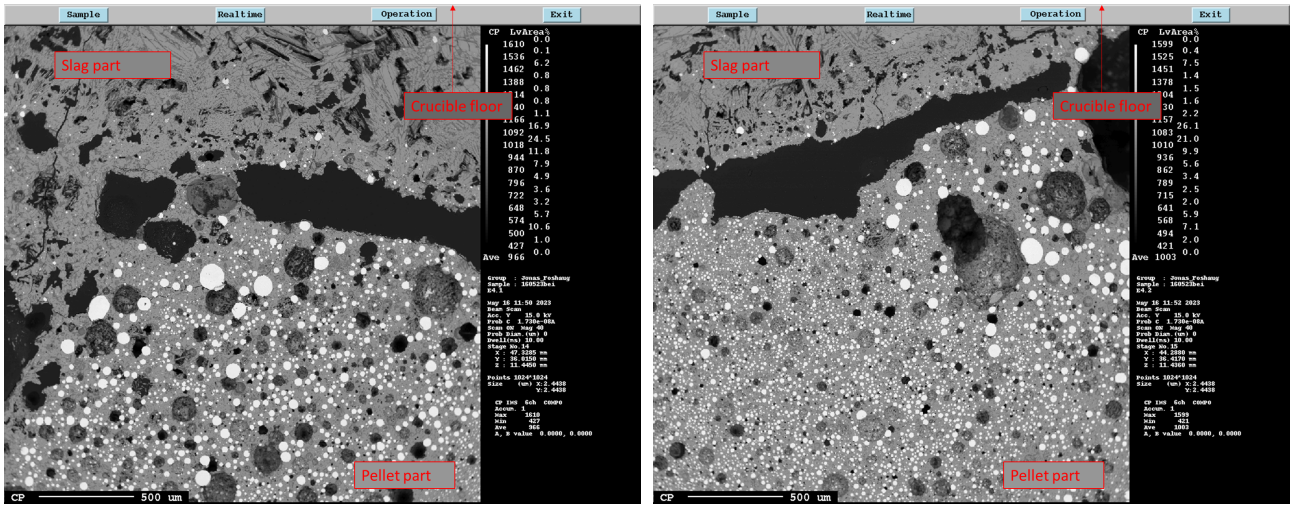

Figure 4.37: Two overview EPMA images at 40x zoom of the E4 sample. Here the crucible floor is further upward in the images, indicated by arrows in the images. The bottom part with all the metallic phases is the pellet part, while the top part is the slag.

The overview images seen in figure 4.37 give a clear indication of the difference between the slag and the pellet. The bottom part of the images shows the pellet part, with a big amount of metallic iron phases. The top part is the slag, it is seen to have a lamellae/plate-like structure further up. Above the Epoxy/hole, the pitch black part, it is seen that the pellet has reacted with the slag, just broken off where this cross section is taken from.

EPMA mapping

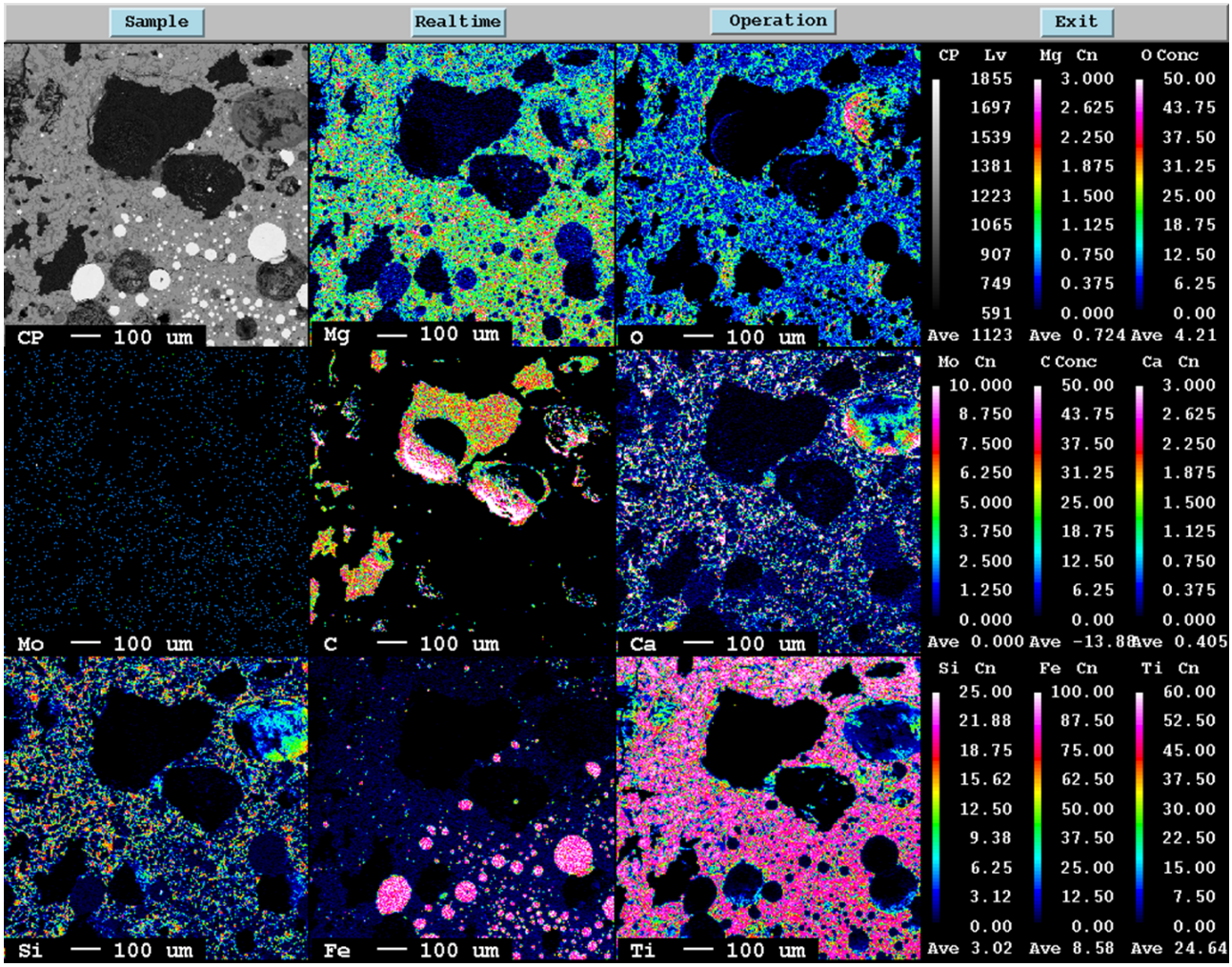

Figure 4.38: EPMA mapping of sample E4, showing the interface between pellet and slag.

The mapping of the intersection for experiment E4 can be seen taken from the leftmost image in figure 4.37. At least it can be believed to be the interface, however, it is possible it is still part of the pellet, just melted further. It can be a bit hard to see but the mapping shows a higher Mg concentration the closer you get to the pellet. The top of the Mg mapping shows a decrease in concentration. The Mo is irrelevant here and only included due to it being analyzed at the same time as the H series. The Si is also seen being non-existent in the big metallic iron phases.

4.4.5 Main findings E-series

Table 4.15: Some of the main findings for the E-series, the experiments using G3 pellets in SiC crucibles.

Findings	**Comments**
Black coloration of the slag	
Climbing of slag in the crucible	High wettability between slag and crucible
A reaction between slag and crucible	Crucibles seen corroded Si seen throughout the slag
Non-melted pellet parts visible in E4	Clear interface between slag and pellet Pellet part full of smaller metallic iron phases (spheres)
No pellets visible in E1, E2 and E3	E1 is increased temperature E2 and E3 is increased melting time before quench
Creation of big metallic iron phases	Gray ring around the bigger ones made of TiC TiC around the edge of the big metallic phase Reduced with the help of the SiC crucible
Si present in the metallic phases near the crucible	Reaction from the crucible Si not present in metallic phases near and in pellet
Si also present throughout the slag	Si-O phases

4.5 F-series EPMA analysis and mapping

Table 4.16: Parameters for the F series experiments.

Identification	Pellet	Slag composition	Crucible	Coating	Temperature	Time BQ*
F1	G6	85wt%TiO_2-10wt%FeO-5wt%CaO	SiC	BN	1650 °C	0 min
F2	G6	85wt%TiO_2-10wt%FeO-5wt%CaO	SiC	BN	1600 °C	1 min
F3	G6	85wt%TiO_2-10wt%FeO-5wt%CaO	SiC	BN	1600 °C	3 min
F4	G6	85wt%TiO_2-10wt%FeO-5wt%CaO	SiC	BN	1600 °C	0 min

* Time BQ = Time before quench, it refers to the time after the pellet is dropped before the sample is quenched.

The parameters for the F-series are similar to the ones set for the D-series and E-series, the difference being the pellet type. Here the G6 pellets are used, these pellets are reduced with 100% hydrogen, and they achieved a conversion degree of 113%.

4.5.1 Experiment F1 (G6(100%H_2)-SiC-0min-1650)

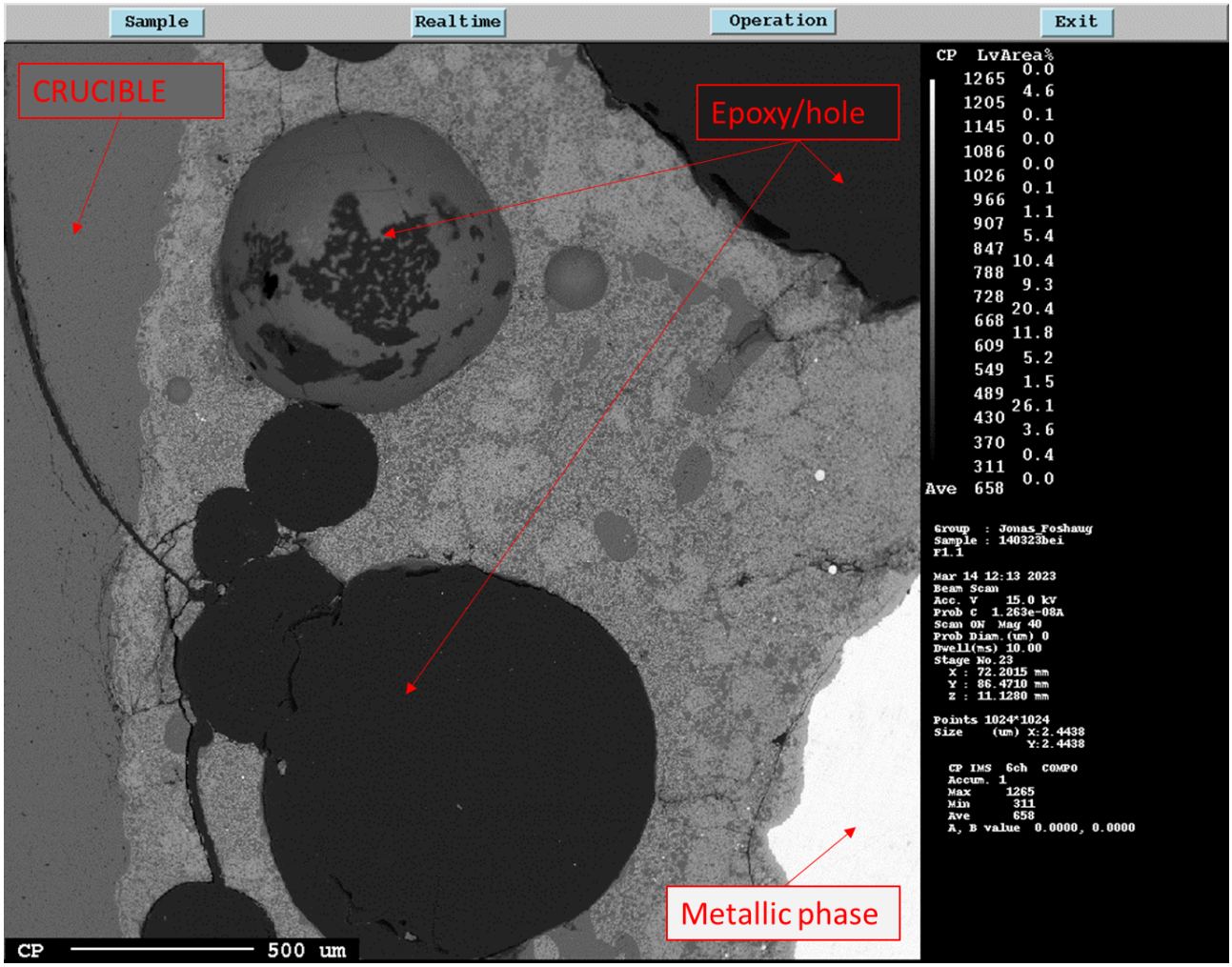

Figure 4.39: An overview EPMA image at 40x zoom of the F1 sample. Here the slag can be seen with the crucible floor to the left. And a big metallic iron phase further towards the center of the sample.

For figure 4.39 the image is rotated, with the crucible floor being to the left. The slag is seen on top with a huge metallic phase present. The crucible seems to be corroded by the slag, noticeable by the rough crucible border.

EPMA mapping

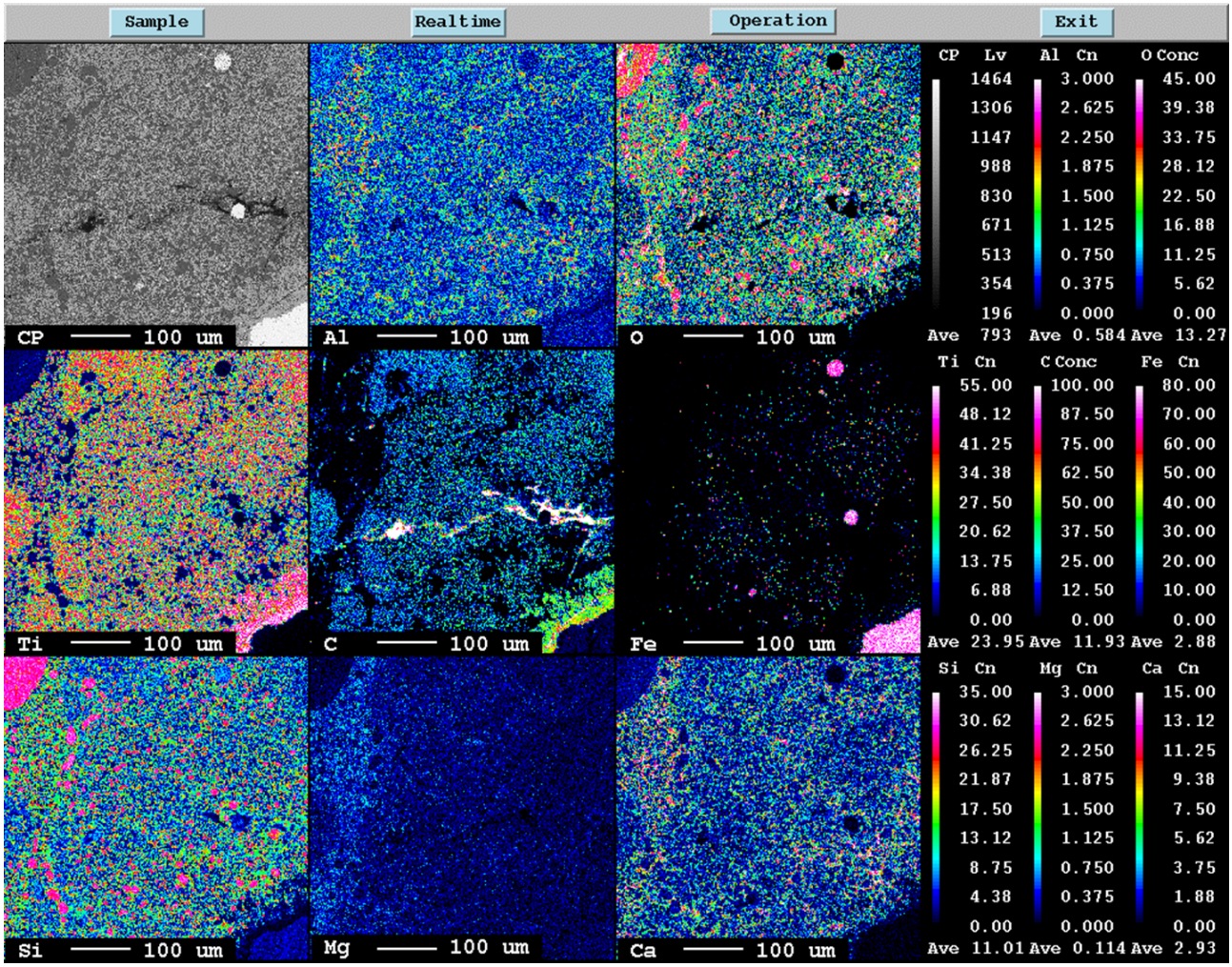

Figure 4.40: EPMA mapping of sample F1, from an image in the centre of the sample.

The mapping of sample F1 seen in figure 4.40 shows a mapping taken near the huge metallic phase. This metallic phase can be spotted in the bottom right corner of the image. In the mapping, a higher concentration of Ti and C is seen close to the metallic phase. Meaning it likely is a TiC phase created, the C concentration seems to follow the Ti concentration. This gives a TiC phase throughout. In the top left, there is a SiO_2 phase, it also looks to be a tiny amount of Si present in and around the metallic phase.

4.5.2 Experiment F2 (G6(100%H_2)-SiC-1min-1600)

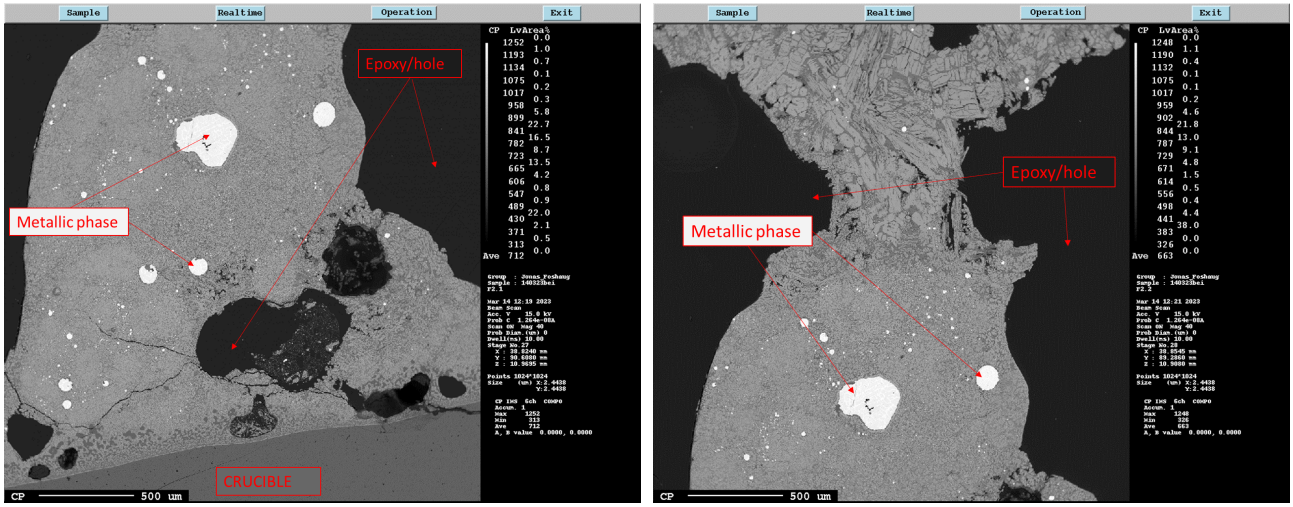

Figure 4.41: Two overview EPMA images at 40x zoom of the F2 sample. Here the crucible floor is seen on the bottom of the left image. The right image shows the sample further towards the centre.

The images in figure 4.41 show the slag from the crucible towards the center. Towards the center the microstructure changes to more of a lamellae/plate-like structure. The crucible is seen reacting with the slag, a SiO_2 phase is one of the resulting products.

EPMA

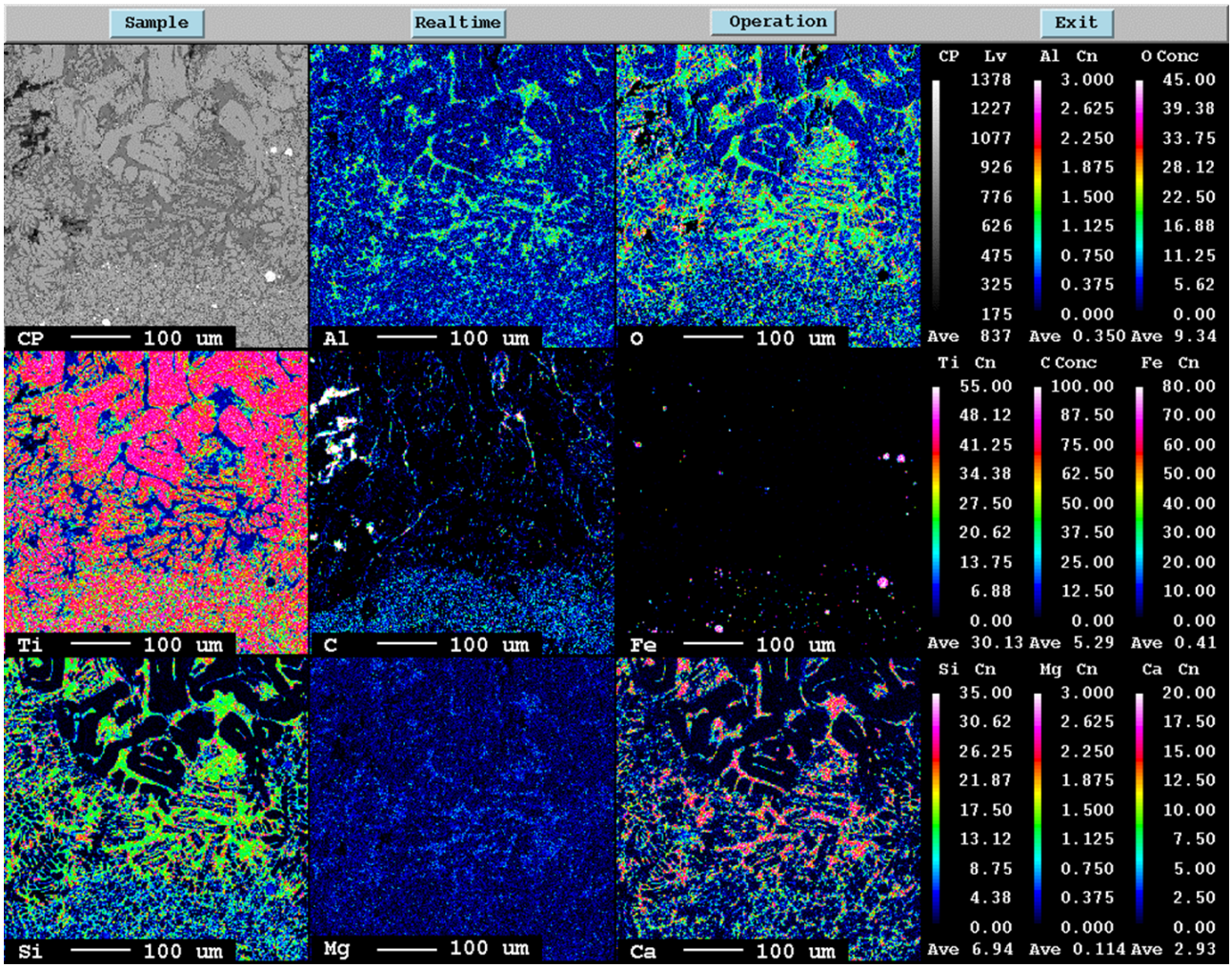

Figure 4.42: EPMA mapping of sample F2, from an image in the centre of the sample.

The mapping of sample F2 is taken from the interface between the two different microstructures seen in figure 4.41. This mapping, figure 4.42, shows that there is a vast difference in Si, C, and Fe concentrations between these structures. The carbon is seen a lot more in the lower structure, this indicates a TiC phase. The darker phase in the upper part seems to be mainly consisting of Si, Ca, and O. In the upper structure, the Ti looks to be in a TiO_2 phase.

4.5.3 Experiment F3 (G6(100%H_2)-SiC-3min-1600)

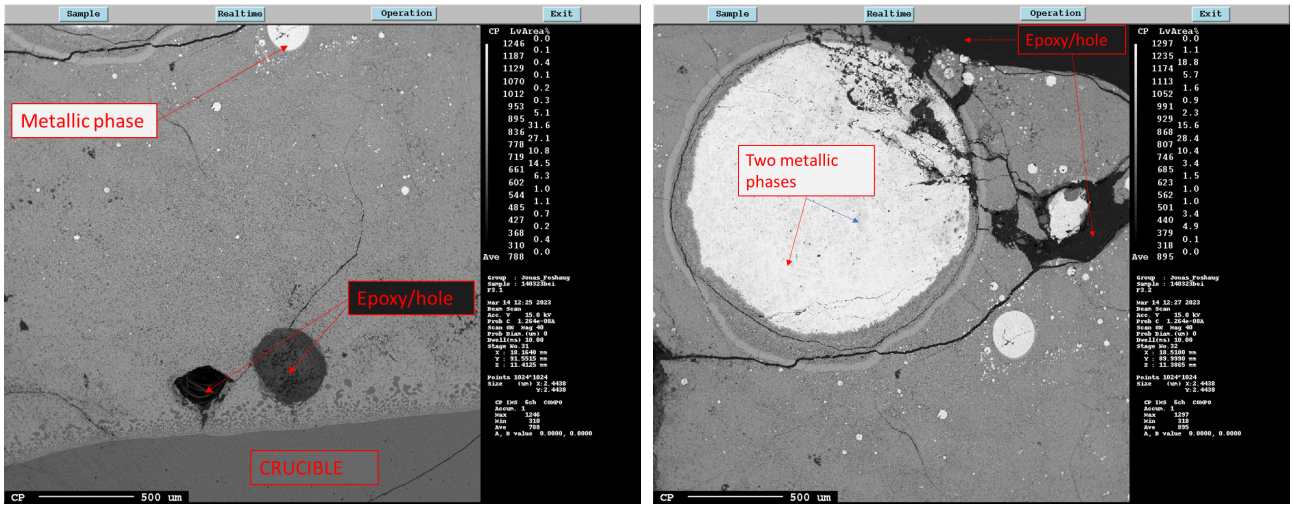

Figure 4.43: Two overview EPMA images at 40x zoom of the F3 sample. Here the crucible wall is seen on the bottom of the left image. The right image shows the sample further towards the centre, with a huge metallic iron phase.

The images in figure 4.43 show the slag on top of the SiC crucible. Further into the slag a metallic iron phase has formed, and around this phase, a light gray ring can be seen. The white metallic phase consists of two phases when looked at more closely, most likely different concentrations of Si.

EPMA mapping

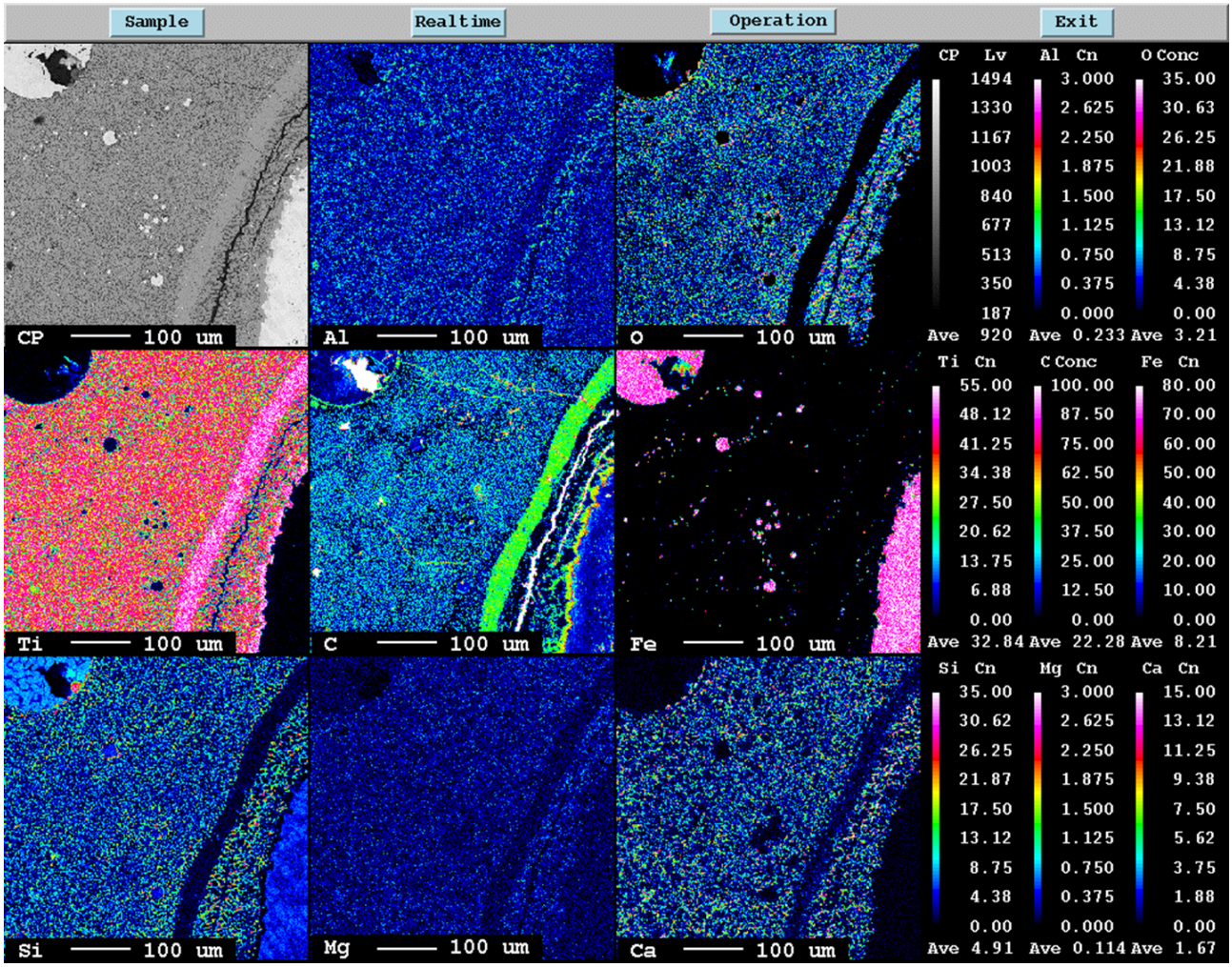

Figure 4.44: EPMA mapping of sample F3, from an image in the center of the sample.

The mapping of the F3 sample is taken close to the ring seen around the huge metallic phase. This mapping, figure 4.44, shows the ring around the metallic phase to be a TiC phase. There is also a TiC phase near the edge of the big metallic Fe phase. Looking at the smaller Fe phase in the top left it is easy to see that there are two iron phases with varying concentrations of Si. This is seen in the Si mapping.

4.5.4 Experiment F4 (G6(100%H_2)-SiC-0min-1600)

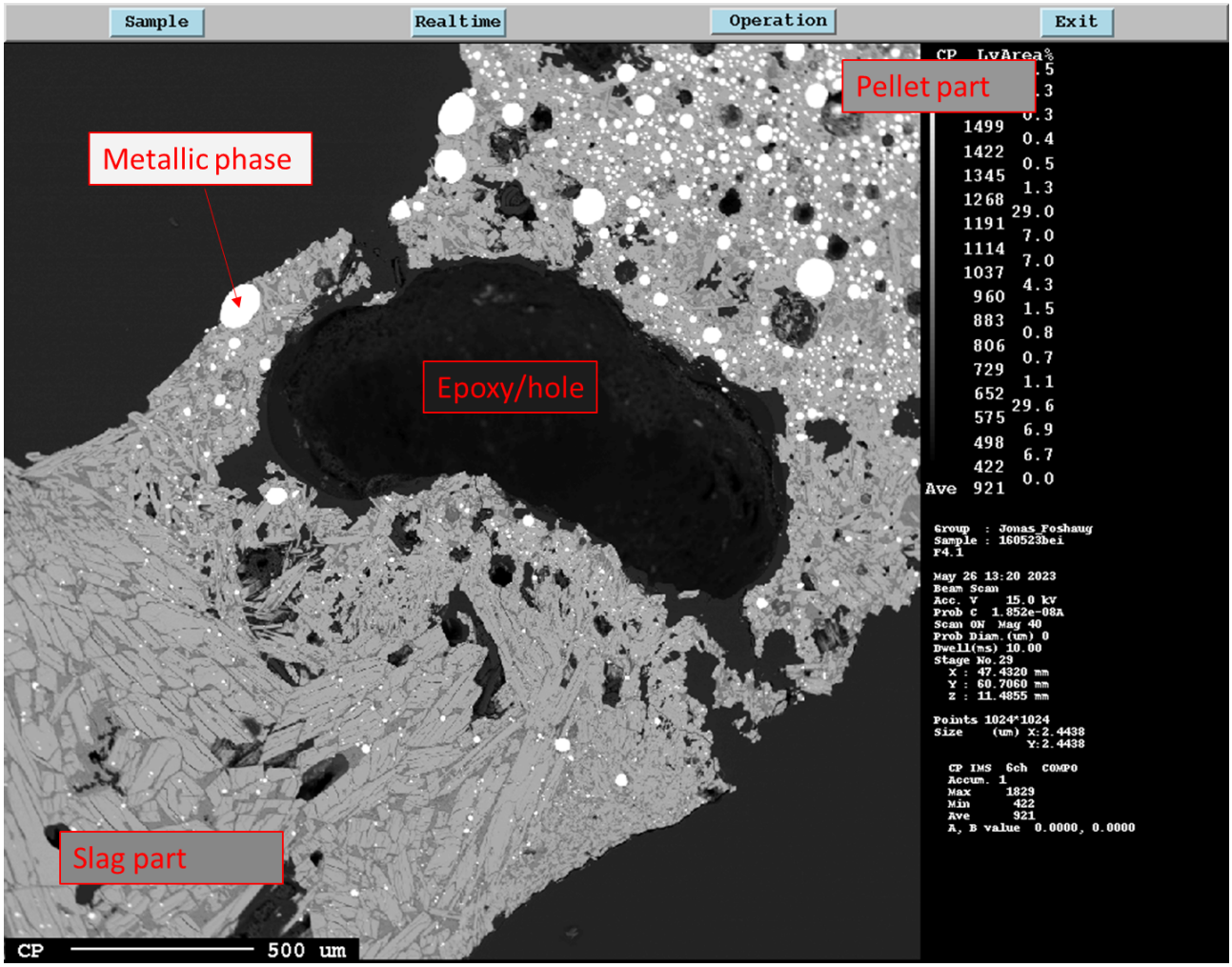

Figure 4.45: An overview EPMA image at 40x zoom of the F4 sample. Taken from the interface between slag bottom left and pellet top right.

The EPMA analysis for F4 (G6(100%H_2)-SiC-0min-1600) is taken quite far up in the crucible since the slag had climbed up, figure 4.45. The slag can be seen in the bottom left while the slag is in the top right. There is a huge structural difference between the pellet and the slag. The slag looks plate/lamellae-like, while the pellet is dominated by metallic phase iron.

EPMA mapping

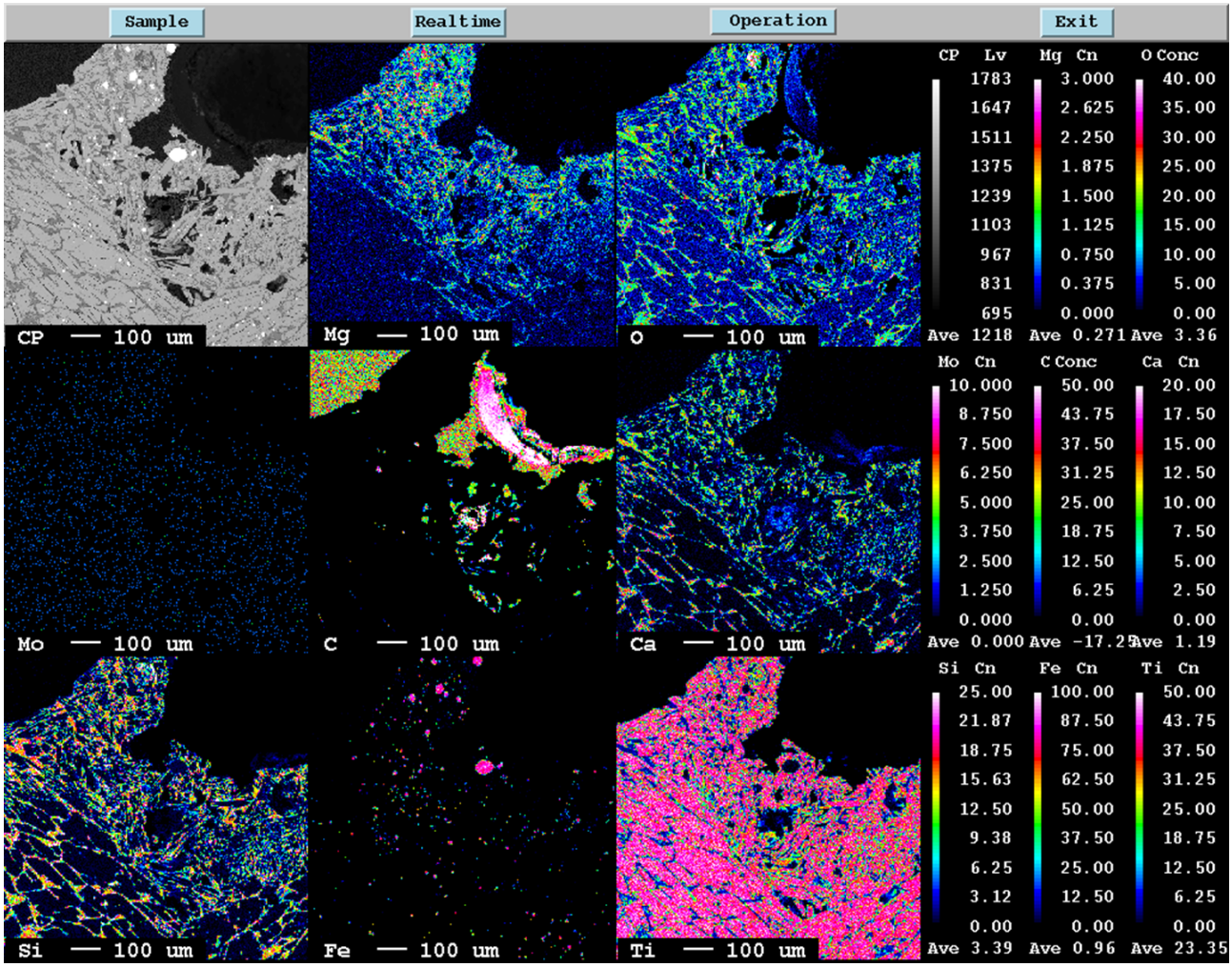

Figure 4.46: EPMA mapping of sample F4, from an image showing the interface between slag and pellet.

The mapping for F4 shows a closer look at the interface between pellet and slag, figure 4.46. One interesting mapping is the Mg mapping, since the Mg only originates from the pellet it is possible to see how far the reaction has gone. The big metallic phases in the pellet part have no inclusion of Si. The carbon mapping only shows a presence in the epoxy parts. There are some presence of all the phases in the black part in the top right, this is due to the black part not being filled with epoxy, it is just a hole, meaning there is some interference from the surface at the bottom of the hole.

4.5.5 Main findings F-series

Table 4.17: Some of the main findings for the F-series, the experiments using G6 pellets in SiC crucibles.

Findings	**Comments**
Black coloration of the slag	
Climbing of slag in the crucible	High wettability between slag and crucible
A reaction between slag and crucible	Crucibles seen corroded Si seen throughout the slag
Non-melted pellet parts visible in F4	Clear interface between slag and pellet Pellet part full of smaller metallic iron phases (spheres) Pellet not seen in the macro image due to being cut out
No pellets visible in F1, F2 and F3	F1 is increased temperature F2 and F3 is increased melting time before quench
Creation of big metallic iron phases	Gray ring around the bigger ones made of TiC TiC around the edge of the big metallic phase Reduced with the help of the SiC crucible
Si present in the metallic phases near the crucible	Reaction from the crucible Si not present in metallic phases near and in pellet
Si also present throughout the slag	Si-O phases

4.6 H-series EPMA analysis and mapping

Table 4.18: Parameters for the H series experiments.

Identification	Pellet	Slag composition	Crucible	Coating	Temperature	Time BQ*
H1	A1 (CO)	85wt%TiO_2-10wt%FeO-5wt%CaO	Molybdenum	-	1600 °C	0 min
H2	A2 (H2)	85wt%TiO_2-10wt%FeO-5wt%CaO	Molybdenum	-	1600 °C	0 min

* Time BQ = Time before quench, it refers to the time after the pellet is dropped before the sample is quenched.

For the H series of experiments, there are some changes to the parameters. These changes are a different crucible type, a Molybdenum crucible, and the A1 and A2 pellets. A1 is 100% CO reduced and A2 is 100% H2 reduced. For these experiments, it was used around 1 g pellet in the drop. The pellets that fit in the TF2 setup were about 0.5 g each and there was space for at least 2 pellets in the drop. There was the possibility for more, but it would just increase the risk of jamming in the dropper tube. The conversion degrees were 76% for A1 and 61% for A2.

4.6.1 Experiment H1 (A1(100%CO)-Mo-0min-1600)

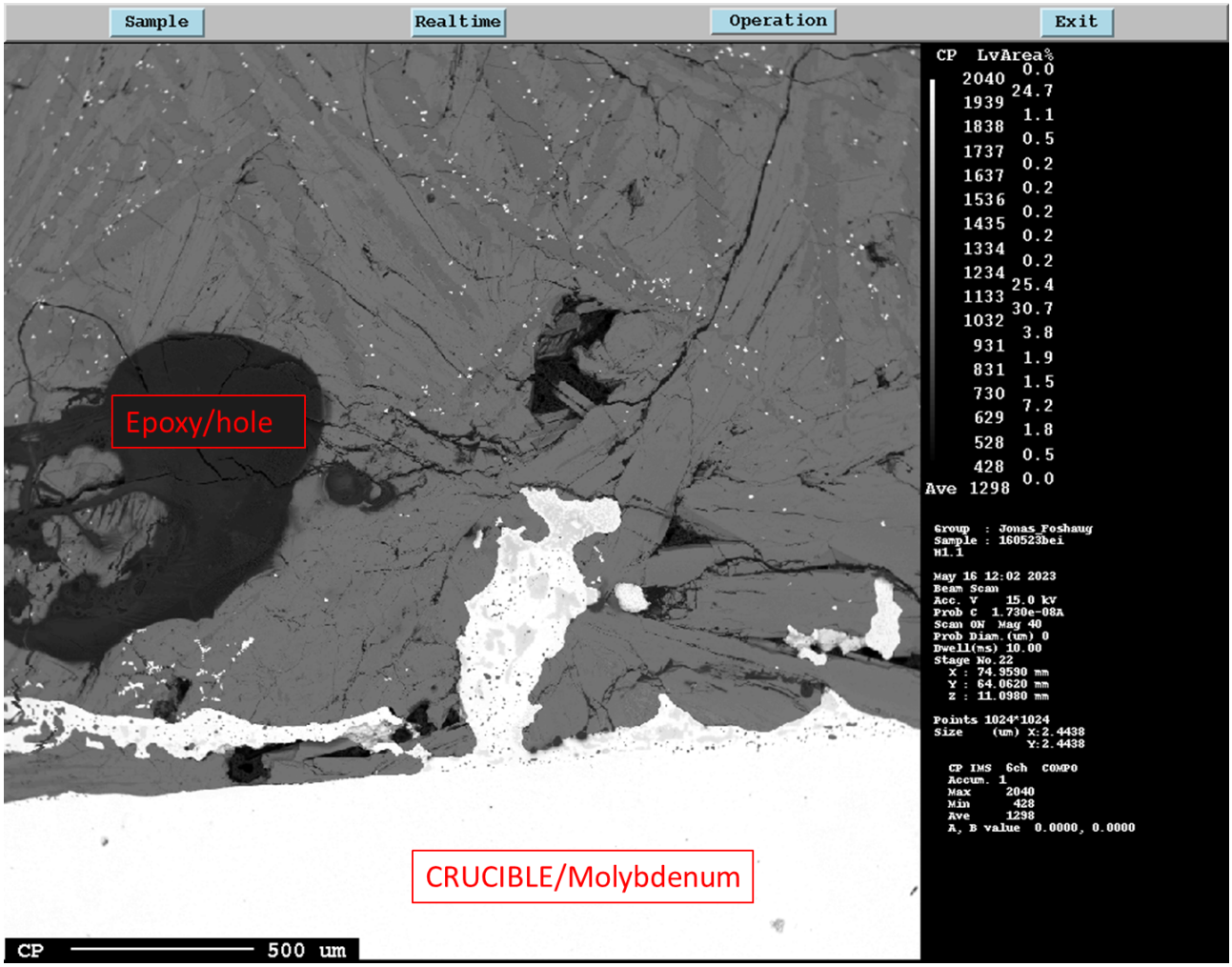

Figure 4.47: EPMA image at 40x zoom for experiment H1.

The EPMA for the H1 experiment is shown in figure 4.47. There is a reaction with the molybdenum crucible, where parts of it can be seen reacting into the slag, the big white metallic phase. The white phases seen in the EPMA images for the H series will no longer be metallic iron but instead they will be Mo phases, since Mo has a much larger atom number. There seems to be two oxide phases in the slag, that have formed in a plate-like structure. These are the light gray and dark gray phases.

Point analysis

For the point analysis, there can be seen three distinct phases in the slag part, the white metallic one, the light gray one, and the dark gray one. The results of these point analysis can be seen in the tables 4.19 and 4.20. The results show the metallic phase to be mostly Mo with a small amount of Fe. The light gray phase is a Ti phase containing Fe, while the dark phase is a mainly Ti-containing phase. The analysis for the gray phases did not include Mo, this is likely an error since it can be seen in metallic phases throughout the sample.

Table 4.19: Point analysis of the white metallic phases seen in the slag fro H1.

Si	P	C	Fe	Ti	Mo	Total
0	0.388	0	4.215	0.757	95.018	100.378

Table 4.20: Point analysis of the gray phases seen in the slag from H1.

Identification	SiO2	MgO	FeO	CaO	Al2O3	TiO2	Total
Light gray	0.005	0.148	17.524	0.21	0.267	83.465	101.619
Dark gray	0.022	0.016	2.204	0.274	0.051	97.097	99.664

EPMA mapping

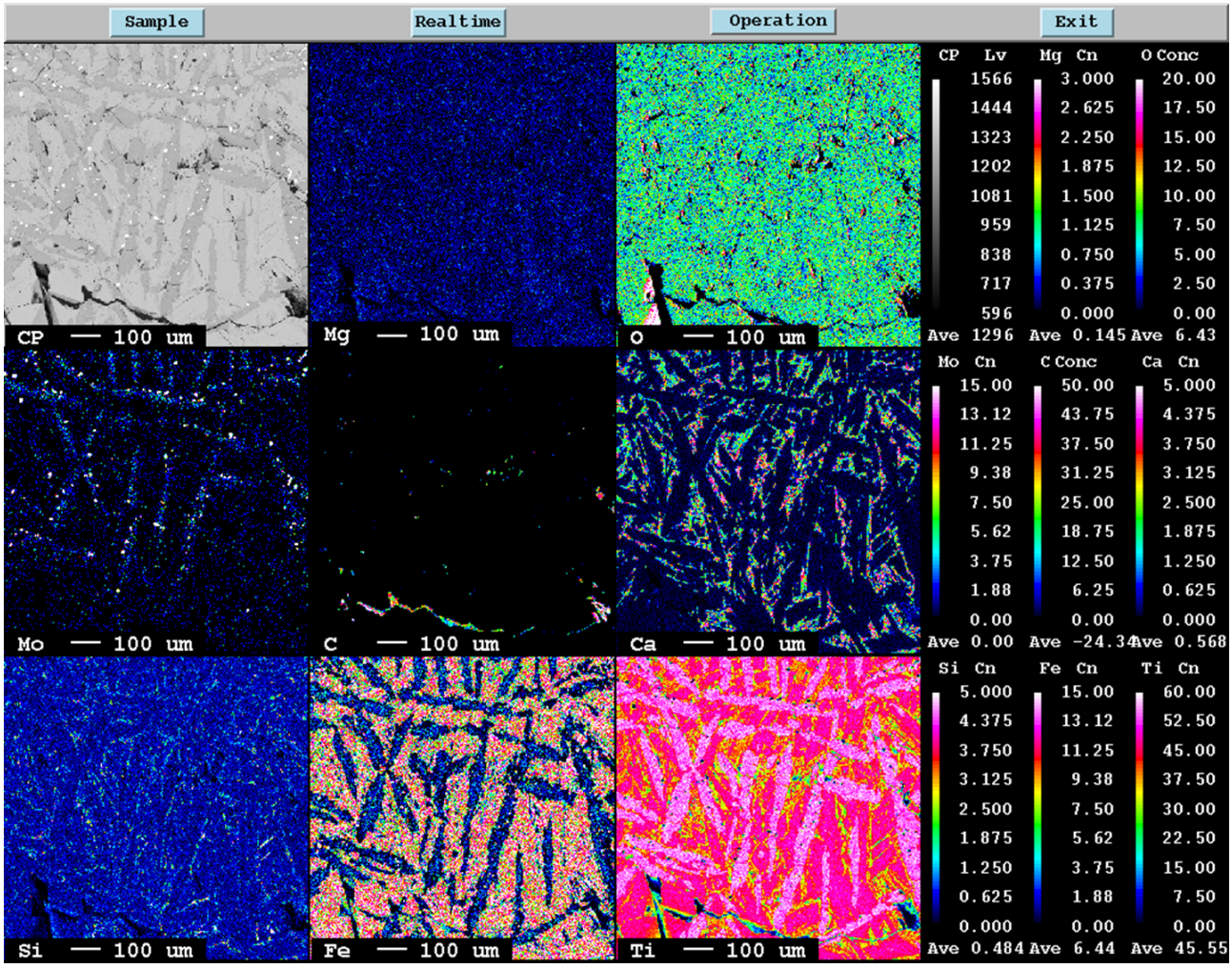

Figure 4.48: EPMA mapping of sample H1, from an image in the center of the sample.

Looking at the mapping of the H1 experiment, seen in figure 4.48, there can be seen three major oxide phases, the two gray phases discussed earlier, and a phase including Ca. More easily seen in the Ti map, light pink, dark pink, and yellow. Mo can be seen present in one of the phases together with Ti, and the metallic phases seem to be only present in and near this phase. The Fe mapping shows the lack of Fe in this Mo-Ti phase but there seems to be some Fe present in the metallic phase. This is difficult to spot since these phases are so small, but it was picked up in the point analysis.

4.6.2 Experiment H2 (A2(100%H_2)-Mo-0min-1600)

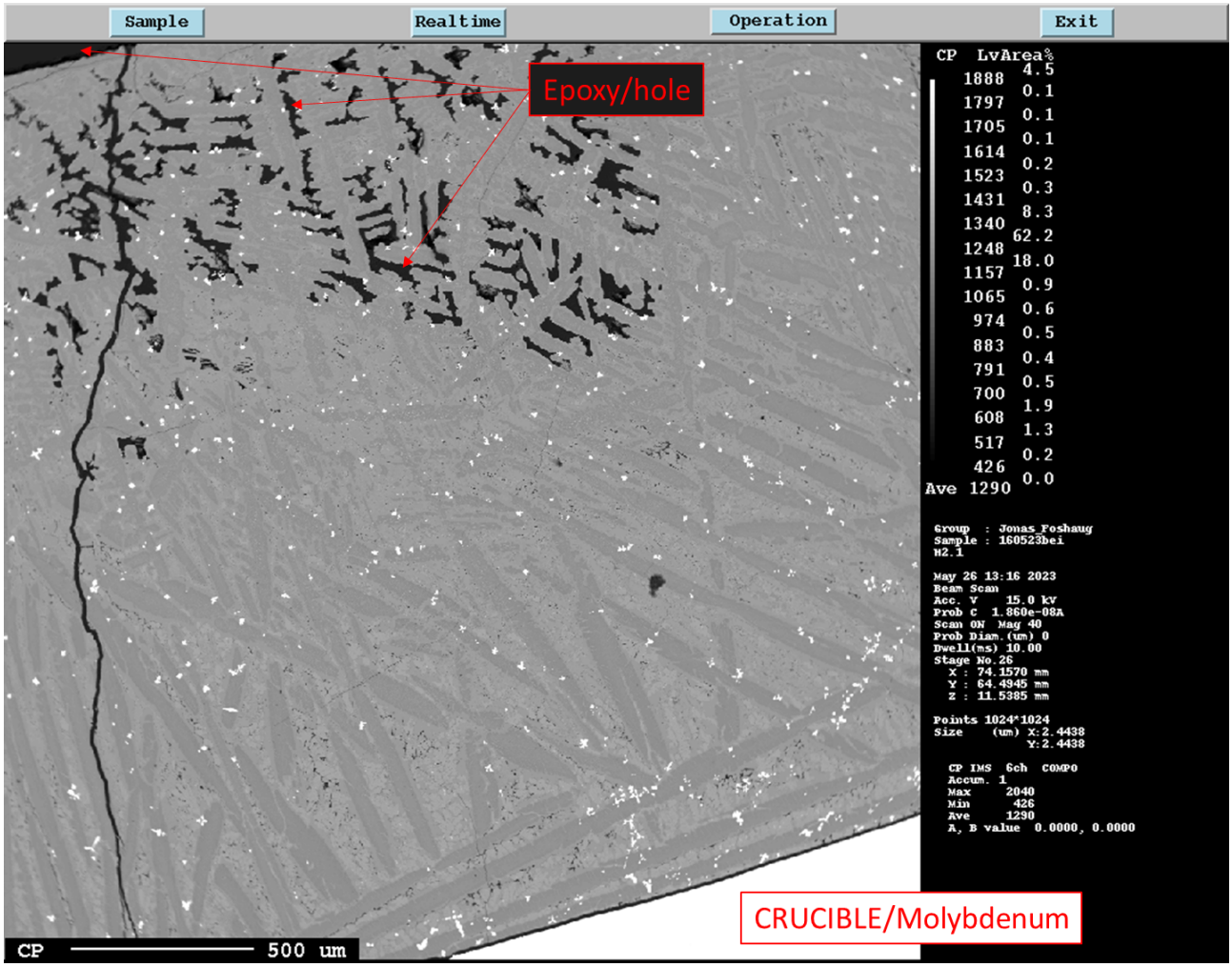

Figure 4.49: An overview EPMA image at 40x zoom of the H2 sample. The crucible is seen at the bottom with the slag on top.

In the EPMA image of the H2 sample there is seen a lot of smaller metallic Mo phases throughout the slag, figure 4.49. This means a reaction of the Mo crucible has taken place in the experiment. Because Mo is a much heavier atom than Fe, the metallic phases of Fe if there are any would be much darker than seen in experiments without Mo. There is seen a structure change with holes in the samples, these were the same one seen in the macroscopic images in figure 4.12. The holes/structure can be seen in both figure 4.49 above and figure 4.50 below. The latter figure shows the corner of the crucible where the holes are even bigger. The reason for the black color of the holes is because of the epoxy they are filled with.

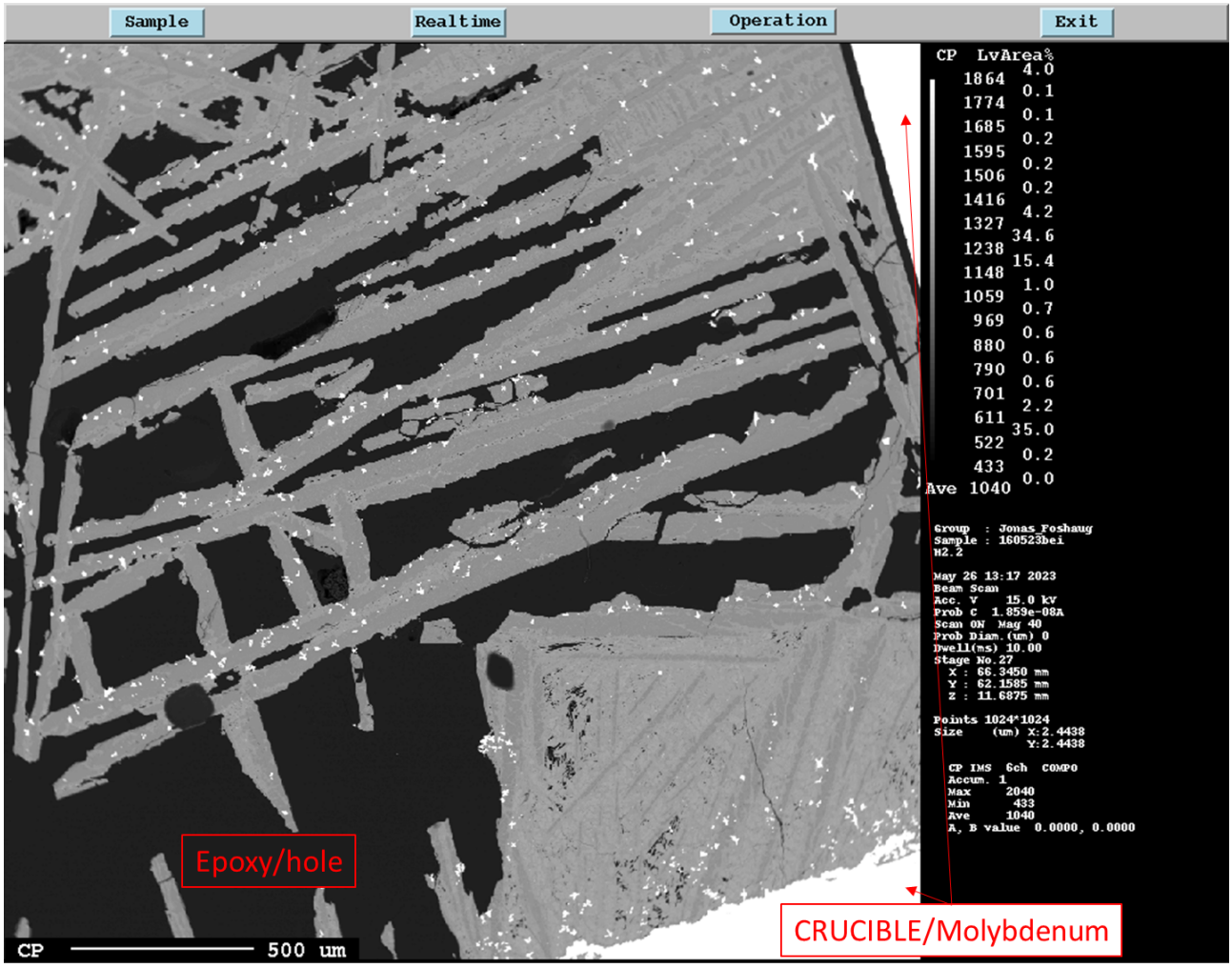

Figure 4.50: An overview EPMA image at 40x zoom of the H2 sample. Taken from the corner of the crucible.

EPMA mapping

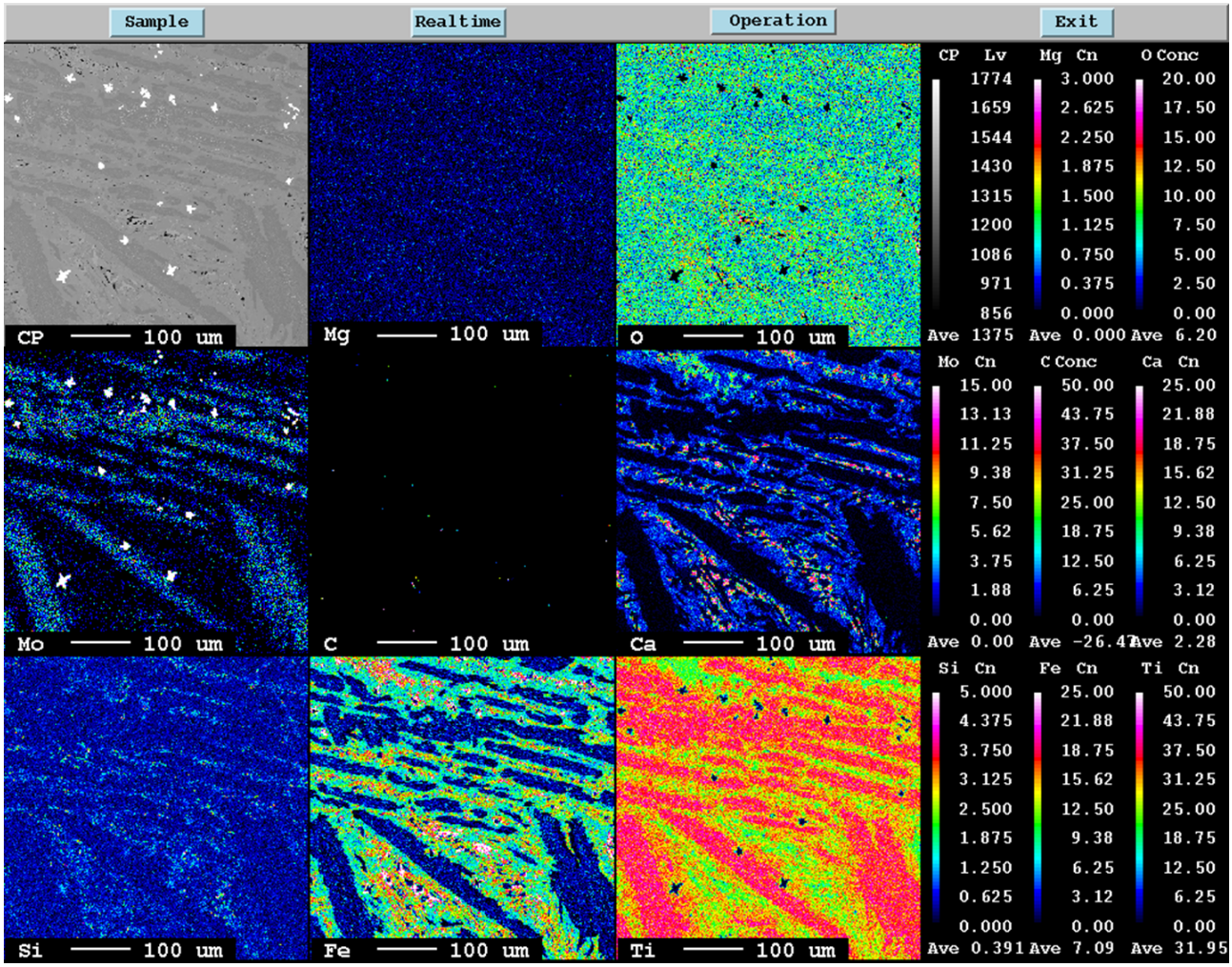

Figure 4.51: EPMA mapping of sample H2, from an image in the center of the sample.

The mapping, figure 4.51, of the H2 sample is taken from a phase near the holes seen in the overview figures above. The mapping shows a small amount of Mo being present in the dark gray phase. While the metallic phases seen, made up of Mo, are dominantly close to or inside the darker gray phases. There seem to be two dominant oxide phases and a mixture phase present in the sample, these are seen clearly in the Ti mapping. The green part of the Ti mapping seems to be a mixture of Ti with elements with a smaller concentration, meaning Ca, Fe, and Si. When looking at the Fe mapping there can be seen a metallic iron phase. This is seen where the Fe concentration is the highest, a white Fe color in the mapping.

4.6.3 Main findings H-series

Table 4.21: Some of the main findings for the H-series, the experiments using A1 and A2 pellets in Mo crucibles.

Findings	**Comments**
Dark gray coloration of the slag	
No/little climbing of slag in the crucible	Low wettability between slag and crucible
A reaction between slag and crucible	Crucibles seen corroded Mo seen throughout the slag
No pellets visible in H1 and H2	Same parameters as for D4,E4,F4 just different pellet/crucible
Macro image shows topography/structure difference	Different structure with air holes
Creation of metallic Mo phases	Mo present in dark gray phase Metallic Mo phases favors being in and around dark gray phases
Fe-oxide present in phases	Not completely reduced Seen in the point analysis and mappings
”Three” dominant oxide phases	Dark gray, light gray and a mixture phase Seen more clearly in the mappings
Almost no metallic iron	There is a lack of metallic iron Some is seen when looking at the highest count of Fe in mapping (H2)

5 Discussion

The table below is included to make it easier to read the following discussion.

Table 5.1: Recap of the parameters for the pellet-dropping experiments including the more informative name.

ID	Pellet	Slag composition	Crucible	Coating	Temperature	Time BQ*	Informative name
D1	G1	x**	SiC	BN	1650 °C	0 min	G1(100%CO)-SiC-0min-1650
D2	G1	x**	SiC	BN	1600 °C	1 min	G1(100%CO)-SiC-1min-1600
D1_1	G1	x**	SiC	BN	1650 °C	0? min	G1(100%CO)-SiC-0?min-1650
D4	G1	x**	SiC	BN	1600 °C	0 min	G1(100%CO)-SiC-0min-1600
E1	G3	x**	SiC	BN	1650 °C	0 min	G3(60%CO40%H_2)-SiC-0min-1650
E2	G3	x**	SiC	BN	1600 °C	1 min	G3(60%CO40%H_2)-SiC-1min-1600
E3	G3	x**	SiC	BN	1600 °C	3 min	G3(60%CO40%H_2)-SiC-3min-1600
E4	G3	x**	SiC	BN	1600 °C	0 min	G3(60%CO40%H_2)-SiC-0min-1600
F1	G6	x**	SiC	BN	1650 °C	0 min	G6(100%H_2)-SiC-0min-1650
F2	G6	x**	SiC	BN	1600 °C	1 min	G6(100%H_2)-SiC-1min-1600
F3	G6	x**	SiC	BN	1600 °C	3 min	G6(100%H_2)-SiC-3min-1600
F4	G6	x**	SiC	BN	1600 °C	0 min	G6(100%H_2)-SiC-0min-1600
H1	A1	x**	Mo	-	1600 °C	0 min	A1(100%CO)-Mo-0min-1600
H2	A2	x**	Mo	-	1600 °C	0 min	A2(100%H_2)-Mo-0min-1600

* Time BQ = Time before quench

** x= 85wt%TiO_2-10wt%FeO-5wt%CaO

Conversion degrees: G1=65% , G3=83% , G6=113% , A1=76% , A2=61%

On the next page there is a comparison table made from all the summary tables seen in the results. Here the rightmost column shows what experiment each of the findings encompasses. Table 5.2 shows a large similarity between all the SiC experiments (D-,E-, and F-series). This implies that there are almost no differences between the pellet types, at least from the results seen in these experiments, something that will be looked into further down in the discussion. There are naturally some major differences between the crucible types, these differences will also be explored further. It is also clearly seen that the pellets melt quite quickly once dropped into the melt, this can be argued because the pellets are only visible in the experiments that operate at a lower temperature and 0 min before quench, the exception being the Mo experiments (H-series).

Table 5.2: Main findings for all the pellet drop experiments. The x-series indicates all the x experiments.

Findings	**Comments**	**Experiments from series effected**
Dark gray coloration of the slag		**H-Series**
Black coloration of the slag		**D-series, E-series, F-series**
No/little climbing of slag in the crucible	Low wettability between slag and crucible	**H-series**
Climbing of slag in the crucible	High wettability between slag and crucible	**D-series, E-series, F-series**
A reaction between slag and crucible	Crucibles seen corroded Mo or Si seen throughout the slag	**D-series, E-series, F-series, H-series**
No pellets visible	Seen in macro images/EPMA	**D1, D2, E1, E2, E3, F1, F2, F3, H1, H2**
Topography/structure difference	Different structure with air holes seen in macro images	**H-series**
	Different structure near crucible than in center of slag	**D-series, E-series, F-series**
Pellets visible macro- and microscopically	Clear interface in EPMA images Low temperature, SiC, and 0 min drop time	**D1_1, D4, E4, F4**
Creation of metallic Mo phases	Mo present in dark gray phase	**H-series**
	Metallic Mo phases favors being in and around dark gray phases	**H-series**
Fe-oxide present in phases	Not completely reduced Seen in the point analysis and mappings	**H-series**
Fe-oxide not present in phases	Seems to be completely reduced to metallic phases	**D-series, E-series, F-series**
”Three” dominant oxide phases	Dark gray, light gray and a mixture phase Seen more clearly in the mappings	**H-series**
Creation of big metallic iron phases	Gray ring around the bigger ones made of TiC TiC around the edge of the big metallic phase Reduced with the help of the SiC crucible	**D-series, E-series, F-series**
Si present in the metallic phases near the crucible	Reaction from the crucible Si not present in metallic phases near and in pellet	**D-series, E-series, F-series**
Si also present throughout the slag	Si-O phases	**D-series, E-series, F-series**

Table 5.3: Advantages and disadvantages of some of the parameters in this master thesis.

	Advantage	**Disadvantage**
Molybdenum crucible	Not a complete reduction of iron Iron is still in oxide phases Little/no climbing of slag (No foaming) No thermal shock during cooling	Metallic Mo phases present throughout the slag Mo present in some of the oxide phases Expensive material Has to be specially ordered
SiC crucible coated in BN	Cheaper materials than Mo crucible No thermal shock during cooling	Fe in the slag reduced because of C in crucible Metallic Fe phases near the crucible have Si inclusions Has to be specially ordered
Hydrogen reduction agent	Faster reduction, less time to reach the same conversion degree H_2O off gas	Not tried on a large scale yet (production industry)
CO reduction agent	More researched (effects known to a larger degree)	CO_2 off gas Slow reduction agent when a high conversion degree is desired

5.1 Macroscopic comparisons and results

Noticeable in all the experiments using SiC crucibles is that the slag seems to climb the crucible walls, which is not the case for the Mo experiments. This can possibly be explained by the slag wettability on these materials. The wettability is higher on the SiC crucible compared to the Mo crucibles. The study by P. Shen et al. [17], found that the graphite crucible had low wettability when the temperature was low but, due to a temperature dependant reaction, it ended up being very adhesive. There was also foaming taking place. A similar reaction is likely taking place in the SiC crucible, meaning that the wettability is high, and there is likely a fair bit of foaming taking place. The foaming is influenced by the creation of CO/CO_2 in the slag as well as the viscosity of the slag. [10, 11] The creation of CO/CO_2 is a very likely product when looking at the metallic iron phases created in the melt. These metallic phases are easily seen, even macroscopically. When considering the viscosity of the slag, it can be assumed to be much higher in the SiC experiments since the FeO content that normally keeps the viscosity lower is reduced to metallic iron. There are ample studies done on the viscosity of TiO_2-FeO slag, the findings indicate the ratio between TiO_2-FeO to be crucial. A study of this was done by K. Hu et al.[19, 18] There is likely a bit of wettability in the Mo experiments as well, as seen by the slag in the corner of the Mo crucibles climbing a bit. The slag is not completely flat in the crucibles.

The color of the slag is a darker black in the experiments using the SiC crucible, while the color of the experiments using the Mo crucible is a very dark gray. The reason for the color difference is correspondingly due to a reaction between slag and crucible. This color difference was something that was observed in the forerunning project work as well. [20] In the project work it was suggested that it could be due to the BN coating used on the crucible because in pure form Boron is dark/black. Another explanation might be that the color comes from the TiC phase that has been seen to have a presence in all the SiC experiments. TiC is known to have a black color. This would explain why the color of the SiC crucible experiments is darker since the Mo crucible does not have a source of carbon to create the TiC phases.

The pellets can be visually seen in the experiments that have the parameters of SiC crucible, low temperature (1600 °C), and a time till quench of 0 min. The exception is the D1_1 (G1(100%CO)-SiC-0?min-1650) experiment since it was at 1650 °C, however, the temperature was likely a little lower during the drop because of the negative drop time, meaning the quench "started" before the drop. For the Mo experiments (H-series) there were no pellets visible, the most likely reason being that they are completely melted. The reasons for the difference between the Molybdenum and the SiC crucibles can be many. A possibility might be the liquidity/viscosity of the slag in the Mo compared to the SiC. The slag in the Mo experiments had Fe-oxide phases present, this FeO phase influences the viscosity to a large degree. Meaning the pellets dropped into the Mo experiments got completely engulfed in slag making the melting much quicker. The pellets dropped into the SiC experiments seem to be located on top of the slag, seen from the macro images of D1_1, D4, E4, and F4. From the EPMA mappings, these pellet parts seem to slowly be melting into the slag from the top.

Another reason for the pellets not being visible in the Mo experiments might be the size difference of the crucibles, the Mo crucible is larger than the SiC crucible. This could lead to the Mo crucible quenching slower due to the resting heat in the crucible. Meaning the SiC crucible quenches more efficiently. When looking at the size of the pellets dropped one would think that the results should have been the other way around, since the pellets dropped in the Mo experiments were whole and bigger than the pellet parts dropped in the SiC experiments. However, the ratio between pellet and slag was the same for all experiments, with a little room for error of course. The ratio is ca. 10g slag to 1 g pellet. This ratio was chosen to hopefully more easily see the pellets dropped into the slag. From the project work, the pellet-to-slag ratio for the Mo crucible experiments was 3g pellet/100g slag. Rendering it almost impossible to locate the pellets in the slag. [20] This ratio of 1/10 seems like a viable ratio when looking at the SiC experiments. The Mo experiments do not sell the same story, but it is more likely due to other factors than the ratio of pellet/slag that the pellets were not "found".

As mentioned there are no visible Fe phases seen macroscopically in the Mo experiments. This is likely due to the lack of reducing agents compared to the SiC crucibles. The SiC crucible ends up reducing the Fe in the slag and the pellets creating metallic iron phases. This carbon that does the reducing is not available in the Mo experiments making the slag consist of a larger amount of Fe-oxides instead of metallic iron. There is seen metallic iron when looking at the mapping of the Mo experiments, but compared to the SiC crucibles these are non-existent since in the SiC experiments these are even visible macroscopically.

5.2 Pre-oxidation and DisVaDri reduction

The average temperature seen in the two reductions done for the A1(CO) and A2(H_2) pellets shows CO to be of a higher average than H_2, this is not what is expected when considering the H_2 reduction reaction is more endothermic compared to CO. However, this is likely just due to the H_2 experiment being as short as it was. The trendline for the temperature of the H_2 experiment seems to stabilize at a lower temperature than the CO experiment, meaning if the experiment were run for a bit longer the average temperature would be correct when considering the endothermic argument. Another factor that supports this argument is that the A2 (H_2) pellet is less reduced (61% vs 76%) and should have been reduced a bit longer since the goal was to achieve the same conversion degree.

An important assumption made when calculating the conversion degree is that during the oxidation of the pellets, all the Fe in the pellet got oxidized to a Fe_2O_3 phase. This is likely or at least very likely since the oxidation time and temperature were created with earlier experiences found in the work by S. Lobo in mind. When looking at the EPMA image of the oxidized pellet, no metallic iron phases are seen. This is a good indication of complete oxidation, however, further analysis is needed to ensure that this is actually the case. An analysis such as XRF could be done. There were seen some small metallic phases in the pellets, these were zirconium. It is not unheard of to find trace elements of Zr in the ilmenite since the beach mine in Senegal also produces high-quality Zircon.[7]

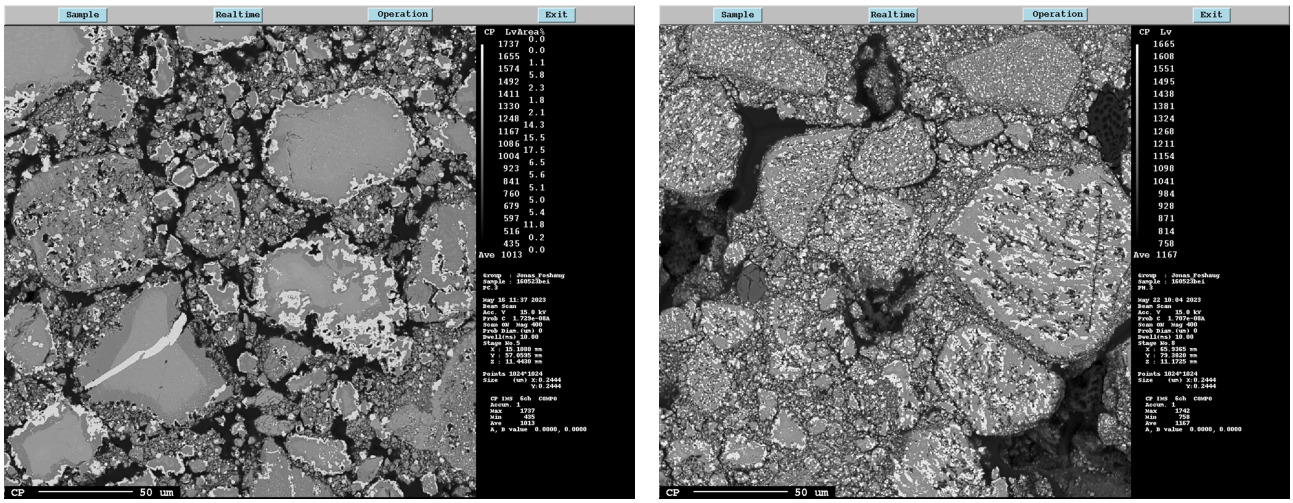

Figure 5.1: EPMA images of the CO and H_2 reduced pellets at 400x zoom. The CO reduced is to the left and the H_2 reduced is to the right.

As seen in the images of the pre-reduced pellets in figure 5.1, there is a noticeable difference in the reduction using CO and H_2. The pellets reduced with H_2 are being reduced throughout the gray round slag phase seen in the image to the right, while the CO reduces at the edges of the gray phases. The reason for this is likely the efficiency of the H_2 gas compared to the CO gas. The hydrogen likely diffuses further into the pellets than the CO is able to. In S. Lobo's work, it was seen a correlation between reduction rate and reduction gas composition. [42] The more H_2 gas used the faster the reduction, more easily seen from the graph in figure 2.4. The reduction using CO went on a fair bit longer than the H_2, 3 hours vs 20 minutes. This could be a reason for why in the CO reduction all the metallic phase is around the edges. There could have been enough time for the metallic phases to conglomerate to the edges in the CO-reduced pellets. While in the Hydrogen reduced pellets, the reduction was stopped before it could conglomerate.

The weight reduction indicator in the DisVaDri furnace was a source of error in the experiments. The start point is misaligned by ca 10g for both A1(CO) and A2(H_2). But even compensating for this, the CO reduction ends up at a weight reduction way too small than what is actually achieved. Since when the pellets were measured after the reduction, the weight reduction was a few grams higher than the DisVaDri instrument indicates. A few grams is a lot in these types of experiments. When compensating for the 10g in the H_2 case the weight reduction ends up almost at what is seen in the measurement after the reduction. Meaning the main problem lies in the CO experiment. One factor that was observed was the creation of soot on the crucible wall in the CO reduction experiment. This could be the reason for the misinforming weight reduction graph seen in 4.1.

The shrinking core model is the simplified model of reduction that was expected to happen to the pellets. When looking at the EPMA images this model is not what happens in the experiments. The reduction is throughout the pellet and even at the core of the pellet there can be seen a reduction to metallic iron. In the LOM image of the CO reduction it is possible to see a hint of what the SCM implies. This was done by tweaking the contrast, meaning it is very difficult to notice. When looking at the gray particles of the CO reduction, figure 5.1, it kind of looks like a microscale SCM, where the core is the gray particles. Here the iron reduces inwards towards the core, and layers of dark gray and light gray phases can be seen.

5.3 Effect of coating and crucibles

The coating and crucible materials are significant parameters for this master thesis, and their effect on the resulting product has to be explored. The SiC crucible with BN coating was used for most of the experiments. There seem to be some blatant drawbacks to this combination, where the main example is the easily seen reaction between the SiC crucible and the slag. The effect of the BN coating is something that is very uncertain, it was used for the precursing project work as well, but the effect was unknown in that work too. There is no debate that the slag reacts through the BN coating. The question is does the coating slow down this reaction by being a kind of barrier, or does it just dissolve once the temperature gets high enough? The latter seems like a more plausible result when looking at how all the experiments using BN coating look. There are studies that have used other types of inert coatings in slag melting experiments, one of these coatings is Y_2O_3. [16] This coating was shown to be a very good candidate for the melting of titanium alloys. This same study looked at BN crucibles and found them to be inefficient and causing major melt contamination. This was for a whole crucible, and considering the layer of BN coating is not very thick it is very likely just being melted into the slag. A problem with the BN is that it is extremely difficult to pick up on in EPMA analysis. This is due to the low atomic number/weight of the B and N. Meaning it is hard to know where in these slag experiments the BN resides.

This same study looked at Mo crucibles as well, however, these crucibles were coated with Y_2O_3.[16] They were shown to be expensive but efficient. The Mo crucible experiments in this master thesis clearly show a reaction of the Mo crucible with the slag, meaning these experiments were contaminated as well. It could be interesting to coat with other inert materials such as Y_2O_3 to see if these would work since none of the crucibles used in this master thesis were without flaws. The question still lies in which ones were the most efficient for these experiments. When looking at the effect of the crucible on the slag, it can be argued that the Mo crucible does the least amount of harm. The Mo reacted into the slag mainly exists in small metallic phases dotted around, it has a small inclusion in one of the oxide phases as well. The Mo does not lead to a reduction of the oxide in the slag, and kind of keeps to itself. This is not the case for the SiC crucible. The crucible gets corroded into the slag in a much more "harmful" way. The Si mixes with the oxide phases and is present throughout, while the C helps in the reduction of iron to metallic iron. The C also forms with Ti to create carbide phases. Overall the SiC crucible completely defines how the resulting slag will look. The Mo crucible does this to a much smaller degree.

It is likely a reduction of Ti in the slag because of the large amount of C present in the SiC experiments. In the study of M. Pourabdoli et al. [21], it was used a graphite crucible in the melting of TiO_2 slag. The additional carbon from the crucible ended up reducing the TiO_2 in the slag. This is not an unlikely parallel in the SiC experiments done in this master thesis. It is further confirmed when looking at the precursing project work. [20] Here it was used a graphite crucible with BN coating, and the resulting slag was analyzed using XRD, finding that the TiO_2 had reduced to Ti_3O_5 and similar phases. The resulting slag from these SiC crucibles has not been analyzed with XRD, and it is therefore difficult to know for sure if a lot of the Ti has been reduced. The only thing known for sure is the reduction of Fe.

5.4 EPMA overview and point analysis

For the point analysis of the experiments, there can be seen a vast difference in the amount of FeO present in the phases. For all the point analysis except for one in the SiC experiments, the amount of FeO in the slag phases is zero. The exception is experiment D1_1 (G1(100%CO)-SiC-0?min-1650). This point analysis is taken further away from the crucible wall and floor, more towards the center. The reason for the difference is likely due to the distance away from the crucible wall. Another

factor might be that the FeO comes from the pellet and has not been reduced completely by the SiC yet. When comparing the point analysis between Mo experiments and SiC experiments the biggest difference is the amount of FeO, and needless to say the SiO_2. A good indication that there has been a reduction of Fe. An explanation for the FeO in the D1_1 experiment might be the uncertain melting time. It is possible that the slag did not have enough time to reduce all the Fe since the experiment got cut a bit short. An argument for this being the case can be the lack of really big metallic phases in the slag.

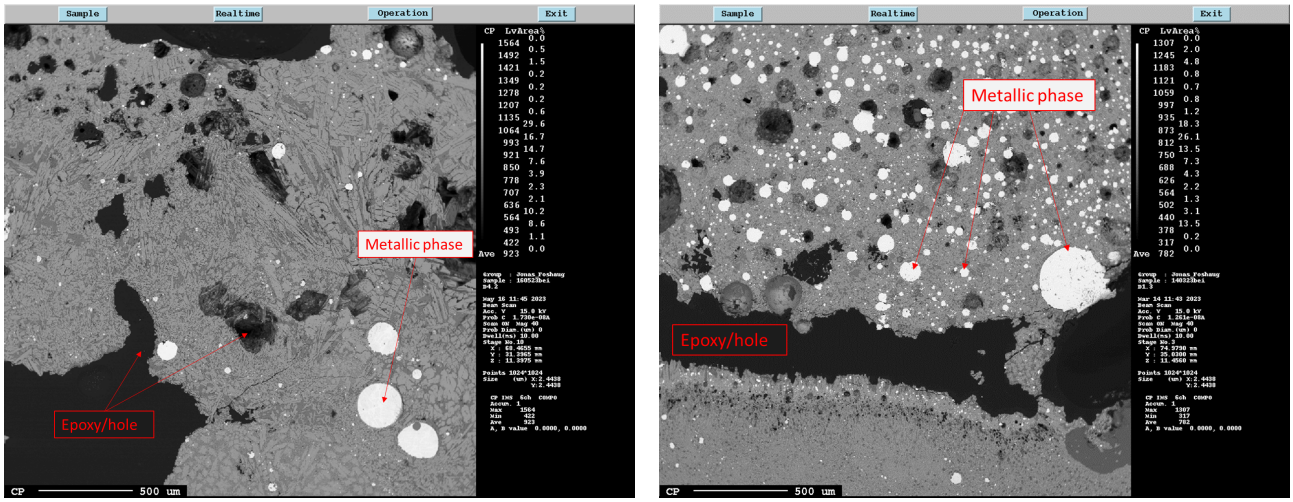

Figure 5.2: EPMA image of pellet and slag for D1_1 and D4.

The pellets that have been seen in these experiments look like the image to the right in Figure 5.2. Here larger metallic phases are seen in the pellet matrix. For the D4 G1(100%CO)-SiC-0min-1600experiment, it looked like a pellet part from the macroscopic pictures. And from the EPMA images taken of the sample it is seen to have a different structure than the ones seen in D1_1, E4, and F4. A comparison is seen in figure 5.2 and the pellet part is the top part of each image. The reason for the difference could be due to the pellet melting faster. This is something experienced in T. van Kaam's work. [44] The pellet that was reduced the least, i.e. the pellet with the least amount of conversion degree seemed to melt at a lower temperature than the more reduced pellets. The pellet used in D4 was the G1 pellet, this pellet had the lowest conversion degree. It is possible that the believed pellet part in the D4 experiment is just a different slag phase. This might be the case when looking at how the pellet looks in D1_1, they are the same pellet, G1, and look very different structurally. When looking at the EPMA overview for the F4 (G6(100%H_2)-SiC-0min-1600) in figure 4.45, the structure just outside the pellet looks a lot like the one seen in D4. Making it likely to be the pellet that just melted a bit more.

In some of the experiments, the structure changes when moving away from the crucible. This structure looks lamellae/plate-like. and is very noticeable in figure 4.31 of experiment E2 (G3(60%CO40%H_2)-SiC-1min-1600). In the EPMA mapping of F2, figure 4.42, it is noticed a vast difference in carbon amount in the different structures. The lamellae/plate-like structure is carbon deprived in comparison. This makes sense since this structure is further away from the carbon source, the SiC crucible. This lamellae/plate-like structure is noticed near and around the pellets in the experiments where these are visible. It could be considered that this structure is a remnant of the pellet (reaction) before the slag and pellet have had time to homogenize. This lamellae structure is what is seen in the part that is believed to be a pellet in D4, figure 5.2.

5.5 EPMA Mapping

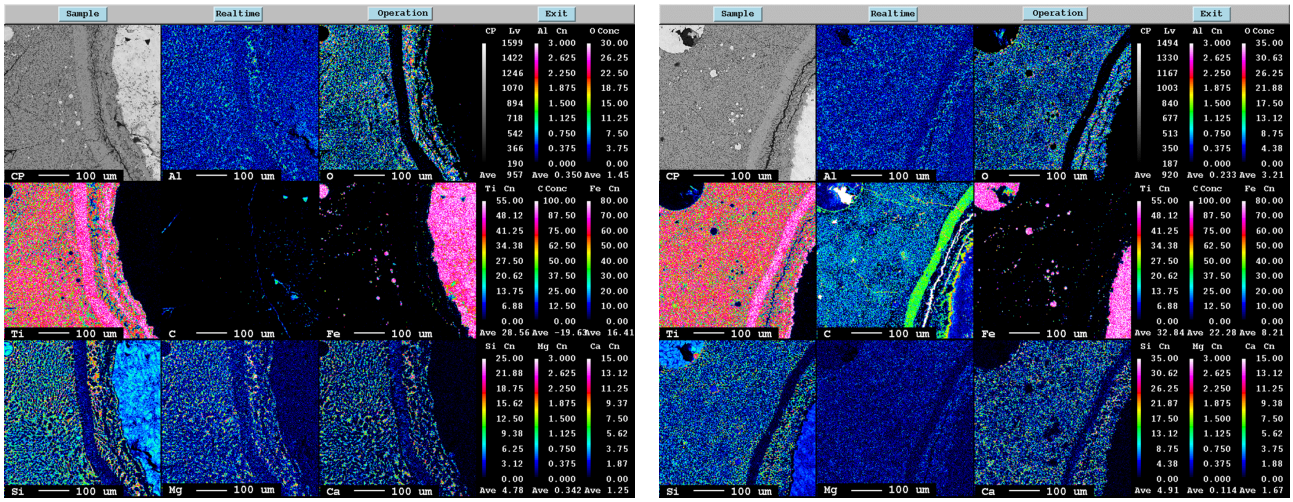

Figure 5.3: EPMA mapping of sample D2 to the left and F3 to the right, both showing mapping near a big metallic phase.

The large metallic phases seen throughout all the experiments involving SiC have a grey ring surrounding them. This ring, from a point analysis of D4, was found to be a combination of Ti and C. And the various mappings done of these surrounding rings shows that to be true. There is only one exemption, the D2 (G1(100%CO)-SiC-1min-1600) experiment. This can be seen above in figure 5.3. Here the mapping of D2 to the left shows no signs of anything but Ti in the ring. These two mappings are however mysteriously similar by the looks of it. And it is much more likely that something has gone wrong in the C mapping of D2. Since all the other mappings and a point analysis show this to be TiC. The C mapping has a problem picking up C in the SiC crucible. This is seen in all the mappings including the crucibles. There is a possibility that the same problem occurred for this one mapping picking up C in TiC. The mapping for carbon in these cases can be calibrated for SiC instead of 100% pure carbon. This can be seen illustrated in figure 5.4 below. This is probably something that could have been done in all the mappings, and this might have made it clearer if there were some TiC phases present. There is also seen to be a creation of TiC at the big metallic phase surface. The creation of TiC is to be expected when there is an abundant amount of C present. This can be seen in the ternary phase diagrams provided by V. Raghavan/S. Jonsson in figure 2.15.

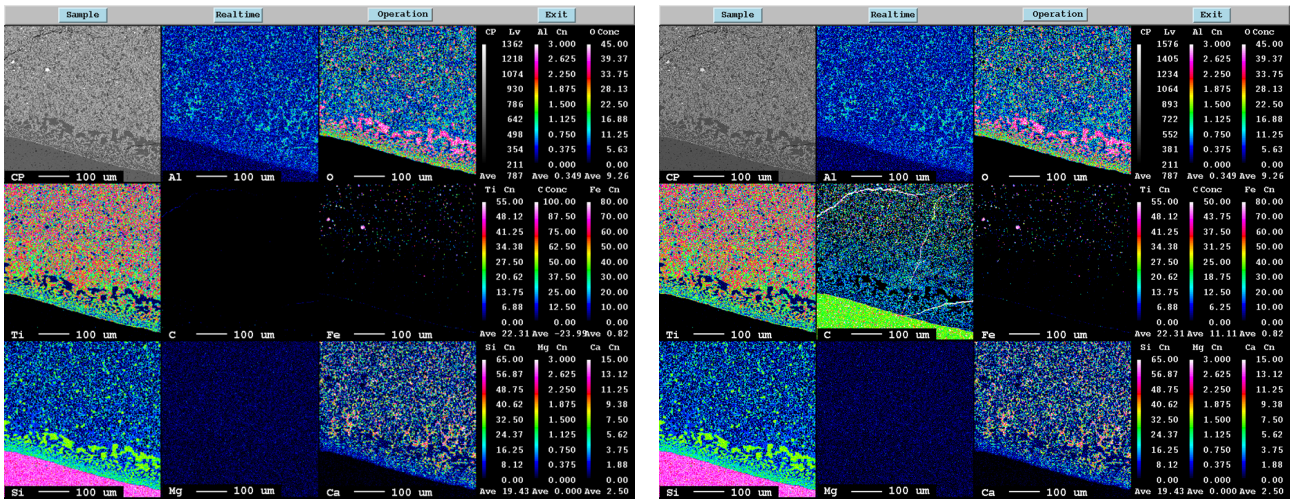

Figure 5.4: EPMA mapping of sample D1_1. The carbon map is calibrated for 100% C on the left while it is calibrated for carbon in SiC to the right.

The interface between pellet and slag was easily spotted in most cases where the pellet parts were visible. The exemption is D4 as discussed before. The images in figure 5.5 below show the comparison between D1_1 (G1(100%CO)-SiC-0?min-1650) and D4 (G1(100%CO)-SiC-0min-1600) at the believed interface. This belief is most likely true for D1_1 where the main evidence is the Mg mapping. For the mapping of D4 it is seen Si present in the metallic iron phase, meaning this iron has most likely been reduced by the SiC crucible i.e. the main interface is a bit further up. This Si in the iron phases is a good indication of where the slag from the crucible has been reacting. When looking at mappings for other interfaces, E4 and F4, it is clearly seen that no Si is present in the iron phases.

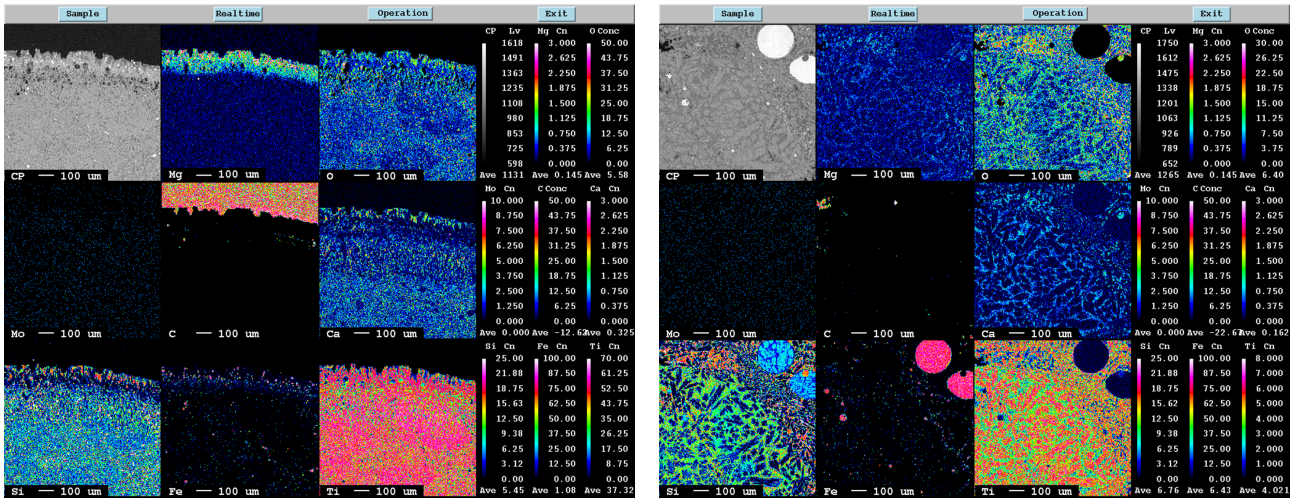

Figure 5.5: EPMA mapping of sample D1_1 to the left and D4 to the right, both showing a mapping of what looks like the interface between pellet and slag.

The Fe mappings for SiC experiments vs Mo experiments show a clear difference. In the SiC experiments, the Fe mapping is almost completely black with dots of Fe around. This indicates no Fe present in the slag phases, just in the metallic phases. For the Mo experiments the Fe is seen present throughout the slag phases i.e. the Fe is not reduced to metallic iron. There are however some metallic iron phases in the slag seen clearly in the H2 mapping, figure 4.51. These metallic iron phases can come from the metallic iron present in the pellets dropped, or the metallic iron the slag was created from. Near the SiC crucibles, the iron diffused to the crucible surface. mixing with Si to create Fe-Si metallic phases. This is the case for all the experiments involving SiC. The SiC from the crucibles

seems to react out into the slag, creating phases of SiO_2, Fe-Si, TiC, and probably some more that include Mg, Al, Ca, etc.

5.6 Hydrogen vs CO

As stated in the table 5.2 the difference between CO and H_2 reduced pellets in the melting experiments are non-existent. This is not necessarily a bad thing considering the goal is to change CO reduced with H_2 reduced pellets. However, the results gotten here are riddled with undesired parameters that have affected the results. The main ones are the crucible types. The crucibles seem to dictate the results to such a large degree that the experiments end up looking the same. For the pre-reduction part, there is clearly a difference in the CO and H_2 reduced pellets. CO is a much slower process and the reduced iron conglomerate at the edges, while H_2 is faster where iron reduces throughout and does not conglomerate. These differences are not found in the melting experiments, the pellet parts even look very similar in all the different cases. This might be due to the reduction continuing when the melting of the pellet begins. Making all the pellets similar. The temperature is very high, and there is a CO/CO_2 evolution in the slag, for the SiC experiments. In the case of the H_2 vs CO in the Mo cases, both these pellets were completely melted and not found. A lower temperature might be needed, or a "negative" drop time, meaning start the quench a few seconds before the pellet gets dropped.

5.7 Experimental difficulties/parameters

There are many parameters in a melting experiment and with many parameters the likelihood of failure or an undesired result increases. One of the significant parameters that had to be changed during this master thesis was the melting temperature. The temperature that originally was planned for all the experiments was 1650 °C. This temperature was to ensure a complete melting of the slag, the melting point of the slag created (85wt%TiO2-10wt%FeO-5wt%CaO) was calculated to be around 1615 °C in Factsage. However, the thermocouples used in the furnace could not handle 1650 °C, and ended up breaking. The temperature was therefore reduced to 1600°C. This is lower than the theoretical melting point, but the furnace is built in such a way that the thermocouple is placed above the crucible. This means that if the thermocouple and crucible are placed in the right spot the crucible should be a few degrees higher than what the thermocouple measures. This is shown from a calibration graph in the methods part, figure 3.8. The result is that the temperature is high enough for complete melting. The inclusion of CaO in the slag was to reduce the melting point so that the furnaces could be used. This inclusion was argued earlier that was insignificant for the results when looking at the viscosity aspect. However, it does include a whole other element to the equation of the slag that has to be considered. And the effect of this inclusion is difficult to say without running a parallel experiment without it.

A parameter is the cooling rate, it is claimed to be a quench in this master thesis. This is only half true, the crucible is pulled down to a colder zone, but this zone is still warm. It is of course a lot colder than the heating zone and there will be a more rapid cooling rate than if the crucible were just left in the heating zone. The quench might be a bit inefficient, and definitely a part of the method with an improvement possibility. The timing of the drop till the quenching commences is understandably a possibility for error and deviance in the experiments. The dropping is very manual and dependent on the user. If the user is experienced and has run a few experiments in short succession the drops more or less will be the same, with a tiny error of a second or two. The problem is inexperience and mistakes. If the user forgets the procedure the seconds add up fast. A way to circumvent this is dry drilling, meaning doing the drop a few times without the furnace being turned on. For the experiments done in this master thesis, the drops are with minimal deviance.

6 Conclusion

This master thesis wanted to look at the interface between different pre-reduced pellets and high titania slag. It was done with the use of synthetically created slag, and pellets made from raw ilmenite. The slag was melted in two different crucibles, Mo and BN-coated SiC.

The main conclusions drawn from this master thesis can be summarized as seen below:

- SiC crucible
  - Strong reaction with the slag at the temperatures.
  - Creation of SiO_2, TiC and Fe-Si phases.
  - Fe-oxides reduced to metallic iron.
  - Climbing of slag in the crucible, high wettability
- Molybdenum crucible
  - Fe-oxides still present in the slag.
  - Pellets completely melted, no "interesting" interface results.
  - Mo reacted into the slag, metallic Mo phases as well as being present in slag phases.
- Different pre-reduced pellets
  - No real difference was found in the G1, G3, and G6 pellets when used for melting in the slag.
  - Clear difference in pellets after pre-reduction, the H_2 (A2) were a faster reduction and the iron did not conglomerate at the edges of the gray phases as it did for CO (A1).

The crucible types both had some significant drawbacks, both of them influencing the slag. The molybdenum crucible influenced to a lesser degree than SiC considering it did not reduce everything in the slag. The SiC also ended up creating carbide phases in the slag. It is important to note that the SiC crucible was coated with BN, which seems to have little to no effect limiting the reaction between slag and crucible. When looking at the pellets, they were only visible in the SiC crucible cases when the temperature was 1600 °C and the drop time was 0 min. For the Mo crucible cases, the pellets were not visible even at the 1600 °C temperature and 0 min drop time. The pellets that were visible and investigated with EPMA looked very similar, meaning no significant difference between the differently reduced pellets. This points to the melting time of the pellets being too fast or to the cooling rate (quench) being too slow.

The goal of this master thesis was to develop a method for and to look at the interface between differently reduced pellets in high titania slag. The method developed for the TF2 is as it stands now an acceptable method of dropping pellets into slag. The problem lies in the type of slag used, the corrosive nature of the slag needs to be solved. This can be done with a change in crucible materials, but that is a problem for future works on this system. The dropping mechanism is easy to use and can easily be applied to other systems as well.

7 Future work

The future work of this master thesis can go many different ways. One of the most important results coming from the thesis is the development and building of the dropping mechanism for the TF2. This can be used for other projects and is not limited to just being used for high titania slag and ilmenite pellets. There are possibilities of dropping more pellets at the same time, and if there is built a bigger holding chamber for the pellets, the possibilities are even higher. It is not a difficult thing to do.

For a more experiment related future work, there is the possibility of changing the crucible type to one that might be less reactive. This could include a crucible coated with Y_2O_3 if the study of S. Fashu et al.[16] holds true. This is a problem that is hard to solve however, since the slag is so reactive. So finding a solution for this might be something that can be a continuation of this work.

The pellets created in this master thesis have the potential for future analysis and experiments. For starters, an XRF analysis could be done of the oxidized pellets to see if all the Fe has oxidized to Fe^{3+}. These pellets were also created to fit the TF2 setup, meaning more experiments could be run with different parameters. The resulting sample series from this master thesis could also be analyzed using XRD to get an idea if the Ti has reduced from rutile to a phase like pseudobrookite. This is especially interesting for the SiC experiments. And the experiments could of course be rerun to ensure validity since there are a lot of parameters that could differ between each run.

The quenching in the TF2 could possibly be improved by using a different inert gas. The inert gas used in this master thesis is argon, but it could be swapped out with helium gas. The inert gas helium is experienced as more efficient in a quenching environment. This is something I noticed when helping running experiments on different slag systems.[57]

Bibliography

[1] Norwegian Evironment Agency. Eramet titanium & iron as. Available from: https://www.norskeutslipp.no/en/Miscellaneous/Company/?CompanyID=5118, 2023. Obtained: 03-05-2023.

[2] R.G. Becher. Improved process for the benefication of ores containing contaminating iron, Aust Patent 247110, sep. 16, 1963.

[3] K. Kanta Sahu, T.C. Alex, D. Mishra, and A. Agrawal. An overview on the production of pigment grade titania from titania-rich slag. *Waste Manag. Res.*, 24(1):74–79, February 2006.

[4] M. Tangstad, H. Elstad, and S. Seim. *Metal production in Norway.* Akademika publishing, 2013.

[5] Mindat.org. Tellnes mines, sokndal, rogaland, norway. Available from: https://www.mindat.org/loc-18742.html. Obtained: 27-11-2022.

[6] Eramet titanium & iron, a pioneer of metallurgy in norway. Available from: https://www.eramet.com/en/eramet-titanium-iron-pioneer-metallurgy-norway.

[7] Grande côte operations. Available from: http://www.tizir.co.uk/projects-operations/grande-cote-mineral-sands/.

[8] TiZir. Tizir titanium and iron. Available from: http://www.tizir.co.uk/projects-operations/tyssedal-tio2/, 2022. Obtained: 09-11-2022.

[9] J. Solheim. *The tyssedal ilmenite smelting process.* Norwegian Institute of Technology, 1988.

[10] I. V. Nekrasov, O. Y. Sheshukov, A. A. Metelkin, A. V. Sivtsov, and M. M. Tsymbalist. Slag conditions in electrosmelting: A review. *Steel in Translation*, 46(6):435–442, June 2016.

[11] G. Handfield and G.G. Charette. Viscosity and structure of industrial high tio2 slags. *Canadian Metallurgical Quarterly*, 10(3):235–243, 1971.

[12] S. Seim and L. Kolbeinsen. Update on the equilibrium between liquid fe-ti-o slags and metallic iron. *steel research international*, 81(12):1051–1055, 2010.

[13] J. Eriksen, E. Robles, and T. Rosenqvist. Equlibrium between liquid fe-ti-o slags and metallic iron. *Steel Research International*, 78:671–675, 09 2007.

[14] S. Seim and L. Kolbeinsen. Alternative approaches for high temperature investigation of high titania slags, 2009.

[15] P. Pistorius. Fundamentals of freeze lining behaviour in ilmenite smelting. *Journal- South African Institute of Mining and Metallurgy*, 103:509–514, 10 2003.

[16] S. Fashu, M. Lototskyy, M. W. Davids, L. Pickering, V. Linkov, S. Tai, T. Renheng, X. Fangming, P. V. Fursikov, and B. P. Tarasov. A review on crucibles for induction melting of titanium alloys. *Materials & Design*, 186:108295, 2020.

[17] P. Shen, H. Fujii, and K. Nogi. Wettability of some refractory materials by molten sio2–mno–tio2–feox slag. *Materials Chemistry and Physics*, 114(2):681–686, 2009.

[18] K. Hu, K. Tang, X. Lv, J. Safarian, Z. Yan, and B. Song. Modeling viscosity of high titania slag. Available from: https://doi.org/https://doi.org/10.1007/s11663-020-02002-8, 2020. Obtained: 09-11-2022.

[19] K. Kai K. Hu, X. Lv, S. Li, W. Lv, B. Song, and K. Han. Viscosity of tio2-feo-ti2o3-sio2-mgo-cao-al2o3 for high-titania slag smelting process - metallurgical and materials transactions b. https://link.springer.com/article/10.1007/s11663-018-1284-x#citeas, May 2018.

[20] J. Foshaug. Pre-reduced ilmenite pellets in high titania slag (prosjektoppgave). *MTMT-NTNU HØST*, 2022.

[21] M. Pourabdoli, Sh. Raygan, H. Abdizadeh, and K. Hanaei. Production of high titania slag by electro-slag crucible melting (escm) process. *International Journal of Mineral Processing*, 78(3):175–181, 2006.

[22] International Iron Metallics Association. Dri production. Available from: https://www.metallics.org/dri-production.html, 2021. Obtained: 13-12-2022.

[23] R. Longbottom and L. Kolbeinsen. Iron ore reduction with co and h2 gas mixtures – thermodynamic and kinetic modelling. Available from: https://ro.uow.edu.au/engpapers/1260/, Jan 2008.

[24] D. Spreitzer and J. Schenk. Reduction of iron oxides with hydrogen—a review. *steel research international*, 90(10):1900108, 2019.

[25] J. Oh and D. Noh. The reduction kinetics of hematite particles in h2 and co atmospheres. *Fuel*, 196:144–153, 2017.

[26] E.T. Turkdogan and J.V. Vinters. Gaseous reduction of iron oxides: Part i. reduction of hematite in hydrogen. *Metallurgical and Materials Transactions B*, 2(11):3175–3188, November 1971.

[27] D.R. Parisi and M.A. Laborde. Modeling of counter current moving bed gas-solid reactor used in direct reduction of iron ore. *Chemical Engineering Journal*, 104(1):35–43, 2004.

[28] A. Ranzani da Costa, D. Wagner, and F. Patisson. Modelling a new, low co2 emissions, hydrogen steelmaking process. *Journal of Cleaner Production*, 46:27–35, 2013. Key Elements (Stages and Tools) for a Sustainable World.

[29] R. Béchara, H. Hamadeh, O. Mirgaux, and F. Patisson. Optimization of the iron ore direct reduction process through multiscale process modeling. *Materials*, 11(7):1094, Jun 2018.

[30] H. Hamadeh, O. Mirgaux, and F. Patisson. Detailed modeling of the direct reduction of iron ore in a shaft furnace. *Materials*, 11(10):1865, Oct 2018.

[31] M.V.C. Sastri, R.P. Viswanath, and B. Viswanathan. Studies on the reduction of iron oxide with hydrogen. *International Journal of Hydrogen Energy*, 7(12):951–955, 1982.

[32] H. Lin, Y. Chen, and C. Li. The mechanism of reduction of iron oxide by hydrogen. *Thermochimica Acta*, 400(1):61–67, 2003.

[33] A. Pineau, N. Kanari, and I. Gaballah. Kinetics of reduction of iron oxides by h2: Part ii. low temperature reduction of magnetite. *Thermochimica Acta*, 456(2):75–88, 2007.

[34] M.J. Tiernan, P.A. Barnes, and G.M.B. Parkes. Reduction of iron oxide catalysts: The investigation of kinetic parameters using rate perturbation and linear heating thermoanalytical techniques. *Journal of Physical Chemistry B*, 105(1):220–228, January 2001.

[35] W. Du, S. Yang, F. Pan, J. Shangguan, J. Lu, S. Liu, and H. Fan. Hydrogen reduction of hematite ore fines to magnetite ore fines at low temperatures. *Journal of Chemistry*, 2017:1919720, Mar 2017.

[36] M. Shimokawabe, R. Furuichi, and T. Ishii. Influence of the preparation history of a-fe2o3 on its reactivity for hydrogen reduction. *Thermochimica Acta*, 28(2):287–305, 1979.

[37] Y.D. Wang, X.N. Hua, C.C. Zhao, T.T. Fu, W. Li, and W. Wang. Step-wise reduction kinetics of fe2o3 by co/co2 mixtures for chemical looping hydrogen generation. *International Journal of Hydrogen Energy*, 42(9):5667–5675, 2017.

[38] I.J. Moon, C.H. Rhee, and D.J. Min. Reduction of hematite compacts by h2-co gas mixtures. *Steel Research International*, 69(8):302–306, August 1998.

[39] A. Pfeiffer, G. Wimmer, and J. Schenk. Investigations on the interaction behavior between direct reduced iron and various melts. *Materials*, 15(16), 2022.

[40] O. J. P. Gonz, M. A. Ram, and A. N. Conejo. Mathematical modeling of the melting rate of metallic particles in the electric arc furnace. *ISIJ International*, 50(1):9–16, 2010.

[41] F.M. Penz and J. Schenk. A review of steel scrap melting in molten iron-carbon melts. *steel research international*, 90(8):1900124, 2019.

[42] S. Lobo. *Experimental Investigations and Modelling of Solid-State Ilmenite Reduction with Hydrogen and Carbon Monoxide*. Norwegian Institute of Technology, 2015.

[43] O. Levenspiel. *Chemical reaction engineering*. John wiley and sons, 3 edition, 1999.

[44] T.P.M. van Kaam. High temperature behaviour ofpre-reduced ilmenite pellets(prosjektoppgave). *MSMT-NTNU HØST*, 2022.

[45] Factsage.com. general information factsage. Available from: `https://www.factsage.com/fs_general.php`. Obtained: 30-11-2022.

[46] K. Borowiec. Phase relations and oxidation studies in the system fe-fe2o3-tio2 at 700-1100°c, 1981.

[47] K. Borowiec. Phase relations and oxygen potentials in the fe-ti-mg-o system, 1985.

[48] M. Allibert. *Slag atlas*. Verlag Stahleisen GmbH, 2 edition, 1995.

[49] A.H. Webster and N.F.H. Bright. The system iron–titanium–oxygen at 1200c. and oxygen partial pressures between 1 atm. and $2 \times 10 - 14$ atm. *Journal of the American Ceramic Society*, 44(3):110–116, 1961.

[50] S. Itoh. Phase equilibria in the titanium-iron-oxygen system in the temperature range of 1173 to 1373 k. *ISIJ International*, 39(11):1107–1115, 1999.

[51] T. Narumi, S. Kawanishi, T. Yoshikawa, K. Kusunoki, K. Kamei, H. Daikoku, and H. Sakamoto. Thermodynamic evaluation of the c–cr–si, c–ti–si, and c–fe–si systems for rapid solution growth of sic. *Journal of crystal growth*, 408:25–31, 2014.

[52] S. Jonsson. Assessment of the fe-ti-c system, calculation of the fe-ti-n system, and prediction of the solubility limit of ti(c,n) in liquid fe. *Metallurgical and materials transactions. B, Process metallurgy and materials processing science*, 29(2):371–384, 1998.

[53] V. Raghavan. C-fe-ti (carbon-iron-titanium). *Journal of Phase Equilibria*, 24(1):62–66, February 2003.

[54] Sintef. Process metallurgical laboratories: Disvadri furnace. Available from: https://www.sintef.no/en/all-laboratories/process-metallurgical-laboratories/disvadri-furnace/, 2023. Obtained: 02-05-2023.

[55] J.S. Gjøvik. Graphite tube furnace. Available from: https://www.ntnu.no/wiki/display/imtlab/Graphite+tube+furnace+-+TF2+translation, 2015.

[56] IMA NTNU. Jeol jxa-8500f electron probe micro analyzer (epma). Available from: https://www.material.ntnu.no/lab/material/equipment/ProdInfoEPMA.pdf. Gotten: 23.03.2023.

[57] S. Haghdani. The study of tio2-sio2-cao-feo slag systems using raman spectroscopy. *NTNU*, 2021.

8 Appendix

The appendix will include the extra images and analysis done on the experiments. It will be divided up into sections for each series. They will not have the same degree of explanation as the ones presented in the results.

8.1 D series

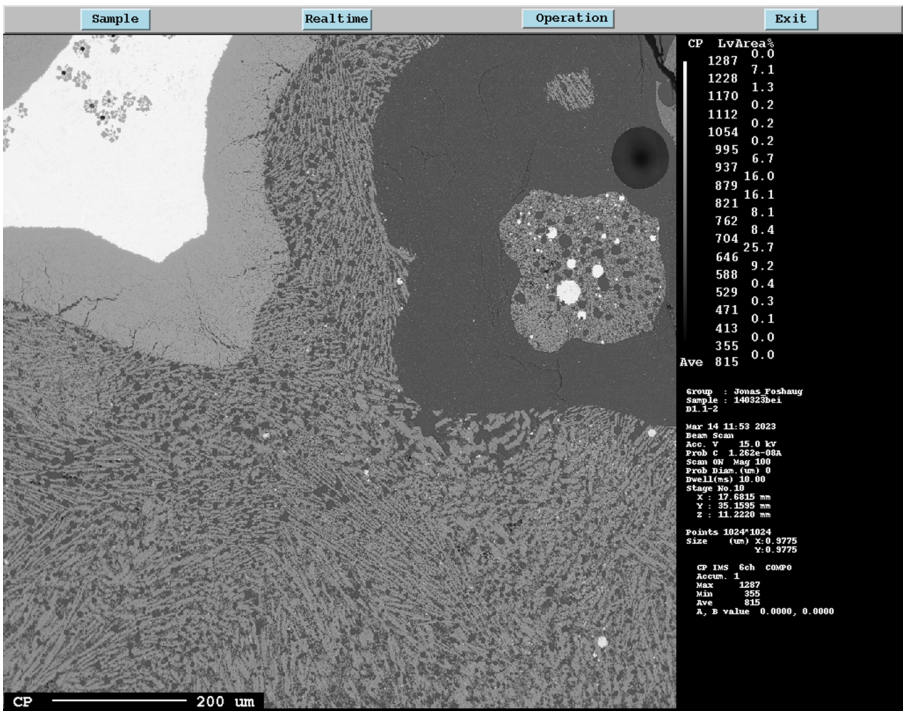

Figure 8.1: EPMA image of D1.

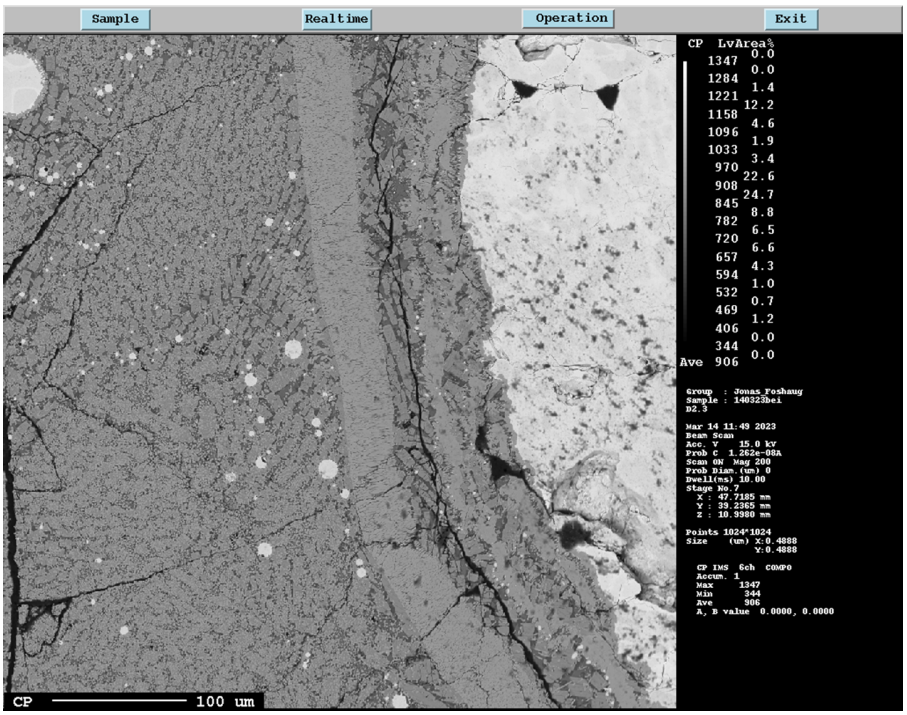

Figure 8.2: EPMA image of D2. Used for mapping seen in results

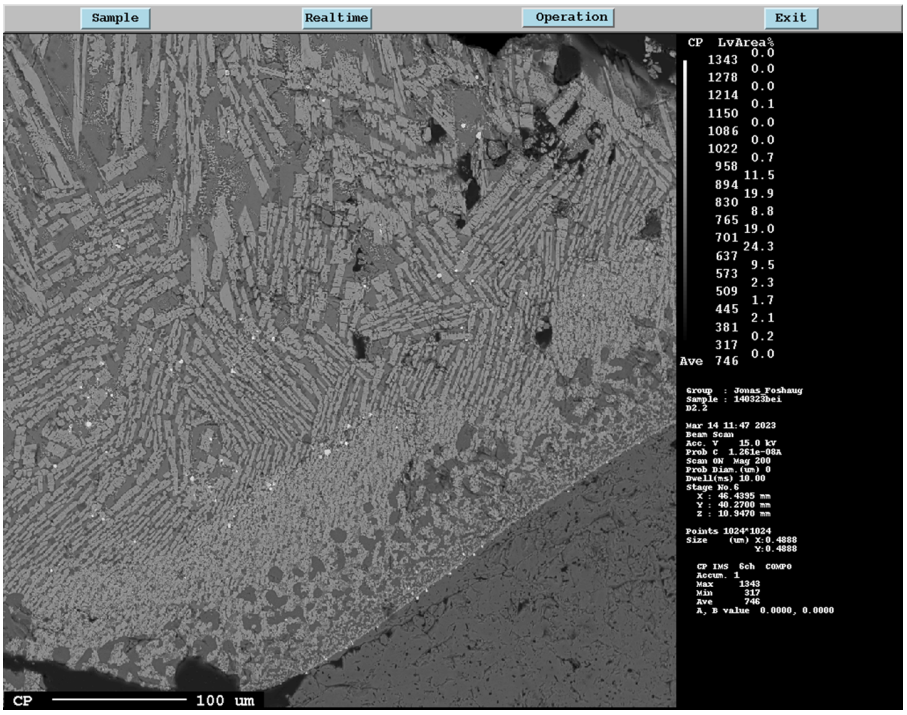

Figure 8.3: EPMA image of D2. Used for mapping seen in results

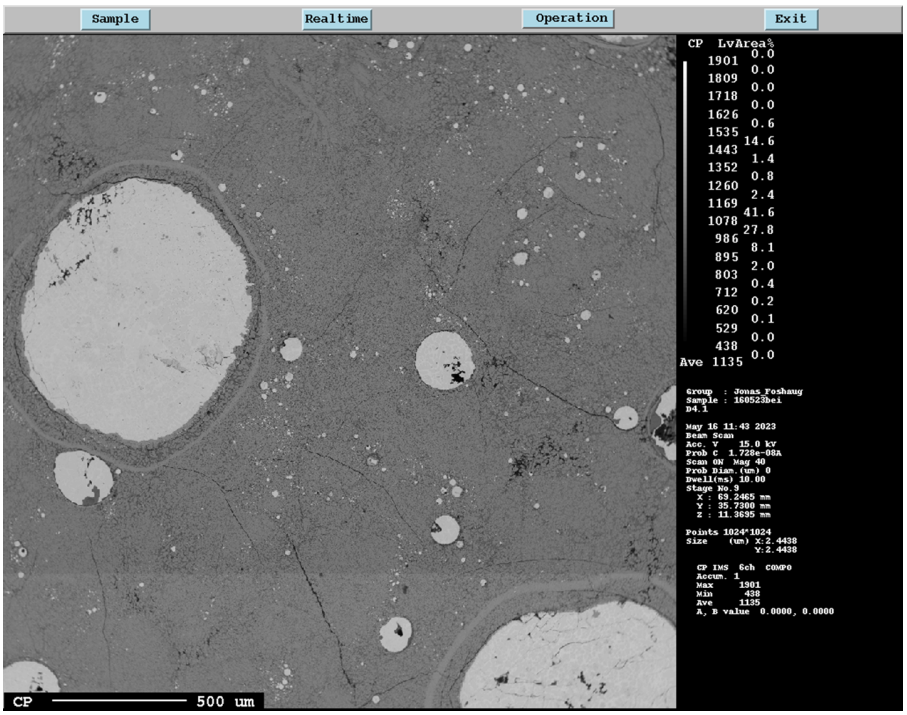

Figure 8.4: EPMA image of D4.

8.2 E series

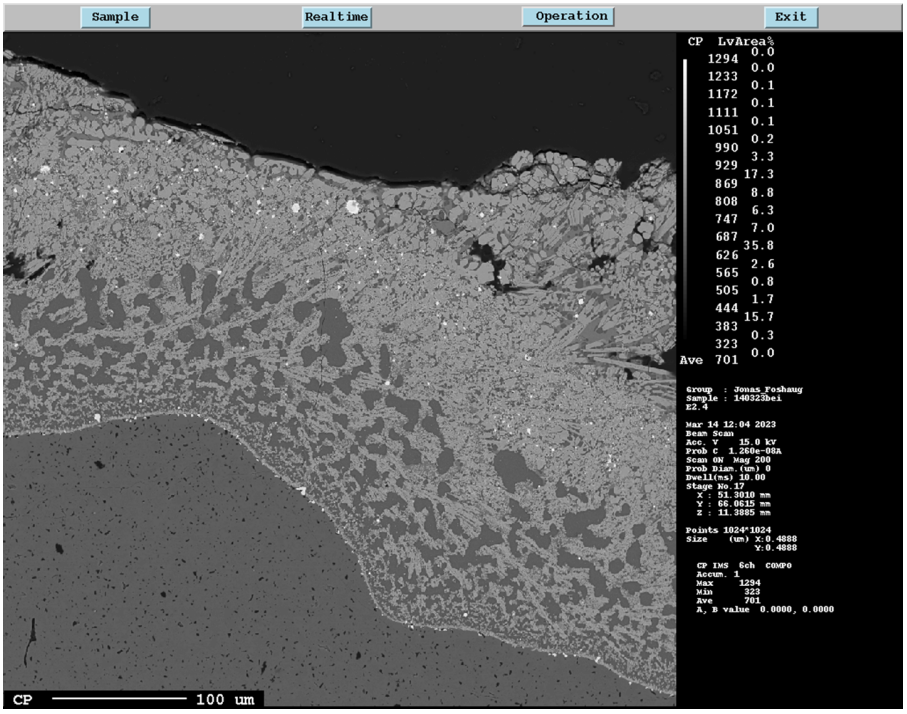

Figure 8.5: EPMA image of E2.

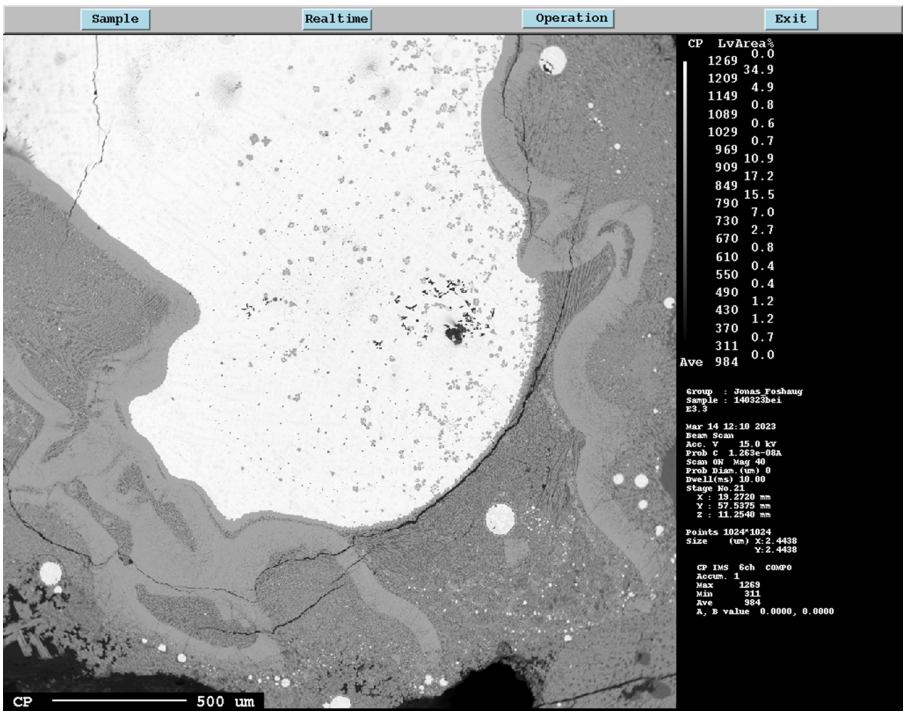

Figure 8.6: EPMA image of E3.

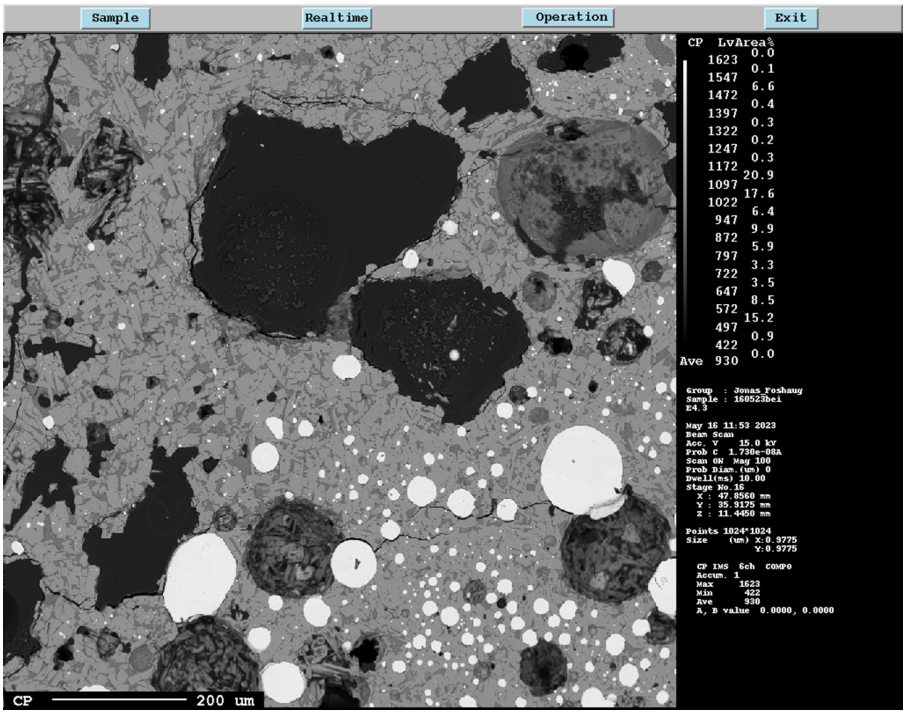

Figure 8.7: EPMA image of E4. Used for mapping seen in results

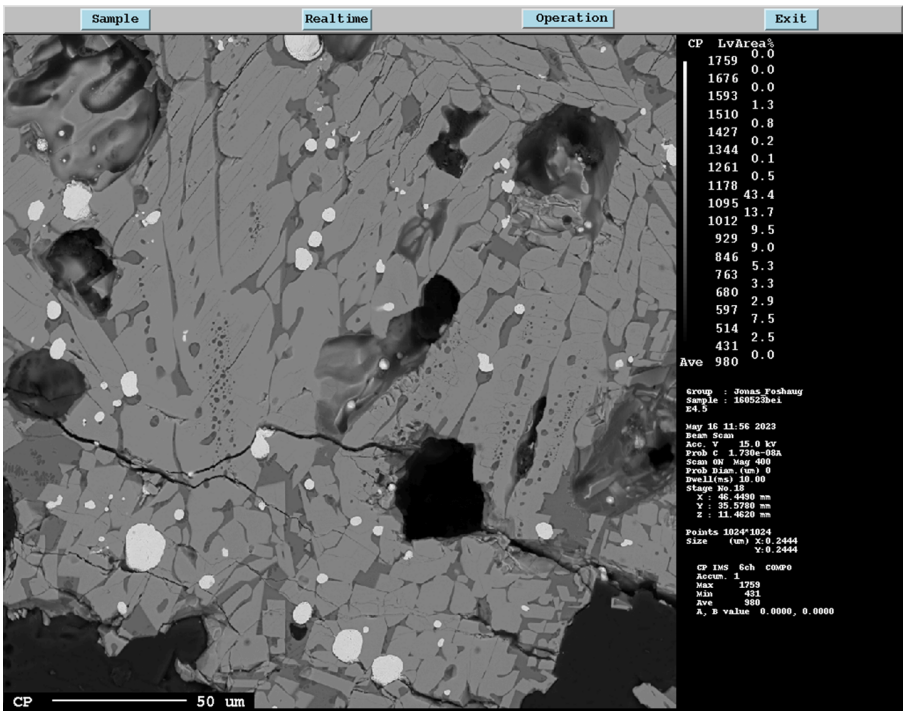

Figure 8.8: EPMA image of E4.

8.3 F series

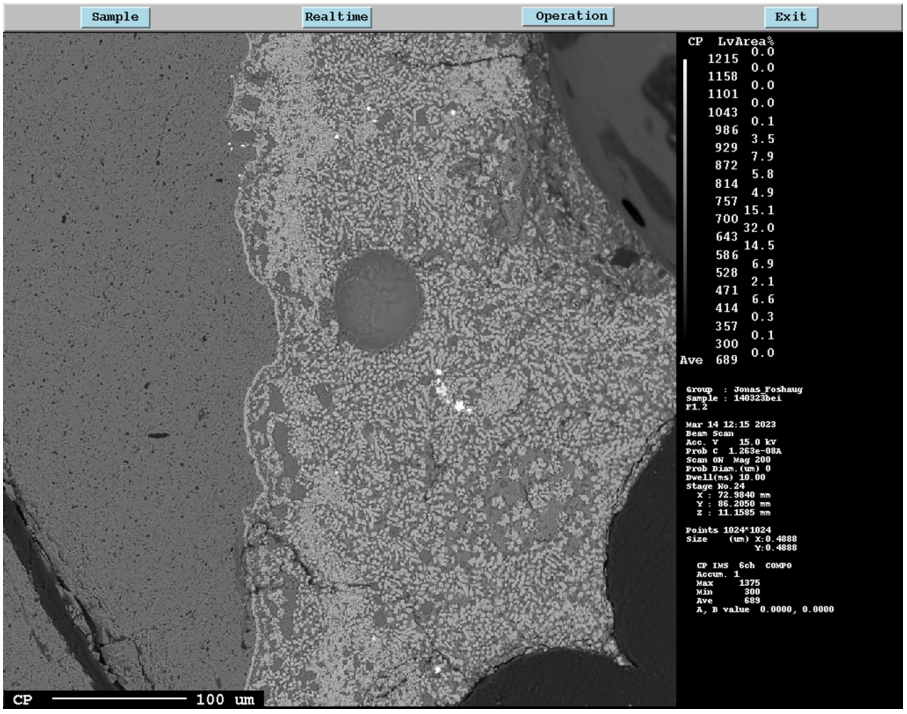

Figure 8.9: EPMA image of F1.

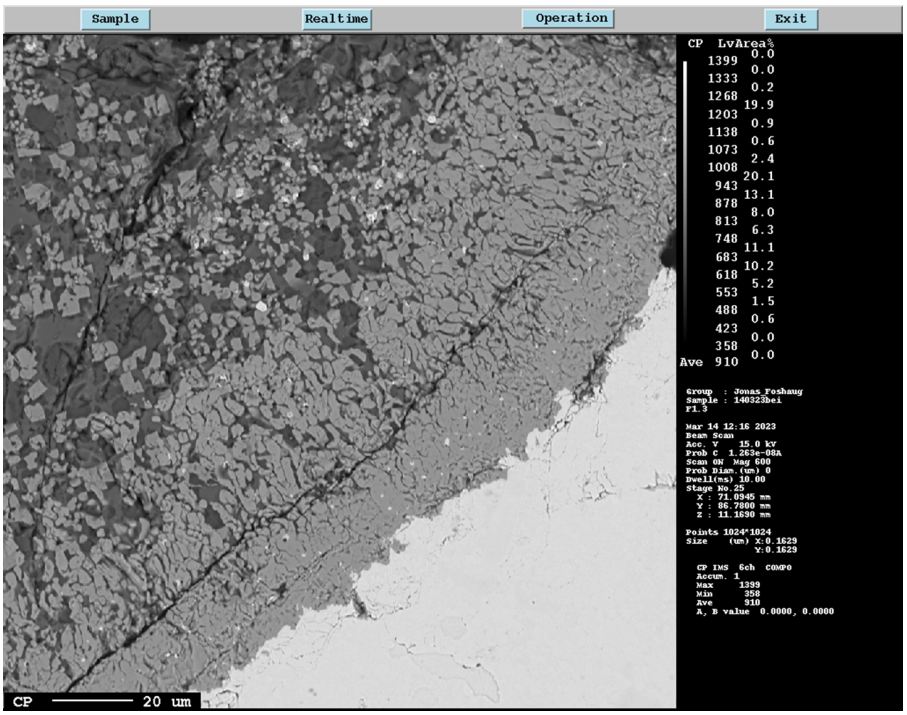

Figure 8.10: EPMA image of F1.

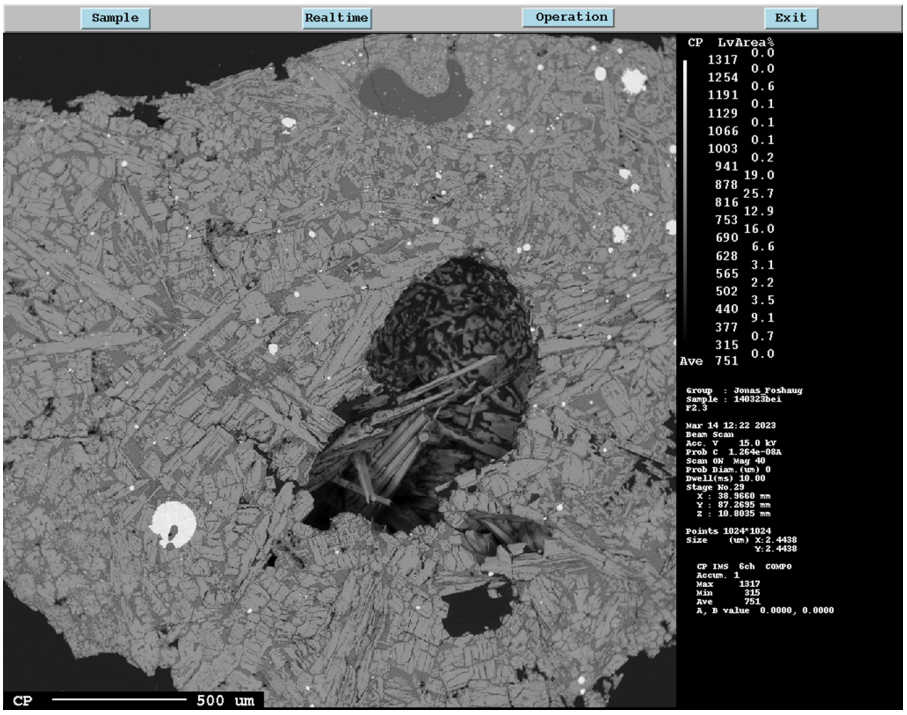

Figure 8.11: EPMA image of F2.

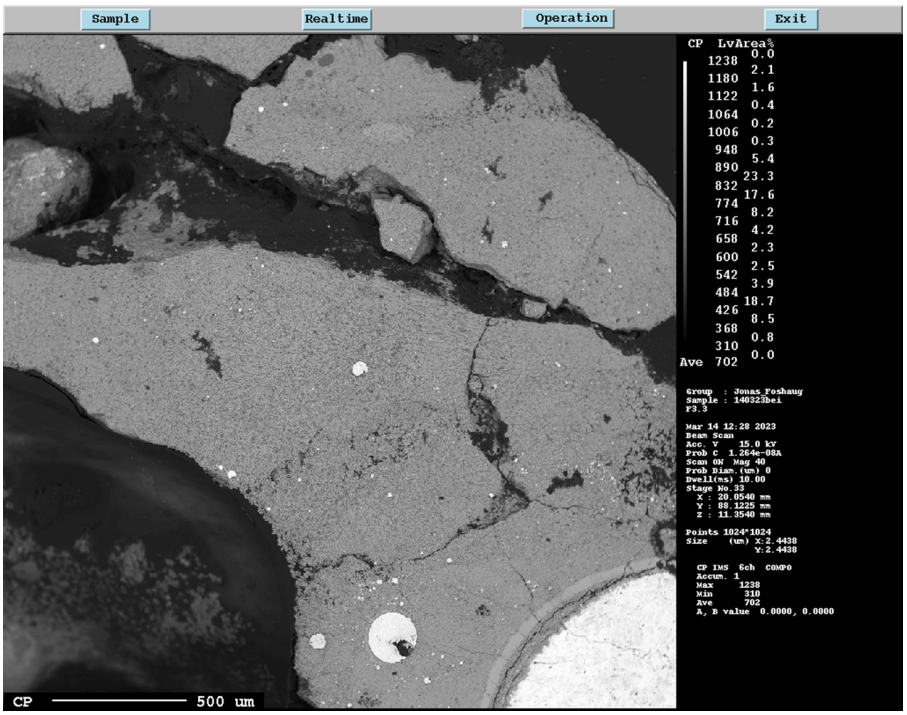

Figure 8.12: EPMA image of F3.

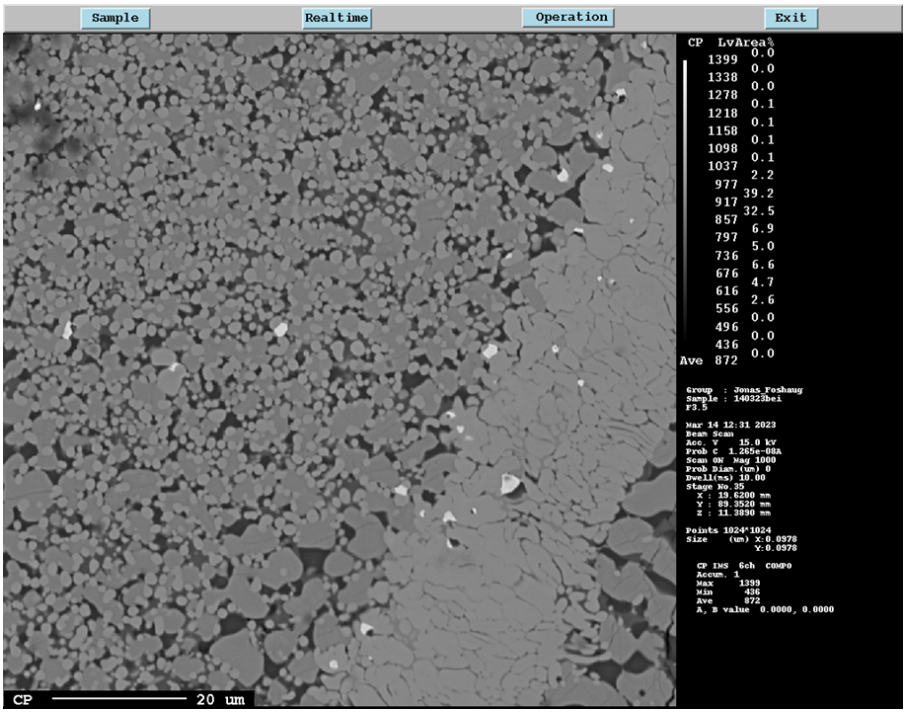

Figure 8.13: EPMA image of F3.

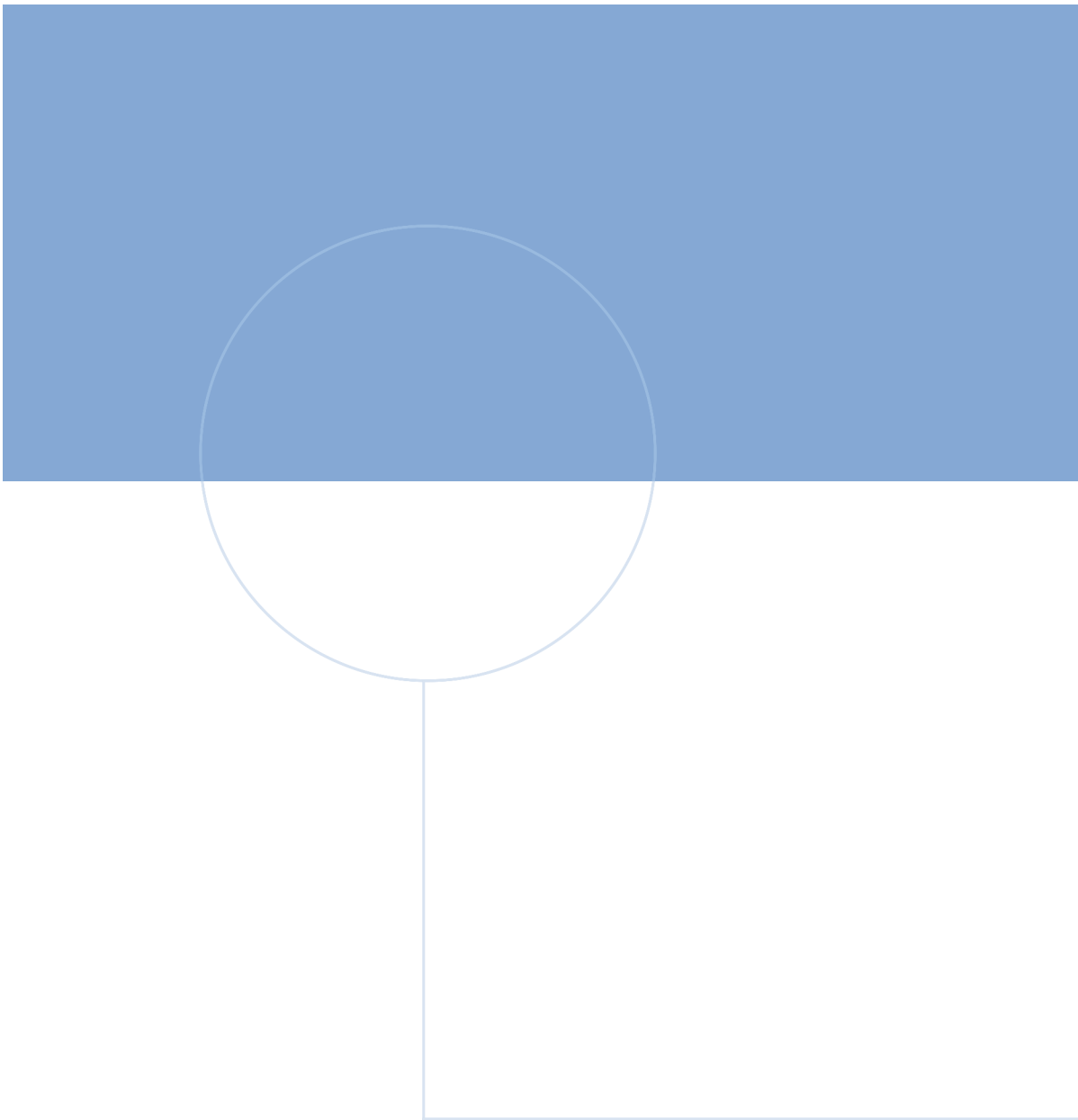

NTNU

Norwegian University of
Science and Technology